PERIGLACIAL FACIES AND ALTITUDINAL TRENDS IN ALASKA AND THE APPALACHIAN HIGHLANDS

By

Raven Jezell Mitchell

A DISSERTATION

Submitted to
Michigan State University
in partial fulfillment of the requirements
for the degree of

Geography – Doctor of Philosophy

2024

ABSTRACT

A century-plus record of work has established the formation pathways by which periglacial processes give rise to entire landscapes. Sedimentological facies, discrete deposits that represent the interactions of climate and topography in an environment, comprise the basis of a concept used in periglacial contexts to interpret paleoclimatic depositional processes and to better characterize landforms. Geographical periglacial geomorphology, a once popular trend in the German literature, established that regional-scale relationships exist between periglacial landform assemblages and the climatic snowline, thus outlining the three-dimensional distribution of upland periglacial features.

Recent periglacial literature calls into question the ability of periglacial processes to generate landform-scale terrain. Motivated by such skepticism, this dissertation focuses on quantitative and qualitative characterization of periglacial regions. Four interrelated but independent chapters in this dissertation use facies and geographical periglacial geomorphology frameworks to 1) identify trends in periglacial feature elevations in relict periglacial environments; 2) identify periglacial facies in known periglacial realms; 3) characterize and map facies; and 4) apply findings from facies and spatial-analytical studies to interpret enigmatic features of hypothesized periglacial origin.

Chapter 2 is a regional-scale spatial analysis of periglacial features in the Appalachian Highlands providing unifying and important spatial context for the subsequent periglacial studies put forth in this dissertation. A synthesis of published periglacial features and locational information shows that a strong correlation exists between periglacial feature elevation and reconstructed climate trends from the Last Glacial Maximum, lending support to the climatic

interpretation of upland Appalachian terrain. Chapter 3 focuses on quantitative characterization of the composition and spatial distribution of upland “periglacial facies” in the Alaskan interior. Sedimentological and remotely sensed data demonstrate that cryoplanation surfaces are comprised of areas delimited by distinct topographic and sedimentological characteristics. Chapter 4 focuses on periglacial terrain at Spruce Knob in West Virginia’s section of the Appalachian Highlands. Data collection and analysis of this hypothesized cryoplanation landform and comparison to the site from Chapter 3 supports the interpretation that the periglacial components of Spruce Knob align with the morphological characteristics of an upper side slope facet. Chapter 5 is a case study that utilizes methodology from previous chapters to elucidate the formation of the enigmatic Hickory Run Boulder field (HRBF), located in northeastern Pennsylvania. Field data show that the HRBF likely formed via an allochthonous pathway characterized by tributary-like flow of blocky material from bedrock outcrops. Evidence for the integration of clasts from an under investigated area of the boulder field was found, offering new insights into the feature’s formation.

Results from this dissertation show that the periglacial imprint is evident and observable, based on periglacial facies, which impart a distinct “footprint” on the landscape. Major findings indicate that 1) the areal distribution of periglacial features in the eastern USA aligns with European findings showing trends in feature elevations; 2) periglacial cryoplanated terrain is composed of faceted surfaces representing topographic and microclimatic variations; and 3) paleoperiglacial processes, combined with glacio-fluvial activity, can result in the formation of large boulder (block) fields that can accurately be described as periglacial features.

This dissertation is dedicated to Fritz Nelson.

ACKNOWLEDGMENTS

Several University and organizational entities helped make this degree possible. I would like to first acknowledge the Michigan State University (MSU) College of Social Science and Graduate School whose Research Scholars Award and Rasmussen Graduate Fellowship helped fund my research. The MSU Geography Department, through the work of academic coordinators, department chairs, and graduate directors, helped me seek funding sources and provided resources which resulted in support for fieldwork and conference travel. Fieldwork required for the completion of Chapter 5 of this dissertation was supported by The American Association of Geographers Marcus Award. The American Geophysical Union's Cryosphere Flash Freeze Competition Award funded my early dissertation research in Appalachia. I would also like to acknowledge the Circumpolar Active Layering Monitoring Program which funded several of my research assistantships and travel between Alaska and Michigan spanning both my master's and PhD programs. The research component of my PhD program was greatly improved by the advisory of my guidance committee comprised of my co-chairs, Drs. Fritz Nelson and Ashton Shortridge, and Drs. Alan Arbogast and Grahame Larson. Without their support and professional advice, this project would not have been possible.

The work presented in this dissertation required data collection that took place over the course of three summers during which I was assisted by several dear friends and colleagues. Dr. Kelsey Nyland accompanied me throughout my master's and PhD fieldwork and offered invaluable field sampling design insight in addition to helping me formulate hypotheses and helping me to forge a path toward dissertation completion in the final semesters of this program. Her mentorship and guiding presence were and are indispensable not only in

research, but also in life. Vasily Tolmanov assisted me in the field in the Appalachians and in Alaska for several months, which included drone piloting and data post-processing that supported analysis included in several chapters of this dissertation. His field and cryosphere expertise and his excellent hiking abilities contributed immensely to my field design and overall project conception. I am forever grateful for his companionship, his big heart, and persevering spirit. I am also grateful for Jacob Tafrate who assisted me during the first summer of data collection in Alaska and for Anya Tolmanov who kindly assisted fieldwork in Pennsylvania and West Virgina.

Lastly but certainly not least, I would like to thank my family. My mom, Courtney, my Grandma Roxanne, and sister, Rachel, supported me in every way during my graduate studies. My in-laws Drew and Therese Milam housed me for semesters at a time and were always there to listen. Finally, my girlfriend Ally, served as my longtime-advisor, support system, late night paper reader, professional data enterer, and field hand. Ally, your unwavering support sailed me through the times when I wasn't sure that I could succeed in this program.

This project took a village to complete. Without the assistance of those mentioned above, the work presented here would have been impossible and certainly much less fulfilling. It would take up entire dissertations-worth of paper to name all those who made this degree possible. To all of you and to those named here, thank you.

TABLE OF CONTENTS

CHAPTER 1. INTRODUCTION

Background

Periglacial regions are characterized by cold but nonglacial conditions in which frost action processes are dominant (Van Everdingen, 2005). Features often encountered in periglacial environments include patterned ground, cryoplanation terraces, boulder fields, angular block deposits, nivation hollows, and solifluction lobes, many of which occur as "assemblages" (Queen, 2018). Some researchers have posited that these assemblages characterize distinctively periglacial terrain and give rise to entire landscapes (Queen & Nelson, 2022). Workers have begun to isolate and distinguish this terrain by applying geomorphometric techniques (Harriott & Evans, 2022; Queen & Nelson 2022) and have determined that upland periglacial landscapes vary substantially from the inselbergs and pediments of warm desert climates, further establishing that periglacial processes generate distinctive landscapes (Queen & Nelson, 2022).

Despite the well-documented inventories and process-based studies linking periglacial climates to assemblages of periglacial features and landscapes, recent trends in the literature call into question the existence of characteristic periglacial terrain (André, 2003; French, 2016). Critics have raised issues with the past "overrating of the role of freeze-thaw mechanisms in the interpretation of cold-region geomorphic features" (André, 2003) and emphasized that even under the influence of periglacial conditions for millions years, a truly periglacial environment is rarely achieved (French, 2016). Specifically, speculation surrounds the ability of periglacial erosional pathways or "periglaciation" to produce a distinctive periglacial footprint on the landscape (French, 2016). Contention surrounding the existence of characteristic periglacial

terrain is bolstered by a lack of studies attempting to identify and characterize such realms using contemporary research methods and by the lack of models of periglacial landscape evolution (French, 2016). Despite the record of research on periglacial processes and landform evolution pathways, a consensus about what constitutes a periglacial environment seems precarious.

The term “facies” describes a “body of sediment or rock with specified characteristics, namely colour, bedding, geometry, texture, fossils, sedimentary structures and types of external contacts” (Hambrey, 1994, p. 15). The facies concept has been used as a framework to examine sequences of sediments and emphasizes the identification of stratigraphic units and their relation to environmental conditions (Madole, 1972; Olyphant, 1985). Periglacial facies, first described by Lozinski (1909), are comprised of blocky, rubble-covered surfaces that typify periglacial uplands (von Łoziński, 1909; Martini et al., 2011) and are the “shallowest layer of the lithosphere in a periglacial environment” (Dobiński, 2024, p. 212) . The facies concept has been used to infer the existence of past periglacial conditions (Hambrey, 1994, p. 171) and studies conducted establish 1) that quantitative links between periglacial features and climate exist (Madole, 1972; Olyphant, 1985; Martini et al., 2011); 2) that facies can be used as indicators of contemporary and past topoclimatic and microclimatic conditions (Olyphant, 1985); and 3) that facies analysis may serve as a useful model for the design of field experiments (Madole, 1972). Although it has been more than a century since periglacial facies were first described, and despite previous work establishing that periglacial facies can be used as a methodological framework to characterize periglacial landscapes, there is no extensive record of publication in which the facies conceptual model has been used to address issues in periglacial

geomorphology. There appears to be a lack of standardization or reference regarding the implementation of facies identification in periglacial geomorphology, a situation that has hindered the application of this methodological framework.

Geographical periglacial geomorphology outlines the relationships between periglacial feature elevations and geographical position (latitude and longitude) across broad, regional scales (Poser, 1977). An outstanding finding from this style of research is the close relation between snowline and periglacial feature elevation (e.g., Graf, 1973; Poser, 1977; Karte, 1979; Nelson & Nyland, 2017). This body of research lends clear and quantitative support for the climatic interpretation of periglacial feature assemblage formation and emphasizes the notion that the spatial distribution of periglacial landform assemblages gives rise to periglacial landscapes (Poser, 1977). Despite prevalence in the German literature, geographical periglacial geomorphology has not been embraced in the Anglo-American literature, and very few regional inventories of periglacial features with respect the altitudinal trends of periglacial features exist.

Dissertation motivation and organization

Based on criticisms raised in the literature, this dissertation responds to the following questions:

1.) Is there a periglacial "signature/footprint" or identifiable facies associated with certain periglacial deposits? Can the identification of facies be used to investigate formation pathways of enigmatic features such as the Hickory Run Boulder Field in the eastern USA?

2.) Can the periglacial facies concept be used to identify facets of periglacial features in unglaciated Beringia? Similarly, can the identification of facies be used to reveal

information about periglacial land formation in relation to periglacial environments that have existed throughout the Quaternary?

3.) Can advanced understanding of periglacial facies in a known periglacial environment be used to identify and characterize hypothesized periglacial features in relict periglacial settings?

4.) Do periglacial features in the eastern USA follow trends explained in the German geographic periglacial geomorphology literature?

Together, the facies concept, which has been used as a theoretical underpinning by which to conceptualize the spatial distribution of periglacial deposits, and geographical periglacial geomorphology, which emphasizes the climatic and scale-based relationships of periglacial features, serve as the theoretical foundation for this dissertation. Using sedimentological relative weathering indices and clast orientation as data input, this dissertation attempts to discern a "periglacial footprint" through a quantitative, field-based methodology conducted at sites in Alaska, Pennsylvania, and West Virginia, as well as across a latitudinal transect spanning much of the eastern USA (Figure1).

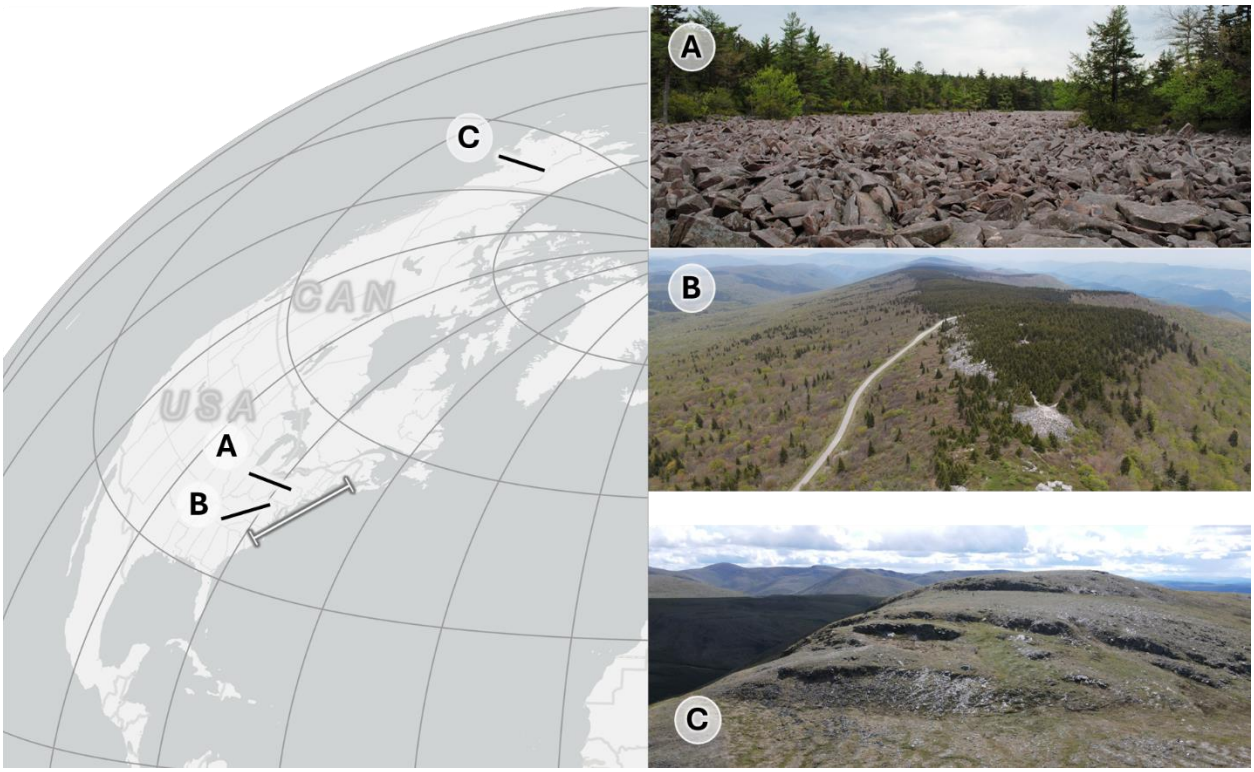

Figure 1. Geographical Extent of Dissertation Study Areas. *Photos in the panels on the right show field conditions at the sites that supported in-situ data collection corresponding to three chapters of this dissertation. The bar located in the map on the left indicates the extent of the study transect for the identification of periglacial features and elevations from a literature review.*

Chapter 1 sets the tone for this dissertation through an exploration of periglacial feature elevations in the eastern U.S. Work from this chapter serves to outline the regional-scale periglacial imprint on the landscape, substantiated by findings in alignment with the European geographical periglacial geomorphology literature. This work also contributes to a subcontinental-scale inventory of periglacial features for the Appalachian Highlands. Cryoplanation terraces, which are abundant in periglacial regions, are used as sampling sites for Chapters 3 and 4 because of their association with periglacial climates and periglacial erosional pathways (Reger, 1975; Nyland & Nelson, 2019; Queen et al., 2021; Mitchell et al., 2023). The substantive work in this dissertation concludes with a case study on the Hickory Run Boulder

Field that incorporates findings and insights from the previous chapters in this dissertation. Chapter 6 summarizes main findings, provides commentary on suggestions for future work, and elaborates on the importance of this work in the context of geomorphology and society.

CHAPTER 2. THE PERIGLACIAL REALM IN THE APPALACHIAN HIGHLANDS DURING THE LAST GLACIAL MAXIMUM

Introduction

The Appalachian Highlands is a mountainous belt extending more than 1100 km south of the Last Glacial Maximum margin (Fenneman, 1946; French & Millar, 2014). This region experienced periglacial conditions during glacial stages owing to its proximity to the Laurentide Ice Sheet (French & Millar, 2014; Bierman et al., 2015), which facilitated July air temperatures 5-12˚C cooler than at present (Woodcock & Wells, 1990). Periglacial features found in the Appalachian Highlands include block fields, block streams, patterned ground, and ice wedges (French & Millar, 2014).

Climatic geomorphology, of which periglacial geomorphology is an important component, is the subdiscipline dedicated to investigations focusing on the relationship between cold climate nonglacial landforms and climate (Peltier, 1950). Climatic geomorphology was proposed as an extension of the Davisian cycle of erosion (Davis, 1909) in the mid-1900s (Peltier, 1950). The results of work pursued in the climatic geomorphology tradition outlined the climatic imprint on landscapes existing outside the latitudinal and altitudinal boundaries of temperate and humid conditions, such as periglacial regions (Caine, 1978).

Geographical periglacial geomorphology (GPG) is the research area focusing on the distribution, altitudinal zonation, and elevation trends of periglacial features and, as such, is a definitive example of climatic geomorphology (Caine, 1978). This line of research became popular in the German-language literature beginning in the mid-twentieth century, a trend that led to development of inventories of periglacial features and their relation to macro- and topoclimate, snowline, and Quaternary history over extensive regions, including Europe, North

Africa, South America, the Middle East, and the cordillera of western North America (Troll, 1944; Graf, 1973; Poser, 1977; Eckelmann, 1988). This trend in European literature provided quantitative support for the climatic interpretation of periglacial features and demonstrated that the altitudinal trends of many such features are similar to that of the climatic snowline (Karte, 1979).

Elaborations of the GPG conceptual framework defined the spatial distribution of periglacial landform assemblages or "form communities" (Poser, 1977) of periglacial features, which is characterized by the steady and consistent rise in elevation of periglacial features as one moves away from the poles and from maritime influences (Graf 1973; Poser, 1977; Karte, 1979; Nelson & Nyland 2017). More recently, the GPG concept has been embraced by periglacial studies asserting that periglacial assemblages give rise to erosional periglacial landscapes, rather than periglacial features simply having been superimposed on preexisting terrain (Queen & Nelson, 2022; Queen et al., 2024, submitted). The overall contributions of the GPG and climatic geomorphology include establishment of periglacial feature elevation trends over large areas, thus defining the climatic imprint on the landscape and providing quantitative support for the characterization of periglacial terrain.

Although the diffusion of the GPG research vein was central in advancing past and current understanding of periglacial conditions and landform development history, large areas remain "uncovered" with respect to geographical periglacial geomorphological analysis. One such region, the Appalachian Highlands of the eastern USA, contains an abundance of periglacial features (Merritts & Rahnis, 2022), but a systematic and integrated regional inventory and determination of altitudinal trends are largely absent, creating a substantial gap

in understanding of the origins and climatic affinities of hypothesized periglacial features in the region.

Following the model of GPG set forth by earlier works in the European literature (e.g., Troll, 1944; Graf, 1973; Poser, 1977), this chapter examines and relates the elevation trends of selected periglacial features to topography, paleoenvironmental reconstructions, permafrost occurrence, and climate observations along a transect from Maine to North Carolina. This examination is achieved through the hypothesis that relict periglacial landforms in the eastern USA follow well-defined altitudinal trends, increasing in elevation from north to south in response to increasing summer air temperature and decreased retention of warm-season snowpack.

The methodology and analysis applied in this chapter serve as a unifying theoretical underpinning for subsequent chapters in this dissertation, as the outcomes from this study provide substantial support for the utility of analyzing the spatial organization of periglacial terrain to discern the impact of past climate and geomorphic processes on the landscape. To that end, this study is the first of its kind to be conducted for the Appalachian Highlands and as such will help to clarify the origins of hypothesized periglacial features in the region. The results of this work will help to clarify the Quaternary history and extent of periglaciation in the eastern USA, will contribute to the ongoing worldwide inventory of periglacial features, and can be used to better understand how currently active periglacial landforms may be impacted by global climate change.

Methodology

The area examined here extends along a ~1400 km transect that includes the areas of the Appalachian Highlands between Maine to North Carolina (Walegur, 2001; Walegur & Nelson, 2003) (Figure 2). To support the central investigation of spatial trends in relict periglacial feature elevations in the Appalachian Highlands, periglacial features, their elevations, and latitudinal/longitudinal coordinates were tabulated. Review of literature resulted in 143 periglacial features for analysis. Climate data from a transect of climate stations on Appalachian summits were used to investigate the climatic interpretation of the tabulated periglacial features (Walegur, 2001). Examples from the European GPG literature feature graphical examples of spatial analysis involve plotting periglacial feature elevations against latitude (e.g., Graf 1973; Karte, 1979). Similar methodology is undertaken here to facilitate comparison between Appalachian topography and other regions previously subjected to such analysis, including Europe and the Cordillera of the western USA (e.g., Poser 1977; Eckelmann, 1988).

Periglacial features

Periglacial features used in this study were identified from a thorough review of the literature and are summarized in Table 1 (see Appendix for a complete enumeration). Numerous studies identifying relict periglacial features in the eastern USA exist (e.g., Merritts & Rahnis, 2022) but the present study only integrated data inputs from resources that provided the type of feature, the location, and elevation for areas in the Eastern USA and as such, data used here should not be considered to be an exhaustive list of periglacial features in the Appalachian Highlands. The altitudinal trends of some periglacial features such as blockfields

and cryoplanation terraces have been assessed (Nelson, 1989; Park Nelson et al., 2007) but simultaneous, integrated analysis of several periglacial features provides additional interpretative power in the spatial analysis of the elevation of periglacial feature types. Mean elevation was used for the cases in which feature elevations were reported in the literature as a range (e.g., Clark & Hedges, 1992). Some sources did not explicitly report elevations in the text but provided elevations graphically (Cremeens et al., 2005). In these cases, graphics from the text were used to derive coordinates and feature elevations. Additionally, some feature coordinates were reported using place names such as a town (Marsh, 1987). In these cases, the coordinates of the closest mentioned town were assigned to the periglacial feature elevation. The southernmost limit of LGM ice in the Appalachian Highlands is known to have occurred at approximately 41˚N (Braun, 2011) and alpine permafrost extended as far south as Georgia (French & Millar, 2004).

Climate data

Previous research establishing the elevations of the present-day and last glacial maximum 0˚C mean annual air temperature (MAAT) isotherms in the Appalachian Highlands was used here to investigate the climatic impact of feature development altitude (Walegur 2001; Walegur & Nelson, 2003; Park Nelson et al., 2007). The elevation of the present-day 0˚C MAAT was derived through calculation of lapse rates (Walegur, 2001), the constant rate at which temperature declines with height, also known as adiabatic cooling (Colman & Soden, 2021). Linear depictions of lapse rates appear in applied studies but local variations in topography, among other factors, can introduce deviations to constant adiabatic lapse rate of -6 to -7°C/km (Walegur & Nelson, 2003). To adjust for local conditions, Walegur (2001) used

data from climate monitoring at high-elevation Appalachian summits to calculate an adjusted lapse rate for the area of 0.94˚C for each degree of latitude for the 1500 km study transect employed in this study. (Walegur 2001; Walegur & Nelson, 2003). Each climate monitoring station, located close or atop site summits, included hourly air and ground surface temperature measurements as well as soil temperature measurements at 10, 25, and 50 cm (Walegur, 2001). LGM lapse rates were derived from paleoecological data from the Appalachian Highlands (Woodcock and Wells, 1990; also see Park Nelson et al., 2007). Descriptions of present-day and LGM data can be found in Walegur & Nelson (2003), and Park Nelson et al., (2007), respectively.

Previous research suggesting that a MAAT of 0°C to -1°C is required for permafrost to occur (Walegur & Nelson, 2003 and references therein). Although permafrost is not a diagnostic criterion for periglacial regions, many modern periglacial realms are affected by permafrost (Van Everdingen, 2005) and as such, the level of the 0°C MAAT was used here as an index by which to integrate climatic data into this study to infer the periglacial affinities of features of study (Park Nelson et al., 2007).

Table 1. Periglacial feature data inputs and source information. *See Appendix for more detail.*

Feature	Data source
relict sorted patterned ground	Delcourt & Delcourt (1988); Antevs (1932)
cryoplanation features	Clark & Hedges (1992); Antevs (1932)
blockfields & block deposits	Park Nelson et al., (2007)
block streams	Cremeens et al. (2005)
blocky deposits	Fame et al. (2024)
pingo scars	Marsh (1987)
embryonic rock glacier	Germain & Milot (2024)
0° MAAT Present day	Walegur & Nelson (2003)
0° MAAT Last Glacial Maximum	Park Nelson et al., (2007), Woodcock & Wells (1990)

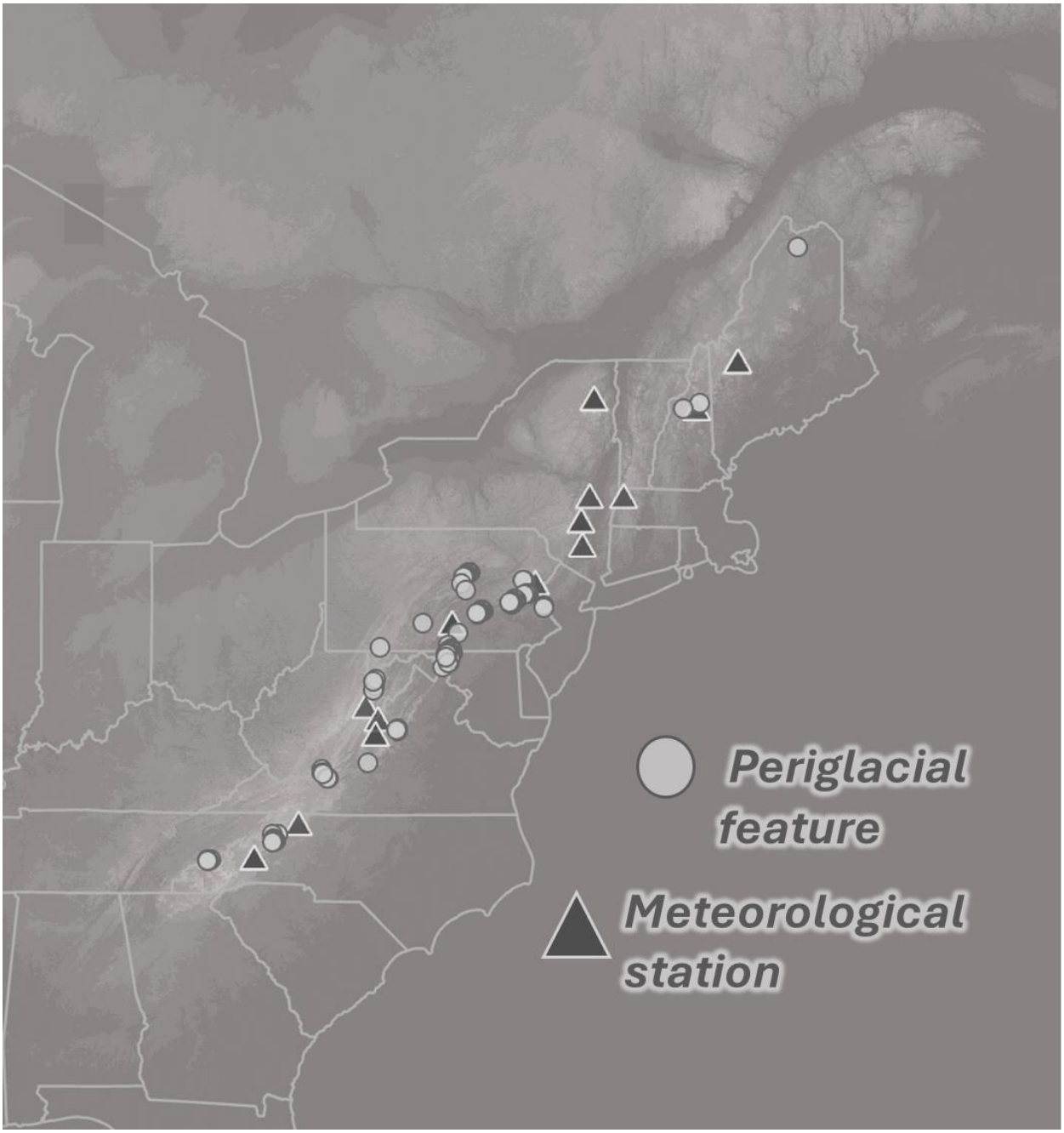

Figure 2. Periglacial feature locations in the Appalachian Highlands*. Lighter areas indicate higher elevations. Meteorological stations were established by Walegur (2001) and were used to calculate the elevation of the present-day 0˚C MAAT (Walegur & Nelson, 2003).*

Results

Elevational trends

Periglacial feature elevations and geographical position, along with the elevation of the present-day and LGM 0˚C MAAT are summarized in Figure 3. Triangles in Figure 3 indicate the location of climate stations whose data were used to derive the elevation of the present-day 0˚C MAAT, which were supported by the calculation of lapse rates (Walegur, 2001). The dotted line represents the study site transect, passing through each of the locations of the climate monitoring stations. The solid line in Figure 3 shows the elevation and latitude of the LGM 0˚C MAAT, which was determined graphically following data and results reported in Park Nelson et al., 2007.

Visual interpretation of this graphic indicates that the close association between periglacial feature elevations and the elevation of the LGM 0˚C MAAT, is in alignment with conclusions from the GPG literature–the elevation of periglacial features increases with decreases in latitude due to increases in mean annual and warmest month air temperatures (e.g., Graf 1973; Poser, 1977; Karte, 1979).

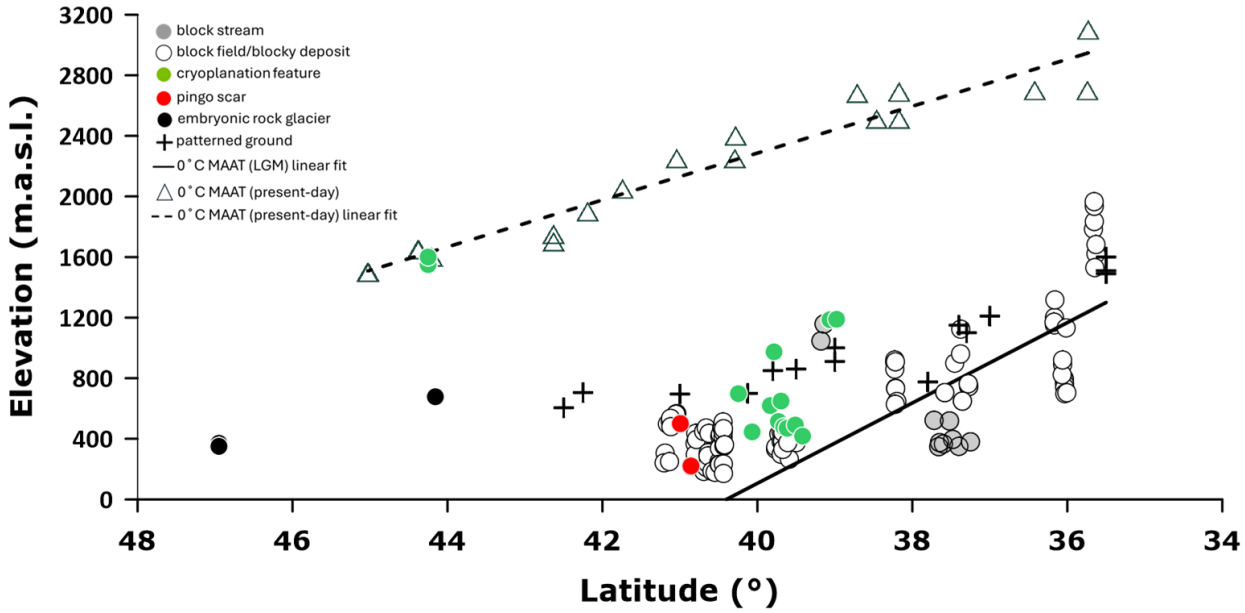

Figure 3. Periglacial feature elevations with respect to LGM and present-day climatic snowlines (0°C MAAT lines). *The LGM ice margin was at approximately 41˚N along this transect (Braun, 2011).*

Results from Figure 3 are indicative of the periglacial affinity of cryoplanation features, blockfields, and patterned ground, evidenced by the fact that many of the periglacial features reported here fall above the elevation of the LGM 0°C MAAT. Trends in elevations here indicate that periglacial features formed in areas above (i.e., cooler than 0˚C) the LGM 0°C MAAT that were affected by intense periglacial activity, and where permafrost was likely to have occurred (Walegur & Nelson, 2003; French & Millar, 2014). Further, the separation between the levels of the LGM and present-day 0°C MAAT lines highlights the fact that periglacial conditions no longer occur in this area and thus, periglacial features in the Appalachian Highlands are relict. This work is suggestive of the presence of an altitudinal zonation of periglacial features and strongly supports a periglacial interpretation for blockfields, sorted patterned ground, and cryoplanation features in the Appalachian Highlands.

Periglacial features below the LGM 0°C MAAT were seldom reported except for cases where site and feature-specific conditions explain the deviation. Regional work in the Appalachian region noting the occurrence of hurricanes and debris flow offers insight into the position of some periglacial features that fall below the elevation of the LGM 0°C MAAT line, such as the clustering of block streams at around 38˚N. Tropical storms, which affect the eastern U.S. are known to displace surface features, including man-made infrastructure, downslope under the influence of debris flows. Over fifty debris flows have been documented in the Appalachian region between 1844 and 1985 (Wieczorek & Morgan, 2008) and some events have been documented to have displaced material as much as 3.6 kilometers downslope (Wieczorek & Morgan, 2008). It is reasonable then to deduce that Pleistocene age periglacial features could have been displaced downslope because of contemporary weather events thus influencing the elevations trends related to LGM climate. In addition, block fields, which are linear accumulations of blocky material, form through emplacement via flow downslope (Ballantyne, 2018). Owing to their formation, block streams may be found downslope from the altitudinal position of original formation (Ballantyne, 2018).

Active rock glacier formation requires MAAT < -2˚C and as such, can be used in paleoclimate reconstruction. The embryonic rock glaciers included in this analysis are early-stage, relict, talus rock glaciers (Germain & Milot, 2024). These features are found downslope from a talus slope, which provides the frost-shattered rock required for rock glacier formation (Matthews et al., 2017; Uxa & Mida, 2017; Ballantyne, 2018, p. 242). The features identified in this study fall well above the LGM 0°C MAAT line, indicating that extremely cold conditions are associated with formation. This finding is in line with the conditions required for rock glacier

formation and their global distribution as actively forming rock glaciers are abundant in areas where MAAT < -6˚C (Ballantyne, 2018, p. 242.). Active rock glaciers are rare in areas where MAAT exceed -2˚C and a positive relationship exists between rock glacier activity and increasing elevation (Ballantyne, 2018, p. 242). The other periglacial features identified for this study tend to be associated with frequent freeze-thaw cycles (i.e., patterned ground, and nivation associated with cryoplanation terrace formation) (Nelson, 1979), and as such, it is expected that these features fall closer to the LGM 0°C MAAT where seasonal temperatures would have fluctuated more frequently about the freezing point of water.

Mt. Washington anomaly

Anomalous elevations of cryoplanation terraces at a high-elevation site on Mt. Washington (points near 44 degrees north, 1600 m.a.s.l) were encountered (Figure 3). The explanation for this site's departure from the elevation trend is related to both this mountain's topographic prominence and the glacial history of the region. Cold-based ice covered the high-elevation periglacial features at the Mt. Washington site and other peaks in northern New England (Bierman et al., 2015). The reduced erosive capacity of cold-based ice, combined with rapid thinning of ice near the summit, could be responsible for the preservation of periglacial features in the upper reaches of Mt. Washington. Fowler (2010) and Fowler et al. (2012) described a "sharply defined boundary" at ~1585 m.a.s.l. on Mt. Washington, below which evidence of glacial erosion is abundant. Above this level, however, evidence of glaciation is scant. Well-preserved periglacial features, including large-diameter sorted patterned ground, turf-banked terraces, and blockfields, are present (Antevs 1932). Also present in the mountain's

upper reaches are large “lawns, benches, spurs, and tablelands,” which Antevs (1932, p. 70) attributed to frost action and noted their similarity to cryoplanation (goletz) terraces in Siberia.

Further evidence for the preservation of periglacial landforms from the upper reaches of Mt. Washington is offered by radiocarbon dates showing that the Mt. Washington summit area was covered by glaciers during and after the LGM (Koester et al., 2021). More than 20 surface exposure dates from Mt. Washington show that clast surface exposures increase in age with increasing elevation, suggesting that the upper areas of Mt. Washington were covered by very cold ice until 18 ka (Koester et al., 2021). The cold-based ice in this region could not erode underlying material, thus preserving the cryoplanation features, patterned ground, solifluction terraces, and glacial erratics observed on Mt. Washington. At lower elevations, LGM ice would have eroded any periglacial features. To this end, Mt. Washington represents an important locality for studying the interplay between periglacial and glacial activity during the LGM, as this site demonstrates the elevation of the upper limit of the Alpine periglacial zone in this region (Antevs, 1932, Dobiński, 2024).

Conclusion

Despite its widespread use in European periglacial literature, geographical periglacial geomorphology has not achieved extensive recognition or use in Anglo-American periglacial literature. This study represents the first systematic and integrated regional inventory and determination of the altitudinal trends of periglacial features in the Appalachian Highlands of North America, a region in which periglacial features are widespread. This gap in our collective knowledge has severely limited the application of periglacial studies to paleoenvironmental reconstruction. This problem has been particularly acute in the central and southern

Appalachians because glacial cirques do not exist south of the Laurentide Ice Sheet border (see Berkland & Raymond, 1973; McKeon et al., 1974) and so periglacial landforms provide one of the few lines of evidence that can be used to construct potential LGM snowline position over the Appalachian Highlands.

The results of this work focusing on the spatial distributions and elevations of relict periglacial features in the Appalachian Highlands show that most of the periglacial features reported here fall above the elevation of the LGM 0°C MAAT, indicating the periglacial affinity of the features. The separation between the levels of the LGM and present-day 0^{o}C MAAT explains the relict nature of periglacial features that exist in the Appalachian region—the periglacial climate required for formation no longer exists.

This work is also suggestive of the presence of a rough altitudinal zonation of periglacial features, which is in line with findings from other works employing this methodology (Eckelmann, 1988; Karte, 1979; Troll, 1944). The departures from this trend observed at Mt. Washington represent the effects of different styles of glacial coverage (Koester et al., 2021). Other site-specific deviations indicate the potential impacts of weather event debris flows displacing relict periglacial features downslope from the position of their formation (Wieczorek & Morgan, 2008). Results from this work inform broader paleoclimatic reconstructions of the eastern USA by outlining the direct relationship between elevation and periglacial features, lending support for the periglacial interpretation of otherwise enigmatic features such as blockfields.

Future work should focus on the insertion of more data points derived from literature sources, which would help facilitate the development of periglacial zonation in the Appalachian

Highlands. At a more local scale, an exhaustive inventory on Mt. Washington would further elucidate the interplay of glacial and periglacial processes. Additional efforts may focus on the use of LiDAR-derived elevation models to verify and characterize relict periglacial features in the Appalachian Highlands, as LiDAR data can penetrate the thick forest cover covering much of the Appalachian region.

CHAPTER 3. PERIGLACIAL FACIES ANALYSIS OF CRYOPLANATED TERRAIN

Introduction

The term “periglacial,” coined by Polish geologist Walery von Łoziński (von Łoziński, 1909), was initially applied to describe the cold but non-glacial environments adjacent to Pleistocene glacial margins, i.e., the “periglacial zone” (von Łoziński, 1912). More specifically, von Łoziński attributed periglacial processes, e.g., frost weathering, to the mechanical disintegration of sandstones in the southern Carpathian Mountains of Europe (French, 2017). “Periglacial” is still used today but is less restrictive as it is applied generally to describe the “conditions, processes, and landforms associated with cold, nonglacial environments” (Van Everdingen, 2005), the definition having since dropped the qualifier of proximity to a glacial margin (e.g., Washburn, 1980).

Elaborating on periglacial terminology, von Łoziński introduced the concept of “periglacial facies” to describe the rock-rubble deposits formed through frost weathering and freeze-thaw that he observed in the Carpathian Mountains (French, 2017). Today, these so-called periglacial facies have been re-imagined, describing the mountain-top detritus occurring on upland slopes in areas that escaped glaciation (French, 2017). Modern-day periglacial facies have been described as expansive angular block deposits (block fields) that are observable components of the periglacial landscape and are attributable to periglacial processes (Dobiński, 2024). The periglacial facies concept has been used recently in studies describing periglacial assemblages comprised of micro and meso-scale features working in unison to modify and preserve landscape-scale features (Brunnschweiler & Nelson, 2022; Queen et al., 2024, submitted). This line of work, employing geomorphometric analysis of remotely sensed imagery

in addition to field-based measurements, emphasizes a faceted environment of which periglacial facies comprise the principal components of upland periglacial landscapes (Brunnschweiler & Nelson, 2022) (Figure 4).

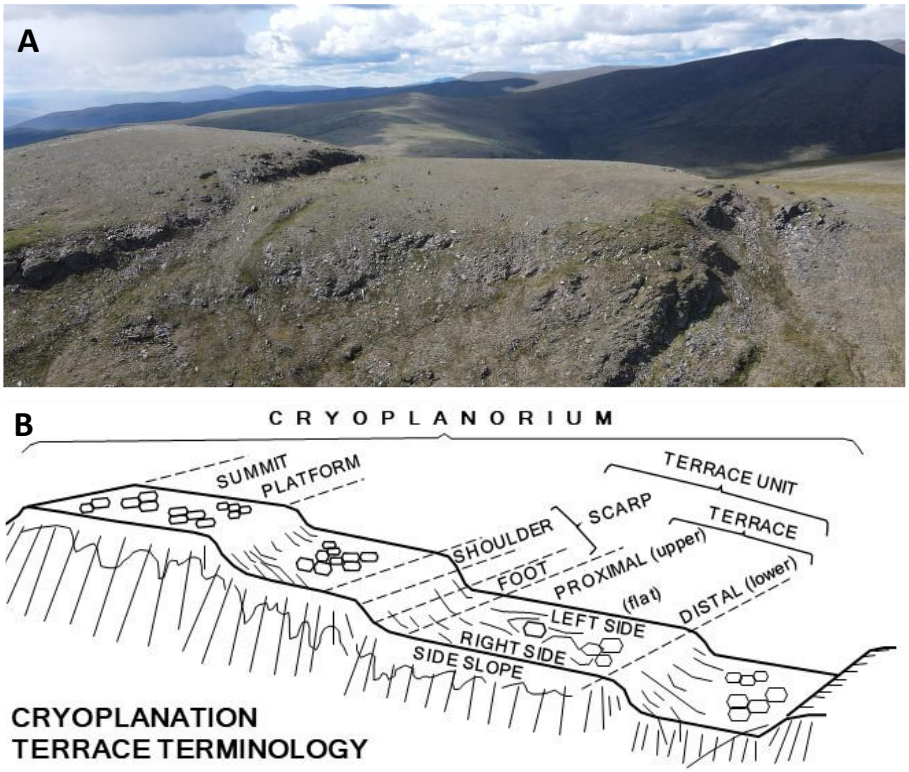

Figure 4. Periglacial facies in Alaska and schematic of cryoplanation facets. *(A) Cryoplanation terrace unit in the interior of Alaska, photo taken via drone by V. Tolmanov, July 2023. (B) Diagrammatical schematic of the "cryoplanorium" (altiplanorium), a group of cryoplanation/altiplanation terraces arranged in a descending series along ridge crests (Brunnnschweiller & Nelson, 2022; Nyland et al. 2024).*

Cryoplanation terraces (CTs) are large bedrock features carved into ridges and hillslopes and are prominent in cold regions that were not glaciated during the Pleistocene (Reger, 1975; Ballantyne, 2018, p. 220) (Figure 4) and as such, they are considered foundational components of characteristic periglacial terrain (Queen et al. 2021; Queen and Nelson 2022; Nyland et al., 2024; Queen et al. submitted). CTs consist of alternating gently sloping treads (generally < 12°) and steep (> 20°) rubble-covered, or exposed bedrock scarps (Demek 1969; Reger 1975). Well-

developed CTs achieve landscape-scale dimensions, with sequences of terraces spanning several kilometers of ridgeline (Demek, 1969; Reger and Péwé, 1976; Priestnitz, 1988; Nelson and Nyland, 2017; Ballantyne, 2018, pp. 220-222)

CTs encountered in active periglacial realms (e.g., eastern Beringia) feature mountain- and ridge-top detritus-mantled surfaces that have previously been characterized based on facets, of which the scarp, tread, upper side slope, and lower side slopes are the primary components (Brunnschweiler & Nelson, 2022; Nyland et al., 2024). The origin and development of CTs remained largely under-investigated and formation mechanisms were poorly constrained until recently (Ballantyne, 2018; Matthews et al., 2019; Nyland & Nelson, 2019, 2020; Nyland et al., 2020; Mitchell et al., 2023). Studies employing quantitative field-based methodologies, remote sensing, and absolute dating of these landscape-scale features have improved understanding of CT formation, which today is largely recognized as the geomorphic culmination of a periglacial process-suite known as nivation (Matthews et al., 2019; Nyland & Nelson, 2019; Nyland et al., 2024).

Periglacial-focused studies have contributed to the Quaternary science literature for ~120 years, revealing the multiple processes and landforms associated with cold climates (Merritts & Rahnis, 2022). Since the introduction of periglacial/periglacial facies terminology, there has been a rise in criticism to the effect that periglacial landscapes, as von Łoziński imagined them, do not exist under the present climate conditions (e.g., French, 2016). Despite the history of the research area and despite the close association between periglacial facies and characteristic periglacial landscape modification processes (i.e., frost weathering and freeze-thaw action), few contemporary periglacial studies feature the periglacial facies concept. This

research deficit leaves the periglacial facies concept underdeveloped, and the existence of modern periglacial regions open to criticism.

This chapter addresses the spatial distribution and organization of periglacial facies to test the hypothesis that CTs are composed of facets reflective of periglacial processes and depositional environments. Existing literature maintains that landscape-scale CTs serve as evidence for long-term periglaciation (Nelson & Nyland, 2017; Nyland et al., 2020; Queen and Nelson, 2022) and as such, are opportune locales for testing and applying facies analysis. The work builds on qualitative investigations by Queen et al., (2024, submitted) and Nyland et al. (2024). Findings from this study will help to investigate the central claim of critics about the concept of "characteristic periglacial terrain," i.e., that periglacial processes are not capable of generating characteristic erosional topography and, therefore, that truly periglacial upland landscapes are rare or nonexistent under modern climate conditions (French, 2016). Findings from this study are particularly relevant given that although permafrost is not a diagnostic criterion of periglacial environments, all environments with permafrost are periglacial (Van Everdingen, 2005; Merritts & Rahnis, 2022). Permafrost is designated as a Climate Change Indicator (U.S. E.P.A., 2016; Murton, 2021) and efforts to better constrain periglacial landscape dynamics will inform the present and future trends in global permafrost distribution.

Background

Sedimentological facies

The term "facies" describes a "body of sediment or rock with specified characteristics, namely colour, bedding, geometry, texture, fossils, sedimentary structures and types of external contacts" (Hambrey, 1994, p. 15). The facies concept is a principle of sedimentology

and was coined in 1838 by Gressly, a Swiss geologist, to describe the lateral changes of strata in the Jura Mountains of central Europe (Jones, 2015) whereby “facies changes” could be characterized based on sedimentary type, grain size, color, texture, and sedimentary structures and fossils (Jones, 2015, p. 3). Derivatives of sedimentological facies include subfacies, which are used to distinguish the aspect of rock or sediment being studied. Examples of subfacies include lithofacies (facies based on sediment characteristics) and biofacies, which are based on fossil content (Jones, 2015).

Traditionally, the facies concept has been applied when interpreting vertical exposures whereby facies transitions represent lateral changes in the environment (Jones, 2015) which then represent the successional change of the environment. As such, facies analysis is particularly relevant in paleoclimatic reconstructions. In cold regions, “cryofacies” are defined based on volumetric ice content and crystal size (Van Everdingen, 2005). Specifically, the facies concept may serve as a useful model for the design of field experiments (Madole, 1972; Olyphant, 1985).

The areal distribution of facies has been described in the cryosphere literature, establishing a link between the traditional conceptualization of lithofacies and the periglacial facies concept proposed by von Łoziński (Madole, 1972; Olyphant, 1985). Madole (1972) identified Neoglacial facies, a series of surficial deposits representative of discrete depositional environments in the Colorado Front Range. Using spatial analysis, Madole (1972) characterized the glacial facies linking the deposits to the microclimatology of the area. Later, Morris & Olyphant (1990), working on alpine lithofacies in the southern Rocky Mountains, both formalized and tested a conceptual model of facies deposition and asserted that facies

distribution in their study area was governed by local and regional-scale controls and that facets were distinguishable based on field-based data.

Madole (1972), advocating for the proliferation of periglacial facies as a conceptual guide in field research, stated that for complex rubble and block deposits typical of periglacial environments, the facies concept can help to clarify the process associations of an otherwise "chaotic mass of contemporaneous rock rubble". Further, Madole (1972) proposed that in deciphering paleoenvironments, geologic history may be interpreted through the horizontal distribution of facies, an assertion rooted in the notion that facies occur in the same succession both horizontally and vertically (Madole, 1972). A concluding summary by Madole (1972) underlined the utility of facies analysis in Quaternary science: "Because of the relationship between climate, landform, and type of deposit, these facies may be of even broader use as indicators of topoclimate and related processes, both past and present."

Periglacial facies

von Łoziński introduced the concept of periglacial facies, which are characteristic deposits, such as blockfields and sorted patterned ground, found where periglacial processes are dominant (von Łoziński, 1909; Martini et al., 2011). Initially von Łoziński used periglacial facies as a blanket term to refer to the angular rubble mantling upland periglacial realms and as such, the interpretation of this term generally emphasizes the occurrence of the exposed lateral distributions of blocky mantling. Having employed the root "facies" in his terminology, von Łoziński's concept, largely applied to describe the lateral positioning of deposits, seems to be at odds with the traditional application of facies in sedimentology and stratigraphy where "facies" is typically applied to describe vertical changes in a sedimentological profile, even though

Gressly's facies terminology precedes von Łoziński's (Boggs, 2006). This gap is possibly attributable to a language barrier.

French (2017), offering commentary on von Łoziński's periglacial facies concept, connected the lateral deposit terminology to the disintegration of bedrock in periglacial environments. More specifically, French (2017) likened von Łoziński's periglacial facies to "mountain-top detritus ('blockfields')" (French, 2017, p. 3) writing "The landscape response is the angular rubble accumulations that veneer many upland surfaces" (French, 2017, p. 197). The concluding sentiment in French's writing stresses that the interpretation of mountain-top detritus is presently unclear but that such deposits are formed under prolonged periglacial conditions through freeze-thaw action (French, 2017).

Few periglacial-focused studies acknowledge the periglacial facies concept despite the vast amounts of work aimed at the investigation of mountain-top detritus and other periglacial block deposits (cf., Ballantyne, 2018). von Łoziński's initial description of periglacial facies and French's later extension of the concept are both underpinned by the operation of periglacial processes and efficacy in modifying surface exposures (von Łoziński, 1912; French, 2017) and as such, the periglacial facies concept is illustrative of characteristic periglacial processes and terrain.

A faceted periglacial environment

More recently, Brunnschweiler & Nelson (2022) described a faceted geomorphic environment, now termed the "cryoplanorium" (a group of cryoplanation terraces arranged in a descending series along ridge crests), whose surfaces are comprised of slope facets (scarps, treads, upper and lower side slopes). This construction is consistent with the occurrence and

formation of assemblages of periglacial features (Queen et al., 2024, submitted) and aisreminiscent of the periglacial facies described by Lozinski (1909). Faceted periglacial environments described in the literature bear striking resemblance to the horizontal facies described by Madole (1972) and later Olyphant (1985). Despite these research threads characterizing the occurrence of horizontal facies, and emphasizing their utility in paleoenvironmental reconstruction, few studies integrating the periglacial facies concept exist.

Scrutiny of periglacial landscape evolution

A central question facing the field of periglacial geomorphology as it applies to both active and relict environments was summarized by Brunnschweiler (Brunnschweiler & Nelson 2022) who in 1965 asked, “To what extent is the surface configuration of Alaska determined by climatic influences and through what agents and processes are the latter manifesting themselves?”. This question is exemplified in a statement by Madole (1972), who indicated that regarding the use of facies for paleoclimate reconstruction, central themes of the work must include identifying the occurrence of facies and determining why these facies exist. Both lines of inquiry echo one another in their calls for improvement in understanding of the relationships between periglacial processes, climate, and long-term landscape evolution. Studies that use the spatial distribution of facies to discern past climates in a periglacial context exist (e.g., Bryant, 1983), but overall, utilization of the facies concept is scarce in the periglacial literature. This research gap has invited criticism of periglacial landscape models due to the lack of quantitative characterization of periglacial terrain (French, 2016). This research deficit is highlighted in the statement by the distinguished periglacial geomorphologist, Hugh French, who near the end of

his career, seemingly critical of the periglacial concept altogether stated, “There is a lack of models of periglacial landscape evolution” (French, 2016).

Models of periglacial landscape evolution are not well constrained and recent studies call into question the existence of characteristic periglacial terrain (French, 2016). Facies analysis has been used to link depositional characteristics to climate and geomorphological processes (Madole, 1972) and has the potential to clarify models of periglacial landscape evolution, but such analyses remain unstandardized in terms of sampling and have rarely been employed in a periglacial geomorphology research context. Exceptions are the works of Bovis (1978), Bovis and Thorn (1981) in the Colorado Front Range and Millar (2006) in the same general area of interior Alaska as the present study. The dearth of methodology aimed at quantifying periglacial facies in modern-day periglacial environments has contributed to the lack of standardized methodologies for field-based measurements in periglacial literature (Madole, 1972).

The work presented here represents an exploratory study focused on applying field-based and remotely sensed data to quantify the hypothesized periglacial facies comprising periglacial uplands of the Alaskan interior. Relative weathering indices, clast macrofabric, and remotely sensed imagery are used to evaluate the central hypothesis: cryoplanation terrace unit surfaces are comprised of distinguishable facies related to depositional microenvironments on slope facets (scarps, treads, upper and lower side slopes) and that sedimentological relative weathering indices employed show statistically significant differences corresponding to those facies.

Study Area

A cryoplanation terrace near Eagle Summit, Alaska (65.48°, -145.47°, 1136.599 m.a.s.l.) was chosen for analysis. North Eagle Summit (NES) is the site name chosen to specify the study location, as the site lies just north of the Eagle Summit Wayside, accessible by the Steese Highway. NES lies within the Yukon-Tanana Upland section of the Northern Plateaus physiographic province (Figure 5), a mountainous region spanning ~77,000 km^2 between the Yukon and Tanana Rivers in eastern Beringia (Wahrhaftig, 1965; Foster et al., 1973). The Yukon-Tanana Upland is underlain discontinuously by permafrost (Jorgenson et al., 2008) and upland areas are subject to periglacial mass-wasting processes (Wahrhaftig, 1965).

The Eagle Summit area remained unglaciated throughout the Pleistocene except for isolated alpine glaciers (Péwé et al., 1967). Glaciation of the area is referred to locally as the Eagle and Salcha glacial episodes (Weber, 1986). The primary components of the NES CT, the tread and scarp, comprise an area of ~12,500 m^2. The NES CT terrace tread is oriented due north and is cut into a ~2.5 km long, northwest-southeast trending ridge (Figure 5). The bedrock at this site has been mapped as Devonian and older quartzite and pelitic schist (Foster et al., 1994). Surface clasts are predominantly quartzite, schistose quartzite, and quartz-mica schist (Wilson et al., 2015).

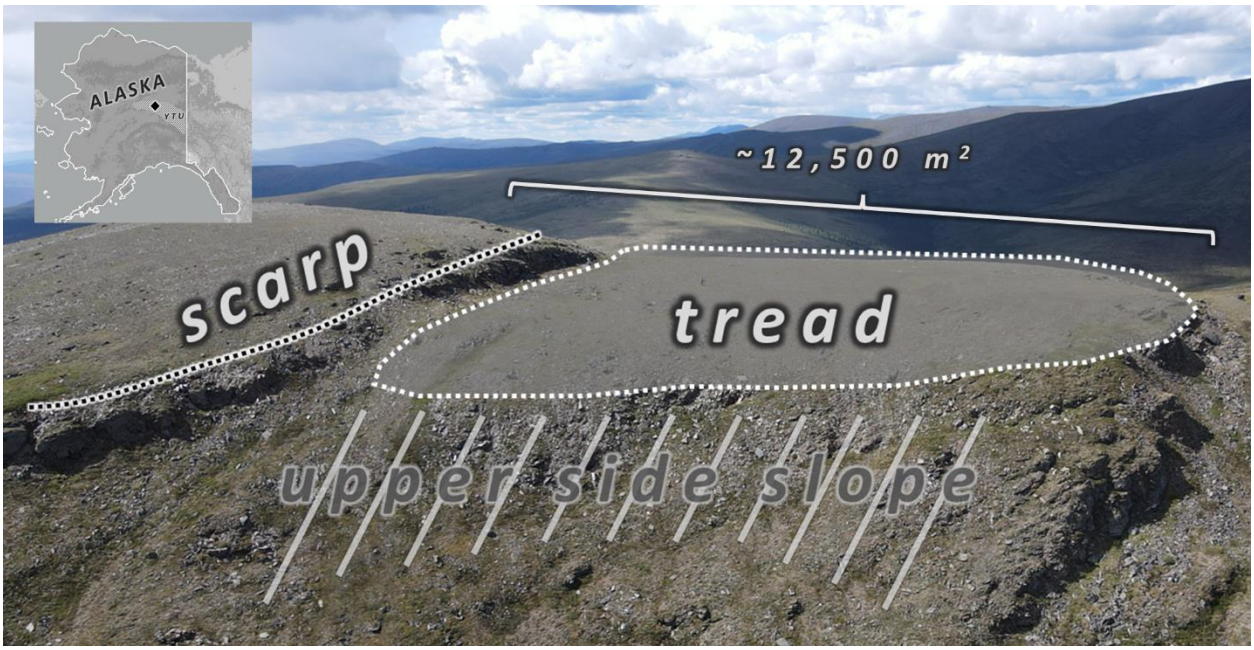

Figure 5. North Eagle Summit cryoplanation terrace unit with primary components labeled. *Inset map with the approximate outline of the Yukon Tanana Upland (YTU) physiographic section.*

The CT unit analyzed was chosen based on suitability for measurement of sedimentological relative weathering indices, road access, and work that had been previously conducted in the area (e.g., Reger, 1975; Nelson, 1985; Millar, 2005; Nyland & Nelson, 2019). The United States Department of Agriculture maintains a Snow Telemetry (SNOTEL)[1] station located ~150 meters from the Eagle Summit wayside. Records obtained from this station (2000-2023) show that the mean annual air temperature at Eagle Summit is ~-6˚ Celsius. Eagle Summit is classified as a Dcf (continental, no dry season, with very cold winters) climate type (Kottek et al., 2006).

[1] Eagle Summit SNOTEL Site, Site no. 960: https://wcc.sc.egov.usda.gov/nwcc/site?sitenum=960

Methodology

The periglacial facies concept was used to guide the sampling strategy implemented at the NES site. The primary facet components analyzed here include CT tread, scarp, and upper side slope, following the classification from Brunnschweiler & Nelson (2022). Relative weathering indices derived from clast volume, in addition to clast rebound (hardness), and clast long axis macrofabrics were sampled from locations across the NES CT.

Sampling design

A subsampling approach (Stewart, 2014) involving stratified sampling was used here to capture continuous dynamics related to clast weathering across the CT tread (Figure 6) (Dixon & Leach, 1976; Lohr, 1999). The subsampling technique allows the analyst to assess spatial variability at various scales, which is particularly important given the aim of this study to evaluate the hypothesis that CTs represent a faceted environment of which the specific scale of the facets is unconstrained. Stratified sampling has been applied in the Earth sciences to estimate the spatial distribution of physical phenomenon (Dobesch et al., 2013; e.g., Fagan & Nelson, 2017) and is a valuable sampling approach as it ensures coverage of the study area and is simple to implement (Dixon & Leach, 1976; Fagan & Nelson, 2017).

Grid sampling

The first component of the sampling strategy included establishing 35 sample sites organized into a regular grid of five 154 m long north-south oriented transects, each with seven sampling locations at 22 m intervals. Grid orientation irrespective of CT facet (Figure 6) was determined based on previous work in the area establishing the time-transgressive nature of CT surfaces, which are characterized by increased weathering from the scarp-tread junction near

the base of the scarp toward the distal end of the scarp (Nyland & Nelson, 2019). Relative weathering data from 10 clasts were collected from each of the sampling nodes. The availability of clasts necessitated a search radius of one to two m about each sampling node. Sample site distance intervals fall on the higher end of acceptable resolution provided in the literature (Lohr, 1999) and were largely guided by the number of available clasts in any given area and on the variable length of the CT tread.

Facet sampling

It is a well-known shortcoming of systematic sampling that periodicities can be missed if physical phenomena occur over distances smaller than the chosen grid interval (Fagan & Nelson, 2017). A second sampling strategy involved intensive sampling of relative weathering indices and clast macrofabric from locations at each facet component and was established to address the potential shortcoming of grid sample frequency (Figure 6). Facet sample sites were nested within the gridded sample locations and center on the hypothesized CT facets, the tread, scarp, and upper side slope. Sites at each facet were established at regular intervals of 10 m. Twenty-five clasts were measured from each of the sampling locations within the CT facets, which included six sites from the scarp and upper side slope, and four sites from the tread component.

Methods to determine adequate sample sizes include implementation of the sample size equation (Dixon & Leach, 1976; Lohr, 1999; Thompson, 2012, p. 54). Data collection generated a sample size n = 750, which is within the bounds needed to ensure accuracy of up to 90% confidence and was determined to be sufficient for the purposes of this study.

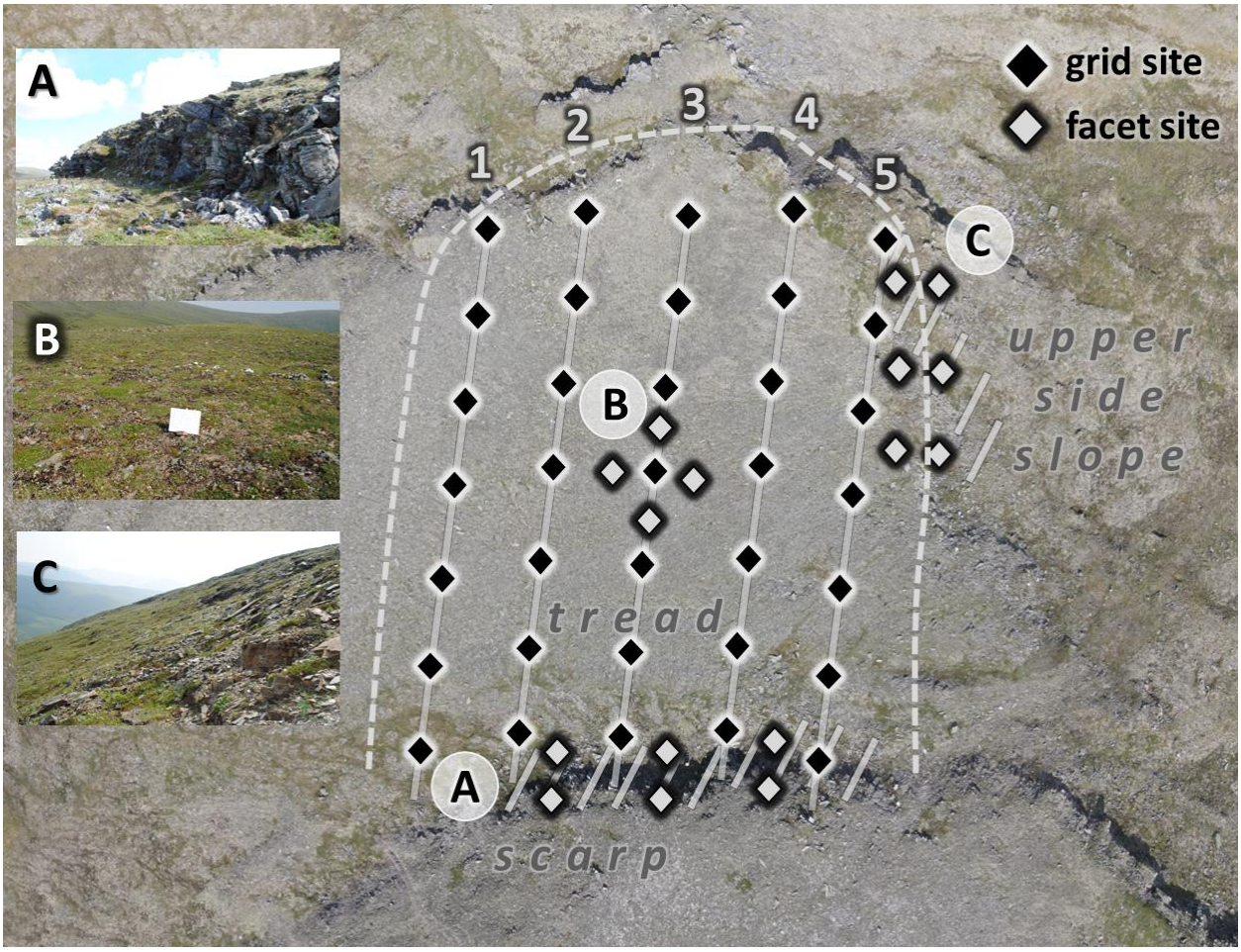

Figure 6. Grid and facet sampling locations and on-the-ground characteristics. *Grid sampling locations are denoted with black diamonds. Facet sampling locations are denoted with a light gray diamond. Sampling transect lines are labeled. The long axis of the tread component is approximately 110 m.*

Field data

Sedimentological relative-weathering indices were collected to capture characteristics of the hypothesized periglacial facies supported by cryoplanation terrace surfaces. Relative weathering indices have been employed in geomorphological research to determine the sedimentological characteristics of surfaces and to infer processes related to feature formation (King & Buckley, 1968; Barrett, 1980; Benn & Ballantyne, 1993; Evans & Benn, 2014). Relative weathering indices have been studied at other areas near the NES site (Nyland & Nelson, 2019)

and as such, analyses of these indices support the comparison between NES and work outside bounds of the present study area.

Shape indices

In periglacial contexts, Krumbein sphericity (Table 2) (Krumbein, 1941), and Cailleux flatness (Cailleux, 1947) have been used to infer the origin and formation of CTs and have been effective in establishing the time-transgressive nature of CT surfaces (Nyland & Nelson, 2019). Although it has been found that flatness and sphericity are inversely correlated (King, 1966) both indices were collected to facilitate comparison between other periglacial studies (Nyland & Nelson, 2019). Clast shape calculations, based on clast volume (Figure 7), were computed following equations outline in Table 2.

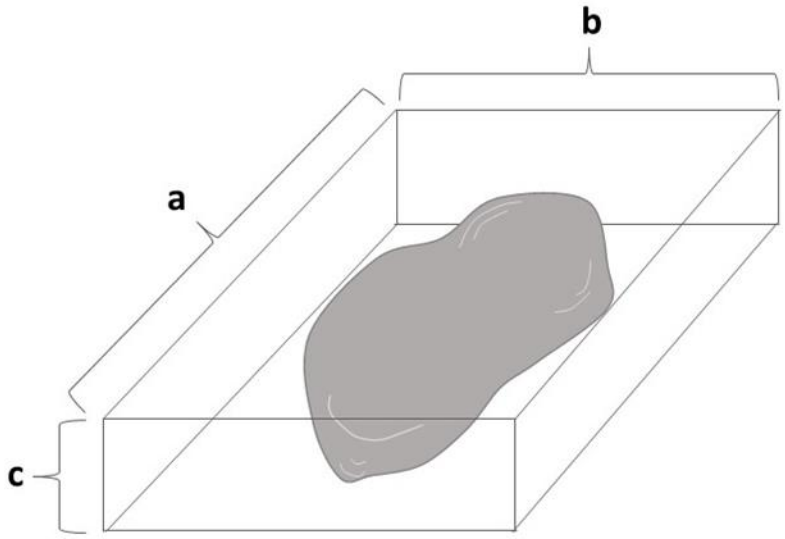

Figure 7. Idealized diagram of clast axes, labeled. *Schematic after (Wedo, 2005).*

Table 2. Relative weathering indices, their descriptions, and relevant equations. *Where "a", "b", and "c", represent the long, intermediate, and short clast axes, respectively.*

Index		Description	Equation
Volume		measure of the disintegration of clasts	$a * b * c$
Rebound (hardness)		measure of clast strength where significant differences among the same lithology can be used to indicate differences in weathering	--
Fabric		the 2D or 3D orientation of a clast in space, used to determine flow behavior in sedimentary environments	--
	azimuth	clast direction with respect to a 360°compass dial where north is 0°, east is 90°, etc.	--
	dip	the angle between a horizontal plane and inclination of clast long axis	--
Cailleux Flatness		shape index where values > 100 indicate increasingly flatter clasts	$1000\left(\frac{a+b}{2c}\right)$
Krumbein Sphericity		shape index that indicates clast similarity to a sphere on scale of 0 - 1 where 1 represents a perfect sphere	$\sqrt[3]{\frac{bc}{a^2}}$

Rebound

Rebound, collected using an N-type Schmidt hammer[2], is a measure of the degree of rock compressional strength (Goudie, 2006). Clast rebound has been used by geomorphologists since the 1960s to indicate relative weathering in clasts of the same lithology where significant differences indicate differences in weathering (Sumner et al., 2002; Goudie, 2006). Following guidelines in the Schmidt Hammer manual and previous research application of clast rebound

[2] Humboldt Concrete Rebound Hammer (https://www.humboldtmfg.com/humboldt-concrete-rebound-hammer.html) model number H-2987H. Humboldt Construction Materials Testing Equipment, Humboldt Scientific Service Center 2525 Atlantic Ave., Raleigh, NC 27604.

(Ballantyne et al., 1989; Nyland & Nelson, 2019) the average of five rebound measurements taken for each clast was used for analysis.

Clast macrofabric

To augment relative weathering indices, clast macrofabric, the two or three-dimensional orientation of a clast in space used to determine the behavior of flows and mass movement in sedimentary environments (Evans & Benn, 2014), was employed to characterize the depositional history of the hypothesized CT facets. Clast macrofabric analysis has been applied in the geomorphic literature, yielding valuable information about paleo depositional environments (Millar, 1995, 2005; Evans & Benn, 2014;). Macrofabrics obtained from periglacial deposits have been cited displaying some of the strongest fabrics among those analyzed from other colluvium (e.g., natural debris flows) even in cases where relict macrofabrics were sampled (Mills, 1990). Clast macrofabrics (clast azimuth and dip) were measured in-situ using a standard Brunton compass[3] (Evans & Benn, 2014). Together, relative weathering indices and clast macrofabics are used to reveal sedimentary characteristics of the CT surface and as quantitative input to test the hypothesis that CTs are comprised of facets discernable by their sedimentological characteristics.

Remotely sensed data

A DJI Mavic Air 2 drone[4] captured imagery of the NES site, including sampling locations to cover a total area of ~0.133 km^2. Aerial image processing was performed using Pix4Dmapper

[3] Standard Transit Brunton Compass: https://www.brunton.com/products/standard-transit.

[4] DJI Mavic Air 2 Drone. https://store.dji.com/product/mavic-air-2?vid=91071.

software[5] to generate; 1) a digital surface model, a georeferenced array of elevation data, and 2) an orthomosaic, which is an orthorectified image mosaic (Hengl & Reuter, 2008). A total of 644 images were used to generate the output rasters, which achieved a spatial resolution of 1.83 cm. The spatial resolution of the output rasters was achieved using at least five images of overlap and was deemed acceptable here given that the average sampled clast is larger than the spatial resolution of the remotely sensed data and because the analysis conducted in this study relies on relative clast locations as opposed to absolute locations. Sample location coordinates were recorded, and site locations were marked using flagging tape so that sites could be identified in the orthomosaic raster.

Analytical methods

Pairwise comparison of CT facets

The Kruskal-Wallis test is a nonparametric alternative to analysis of variance (Kruskal & Wallis, 1952) and was performed using SPSS statistical software[6] to test the hypothesis that there are statistically significant differences in relative weathering indices between the three slope facets: scarp, upper side slope, and tread. Groups with significant differences were treated with the Dunn test, a non-parametric multiple pairwise post hoc procedure (Dunn, 1961). Site-by-site tests of normality indicate non-normal data across all relative weathering indices, necessitating the use of a nonparametric comparison method. Box plots summarizing relative weathering data for each facet were generated to accompany statistical analysis.

[5] PIX4Dmapper version 4.7.5 software. https://support.pix4d.com/hc/en-us/categories/360001503192

[6] IBM SPSS Software Version 29.0.2.0. https://www.ibm.com/products/spss-statistics

Clast macrofabric analysis

Clast macrofabrics were visualized using lower hemisphere equal-area (Schmidt) net projections, in which each data point (azimuth and dip) is the graphical representation of the intersection of the azimuth and dip values for each clast (Millar & Nelson, 2001; Evans & Benn, 2014). The Exponential Kamb contouring method was used to aid the visual interpretations of the Schmidt nets; these were generated using two standard deviation units, highlighting any statistically significant point clusters (Kamb, 1959; Vollmer, 1995; Cardozo & Allmendinger, 2013; Evans & Benn, 2014). Graphics were generated using InnStereo software[7]. Presently there is no quantitative basis by which to determine sample sizes for fabric studies (Evans & Benn, 2014) although examples in the literature typically employ samples between 25-50 (Nelson, 1982b; Mills, 1990; Millar & Nelson, 2001). This study uses sample sizes on the lower end of those published in the literature owing to the limited number of clasts available for sampling in the grid system, although similar sample sizes on relict periglacial colluvium have been reported in the literature (cf. Mills, 1990).

Statistical analysis of the three-dimensional macrofabric data included application of Bingham's U test statistic (Bingham, 1974; Mardia 1975) to all fabric samples collected. Testing was performed in Microsoft Excel following Bingham's U (Equation 1). Bingham's U test was used to test for fabric departures from uniformity and indicate statistically significant fabric shapes indicative of past flow direction. The test statistic requires that each fabric sample be resolved to three orthogonal, normalized eigenvectors representing the primary axes of data

[7] InnStero Stereographic projections for structural geology: https://innstereo.github.io/.

clustering, and thus the shape of clast macrofabrics (Woodcock, 1977) To facilitate shape comparison across sample sites and between fabrics from outside studies, Woodcock plots depicting the natural log ratios of the three principal eigenvalues were generated (Woodcock, 1977). Woodcock plots were used here to facilitate quick interpretation of fabric shape and to support the visual interpretation of periglacial fabrics.

The Bingham U statistic is given by:

$$U = \frac{15}{2}\sum_{i=1}^{3}\left(\overline{\tau}_i - \frac{1}{3}\right)^2 \quad (1)$$

Where $\overline{\tau}_i$ refers to the normalized eigenvalues.

Surface visualization

The NES CT represents a continuous surface and trends in relative weathering indices potentially indicative of depositional and weathering histories remain under investigated. Physical phenomena may not be delimited by discrete boundaries and as such, the visual and analytical interpretation of their distributions may be supported by spatial models to predict distributions in unsampled locations (Mitáš & Mitášová, 1999). Remotely sensed imagery and surface elevation models were used as data inputs to support the generation of prediction surfaces representing the field data collected: volume, sphericity, rebound, and flatness. Sampling locations and the associated relative weathering indices were compiled digitally into tabular format and both raster surfaces (orthomosaic and digital surface model) and the tabular field data were imported into ArcGIS Pro software[8]. ArcGIS mapping software supports the use

[8] ArcGIS Pro Software version 3.2.1. https://www.esri.com/en-us/arcgis/products/arcgis-pro/overview.

of surface interpolation methods including the spline technique, which estimates values based on a mathematical function that both minimizes the curvature of the surface (smoothing) and passes through the input data points while estimating unsampled locations by fitting a mathematical function to a specified number of nearest input points (Franke, 1982; Mitáš & Mitášová, 1988). The result is a smooth, continuous raster surface.

Results

Relative weathering indices

Gridded relative weathering data are plotted by line with increasing distance from the scarp towards the distal end of the tread to reveal trends in indices along the CT unit (Figure 8). Reference imagery for site locations referenced in this section is provided in Figure 9.

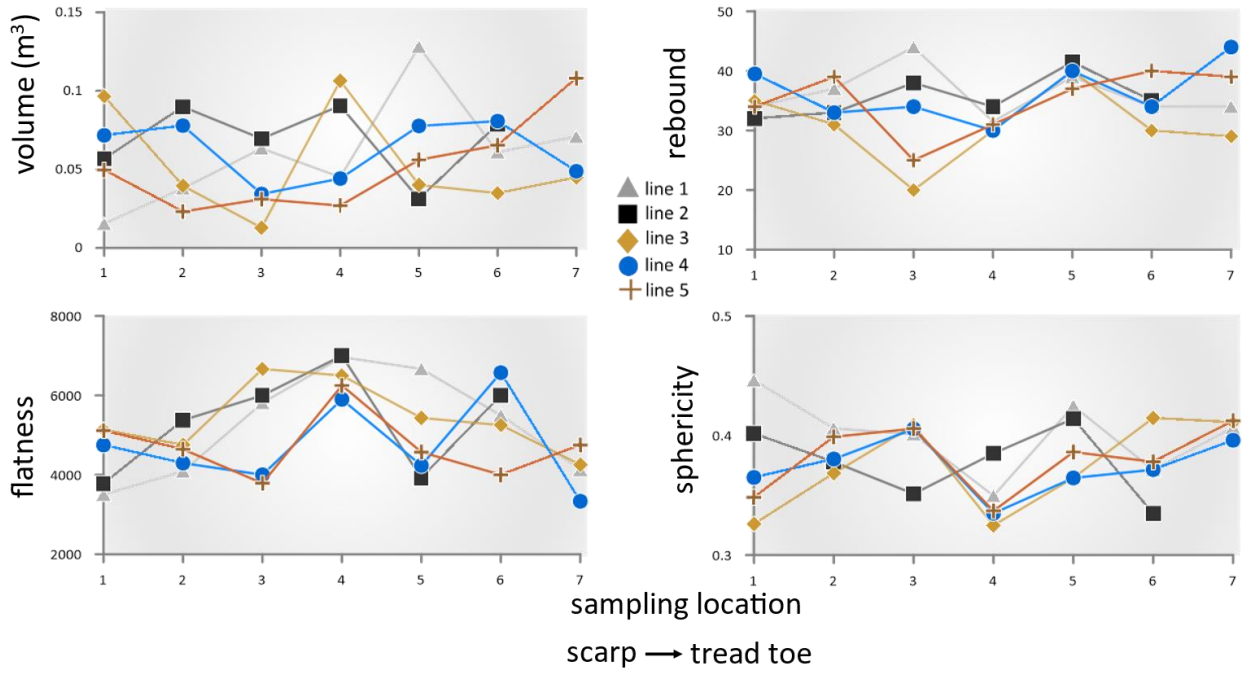

Figure 8. Relative weathering indices plotted with distance from the scarp by transect. *Specific values for each line are indicated by the legend in the center of the figure*.

This graphical organization is supported by findings from a recent study confirming increases in weathering with distance from the CT scarp tread junction (Nyland & Nelson, 2019). Based on the rectangular nature of the sampling grid, Lines 1 and 2 do not cover as much of the scarp component as lines three-five and as such, similarities in relative weathering indices observed in Lines 1 and 2 reflect the aerial coverage of these two lines, which captures the area near the junction of the base of the scarp and the tread, the upper side slope of the western side of the CT unit, and the scarp area of the subsequent CT unit downslope from the primary study area. Lines 3-5 cover the scarp, tread, and eastern upper side slope facets in addition to the scarp area of the adjacent downslope CT unit. Variations between the sampling transects, especially those observed between Lines 1 and 2, versus Lines 3-5 indicated lateral differences in relative weathering in addition to non-linear trends in weathering observed with distance from the scarp.

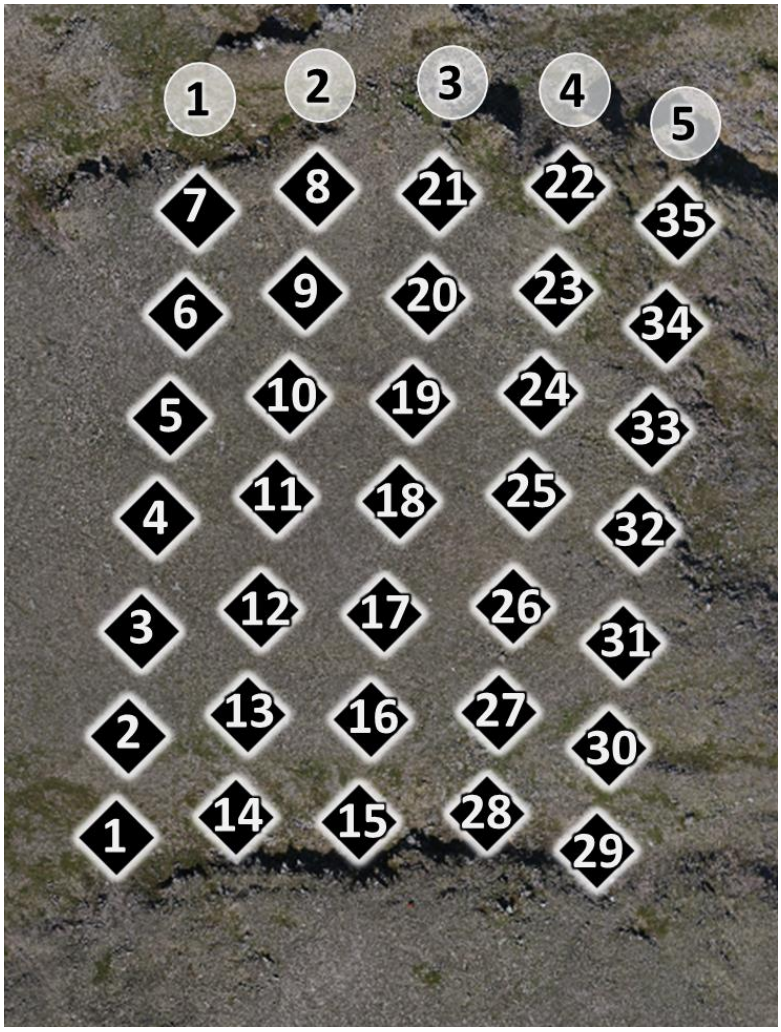

Figure 9. Sample site locations with transects labeled.

Volume

The overall volume of a clast can be used as a measure to indicate the disintegration of clasts via periglacial weathering processes as the disintegration of clasts into smaller fragments is an artifact of physical and chemical weathering (Eppes & Keanini, 2017). Clast disintegration under freeze-thaw cycles is a well-known phenomenon in periglacial regions, where repeated freeze-thaw action can result in the production of angular rocky deposits (Ballantyne, 2018, p. 170; Deprez et al., 2020). Lines 1 and 2 show a volume peak near sample Site 3, which lies at the base of the CT scarp tread junction (Figure 8). Volume then continues to increase near Site

5 through Sites 6 and 7. Peaks in volume near Site 5 occur only in Line 1; this trend is interpreted as indicating the upper side-slope facet where there are observably larger clasts. Near Sites 6 and 7, volume increases represent the area where the subsequent CT scarp is encountered. Overall volume trends are characterized by larger clasts near the scarp base, which is what is expected as frost-riven clasts are liberated from the bedrock, smaller clasts in the tread facet representing extended periods of clasts weathering, and finally, clast volume increases near Sites 6 and 7 near the subjacent scarp, and less clast weathering is encountered.

Lines 3-5 all show strikingly similar patterns in clast volume although these patterns differ from those observed in Lines 1 and 2. In Lines 3-5, which comprise the entire scarp, tread, upper side slope, and subsequent CT scarp components volume trends show decreases from Sites 1-3, which is to be expected as clast weathering increases with distance from the scarp facet. Like Lines 1 and 2, volume then increases towards Sites 5-7 as the next scarp facet is encountered. Line 5 volume trends show a strong signal representative of the upper side slope facet, as indicated by larger relative volumes compared to those observed in Lines 3 and 4. All sample transects show clasts decreasing in size from the scarp toward the toe of the tread. Volume only increases again due to the impact of upper side slope or scarp facet, which comprises the subsequent CT unit.

Flatness and sphericity

Decreases in clast flatness have been used to indicate increased clast weathering (Evans & Benn, 2014). Sphericity, a closely related measure, has been shown to indicate weathering, with higher sphericity values indicating more weathered clasts (Evans & Benn, 2014). Lines 1-3 showed increases in clast flatness with distance from the scarp. Although this trend is at odds

with the hypothesis of increases in clast weathering across the CT tread, a similar result was found in a previous study (Nyland & Nelson, 2019) and in this case, may still indicate clast weathering. Frost shattering is the dominant weathering mechanism at this upland site and as such, platy, highly fractured clasts expressed as flat fragments would be expected. Lines 4 and 5 have patterns differing from those in Lines 1-3 and show that clasts near the scarp and upper side slope are less flat than those encountered at the tread. This is expected as the scarp and upper side slope components are morphologically similar and represent areas of less weathering compared to the tread, where clasts have been exposed to frost shattering processes for longer and as such, are flatter. Sphericity patterns align with flatness patterns, which is to be expected given the inverse relationship between the two indices (King, 1966). Sphericity values indicate that clasts from the scarps and upper side slope tend to be more spherical compared to those encountered on the tread.

Rebound

Rebound patterns, as with the other relative weathering indices show that Lines 1 and 2 display similar patterns while Lines 3-5 show strikingly similar patterns. Lines 1and 2 have almost identical patterns in rebound trends, which show that from the base of the scarp toward the tread toe, rebound values increase subtly. Clast rebound then decreases at sites near the tread and continues to decrease towards the distal end of the tread. Lines 3-5 show almost identical patterns in which rebound decreases from Sites 1 through 3, then steadily increases from Sites 4 through 7. A similar result in rebound with distance from the scarp base was observed by Nyland & Nelson (2019) where increases in rebound occurred with distance from the scarp. At Eagle Summit, weathering in the dominant lithology, quartz-mica schists, results in

clasts near the tread and tread toe being composed primarily of quartz as these minerals weather out last. Quartz is the hardest of the minerals encountered at the NES site and as such, increases in clast rebound may indicate longer exposure to weathering (Goudie, 2006; Nyland & Nelson, 2019)

Identifiable trends in indices from the scarp toward the distal end of the CT tread show increases in weathering from the scarp to the middle of the tread, followed by indications of reduced clast weathering near the scarp of the subjacent CT unit. This trend highlights the primary components of the CT surface, the scarp and tread, which are easily identified by the compilation of relative weathering indices. Clast weathering tends to be less at scarp components relative to the tread components. Grid data including the upper side slope of the CT unit show good agreement with data obtained from the center of the CT unit, indicating that the time-transgressive process formation operates across the entire CT unit.

Facet pairwise comparison

The results of the pairwise comparison of CT components derived from subsampling near facet areas show significant differences in relative weathering between the three facets (Figure 10). Major findings from this analysis indicate that clast rebound differed between the treads and the scarp and upper side slope components (Table 3). Volume differed across all indices, while no statistically significant differences in clast sphericity were achieved. Pairwise comparison of facets indicates that although some differences in clast weathering were achieved, distinguishable characteristics may be difficult to detect on smaller spatial scales as compared to the larger spatial scale captured by the grid sampling which indicated dynamic surface trends in the relative weathering indices employed in this study.

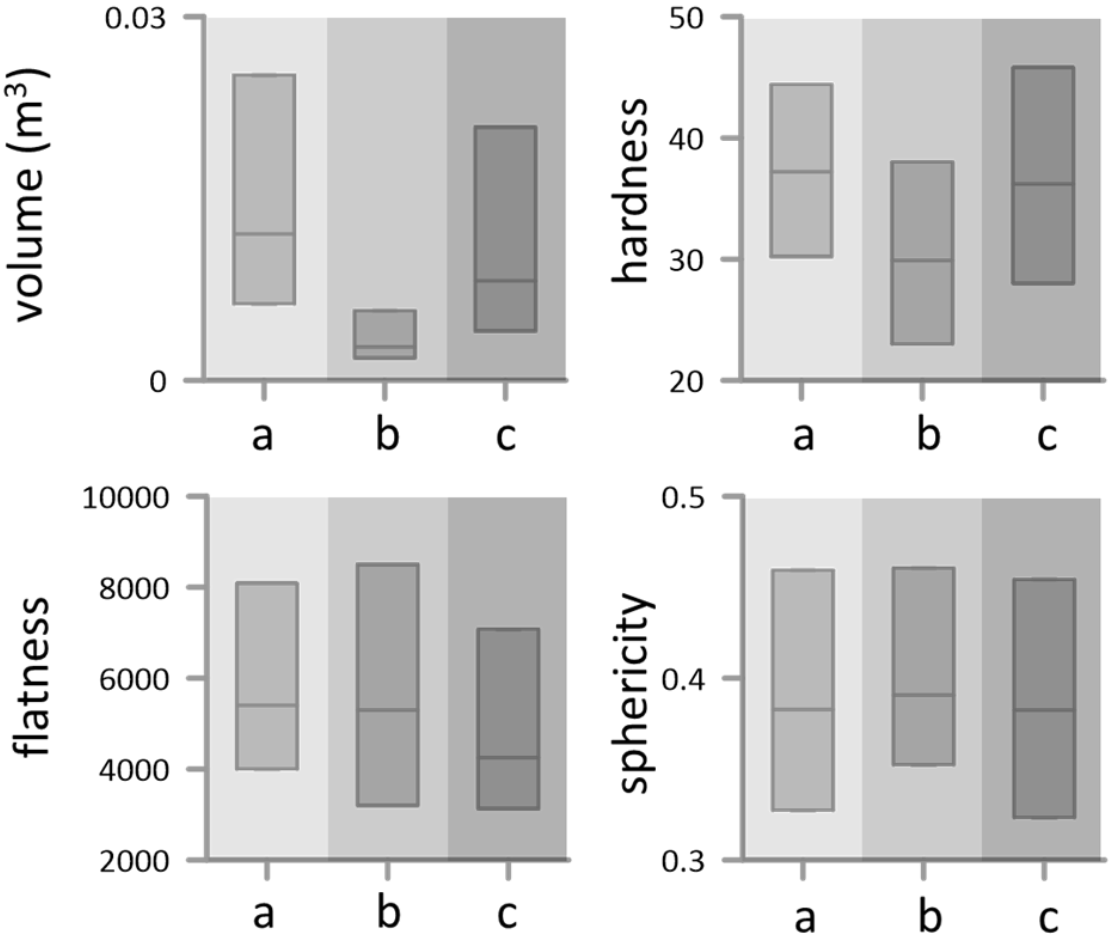

Figure 10. Relative weathering box plots of index values. *Box plot upper and lower limits reflect confidence intervals about the median center line. On the x-axis, (a) scarp, (b) tread, (c) upper side slope.*

Table 3. Output of Kruskal-Wallis and Dunn pairwise comparison of facet data. *Tested results are reported at the 0.05 significance level.*

Site Comparison	Test Statistic	Significance	Reject/Fail to H_o[†]
Volume			
Tread – Upper side slope	21.4	<.001	Reject
Tread- Scarp	57.0	<.001	Reject
Upper side slope - Scarp	9.63	.002	Reject
Flatness			
Tread – Upper side slope	4.96	.026	Reject
Tread- Scarp	.048	.827	Fail to reject
Upper side slope - Scarp	6.84	.009	Reject
Rebound			
Tread – Upper side slope	5.46	.019	Reject
Tread- Scarp	6.66	.010	Reject
Upper side slope - Scarp	.549	.459	Fail to reject
Sphericity			
Tread – Upper side slope	.008	.930	Fail to reject
Tread- Scarp	2.61	.106	Fail to reject
Upper side slope - Scarp	2.16	.142	Fail to reject

Relative weathering prediction surfaces

Spatial interpolation techniques can be generated and used to interpret and assess the spatial variability of physical data (Franke, 1982; Dobesch et al., 2013). Spline interpolation implemented in ArcGIS was used to visualize relative weathering indices and to compare patterns observed in each index across the CT surface that may be difficult to detect based on the plotting of data values on an x and y-axis alone. The interpolated predicted surfaces (Figure 11) show that near the tread, relative weathering indices show that clasts are softer, flatter, smaller, and less spherical.

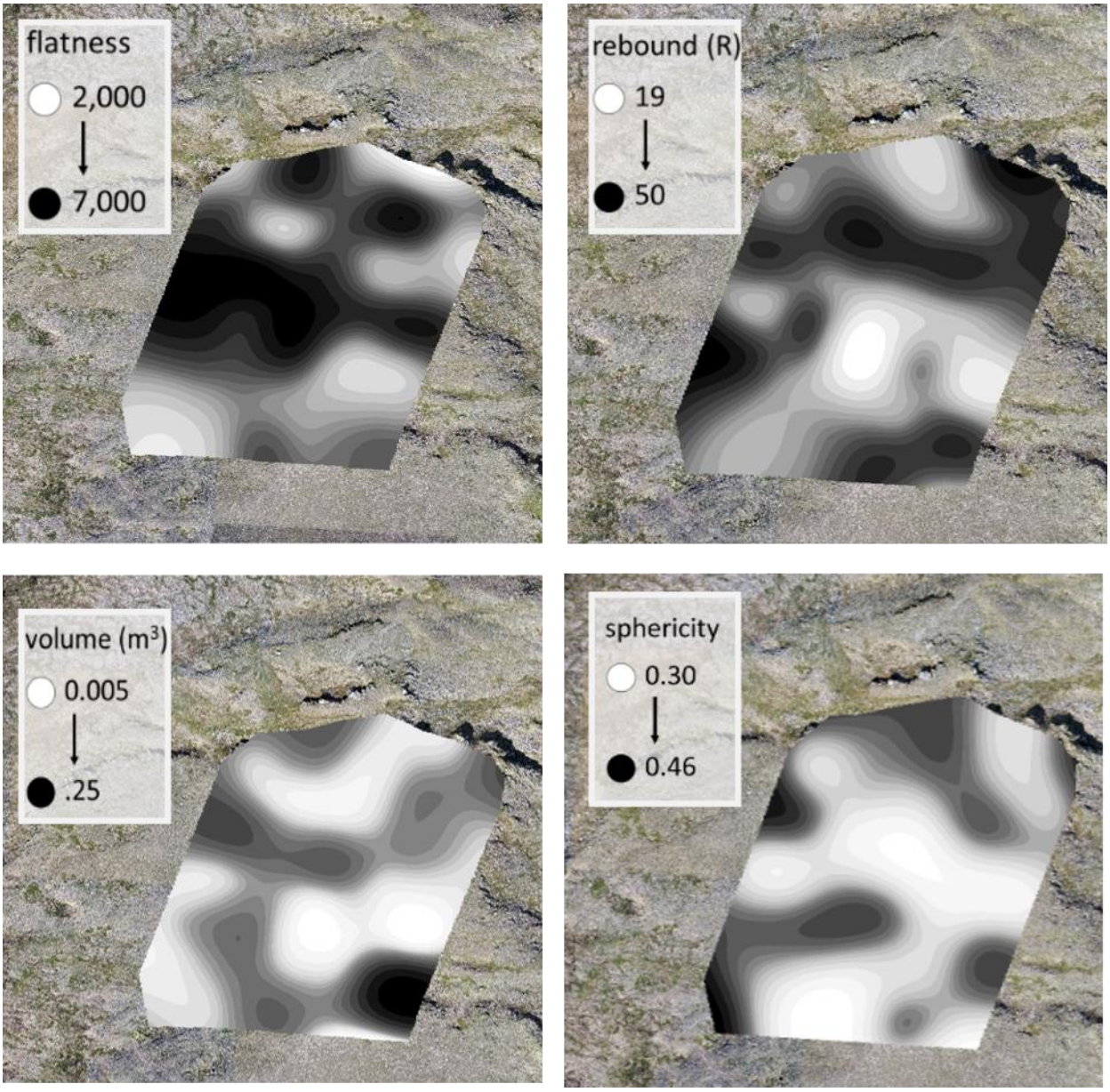

Figure 11. Relative weathering indices prediction surfaces. *Raster surfaces showing relative weathering indices. Input data derived from gridded sampling data. Surfaces were generated using ArcGIS Pro software using the spline interpolation tool.*

Clast macrofabric

Clast macrofabric data from the grid and facet sampling procedures are summarized graphically using Schmidt Net projections (Figure 12). Bingham's U uniformity testing output is summarized in Tables 4 and 5. A Woodcock log-ratio plot summarizing fabric shape is shown in Figure 16. Clast macrofabrics are generally described in terms of girdle, cluster, or isotropic shapes (Evans & Benn, 2014). Clusters appear as isolated, dense groupings of data points that may be bipolar, whereas girdles appear as point distributions distributed around the perimeter of the Schmidt net, or as uniaxial girdles appearing as narrow strips spanning the diameter of the net (Woodcock, 1977).

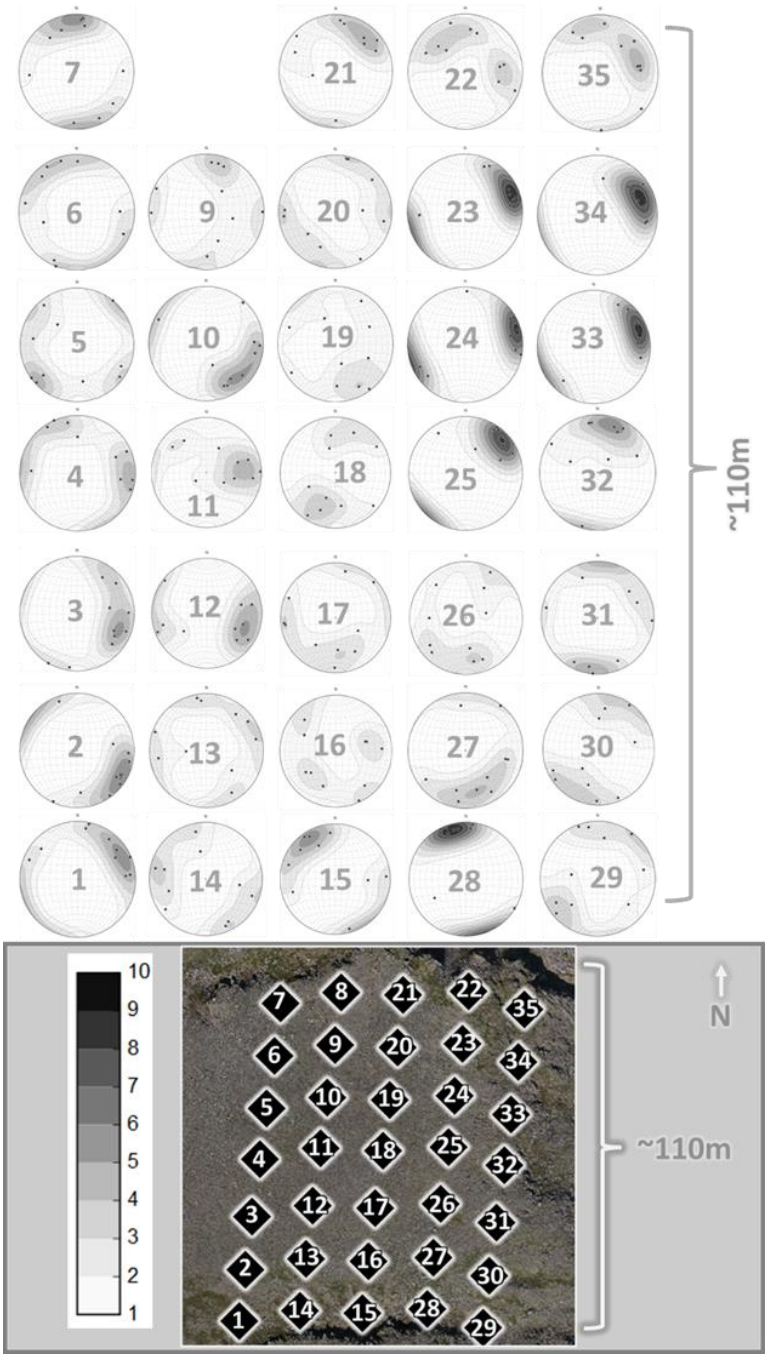

Figure 12. Grid sample equal area Schmidt Nets. *Clast three-dimensional data are plotted on Lambert Equal-Area projections*[9]*. Schmidt net contours were generated using the exponential Kamb method (Kamb, 1959; Vollmer, 1995) and were plotted at 2σ intervals. All net contour intervals are standardized and are depicted by the legend in the lower left corner of the graphic.*

[9] *Macrofabric output was derived using InnStero 4 plotting software Beta 6.* https://innstereo.github.io/.

Table 4. Eigenvalue and Bingham's U test statistic outputs for gridded sampling data tested at the 0.01 significance level. *Site 8 did not have sufficient clasts for sampling and is excluded here.*

Site	Line	$\bar{\tau}3$	$\bar{\tau}2$	$\bar{\tau}1$	Bingham's U	Reject/fail to reject H_0
1	1	0.66	0.315	0.025	1.52	Reject
2	1	0.69	0.265	0.045	1.61	Reject
3	1	0.619	0.351	0.03	1.30	Reject
4	1	0.619	0.351	0.03	1.30	Reject
5	1	0.508	0.381	0.111	0.62	Fail to reject
6	1	0.552	0.368	0.08	0.85	Fail to reject
7	1	0.653	0.267	0.081	1.28	Reject
9	2	0.446	0.395	0.16	0.35	Fail to reject
10	2	0.687	0.254	0.06	1.55	Reject
11	2	0.579	0.318	0.103	0.85	Fail to reject
12	2	0.68	0.236	0.084	1.44	Reject
13	2	0.456	0.384	0.16	0.36	Fail to reject
14	2	0.544	0.286	0.17	0.55	Fail to reject
15	3	0.658	0.254	0.088	1.29	Reject
16	3	0.428	0.343	0.229	0.15	Fail to reject
17	3	0.483	0.395	0.121	0.53	Fail to reject
18	3	0.536	0.283	0.181	0.50	Fail to reject
19	3	0.457	0.329	0.213	0.22	Fail to reject
20	3	0.526	0.337	0.136	0.57	Fail to reject
21	3	0.573	0.308	0.119	0.78	Fail to reject
22	4	0.51	0.421	0.068	0.82	Fail to reject
23	4	0.854	0.114	0.032	3.08	Reject
24	4	0.815	0.147	0.038	2.65	Reject
25	4	0.799	0.14	0.061	2.46	Reject
26	4	0.497	0.263	0.241	0.30	Fail to reject
27	4	0.59	0.338	0.072	1.01	Reject
28	4	0.812	0.158	0.03	2.64	Reject
29	5	0.528	0.311	0.161	0.51	Fail to reject
30	5	0.599	0.203	0.198	0.79	Fail to reject
31	5	0.572	0.356	0.072	0.94	Reject
32	5	0.652	0.228	0.121	1.18	Reject
33	5	0.847	0.126	0.027	3.01	Reject
34	5	0.853	0.129	0.019	3.08	Reject
35	5	0.545	0.416	0.04	1.03	Reject

Grid macrofabrics and statistical output

Macrofabrics summarized by site in Figure 12 show that clast orientation near the scarp and upper side slope facets tend toward strong bipolar point cluster shapes and that the

orientation of these point clusters align with the orientation of the local slope. Conversely, fabrics obtained from the tread show girdle shapes. These fabric characteristics show that fabrics align with local slope, which is greatest at the scarp and upper side slope facets. Previous work on periglacial fabrics established that bipolar fabrics aligning with the local slope support the interpretation that fabrics may be linked to transportation and depositional processes (Nelson, 1985). Previous work on large CT treads noted that although CT treads appear flat, they are slightly convex and as such, periglacial mass movement processes operating on surfaces underlain by permafrost would accentuate the movement of clasts along tread facet surfaces.

The eigenvalue method of fabric analysis has been used in geomorphology to relate macrofabric shape to depositional environments and/or mass movement processes (Mills, 1990). Bingham's U statistic (Table 4) shows that fabrics obtained from near the scarp and upper side slope components display significant departures from uniformity while samples obtained from the tread tend towards uniformity. In the context of depositional processes, significant departures from uniformity can be interpreted as indicating past depositional environments (Bingham, 1974). Conversely, insignificant fabrics may indicate the slowing of clast movement across the CT surface, which is much flatter in the tread area. Fabrics derived from the tread may be displaying the impacts of lateral frost thrusting, which arises from compressional stresses associated with freeze thaw action (Goldthwait, 1976). A similar result was found in fabric analyses of sorted stripes and sorted circles showing how lateral frost thrusting resulted in relaxed clast orientations relative to fabric derived from other periglacial surfaces. (Nelson 1982a, 1982b). Fabric analysis shows good agreement with the relative

weathering trends observed, which show observable and statistical differences based on location on the CT surface. These results support the assertation that the NES CT surface is comprised of a faceted environment and that facets are recognizable based on relative weathering indices and differences in clast macrofabrics.

Facet macrofabrics and statistical output

The results of facet sampling macro fabric data and resulting Bingham's U test statistical output are shown in Figures 13-15 and Table 5, respectively.

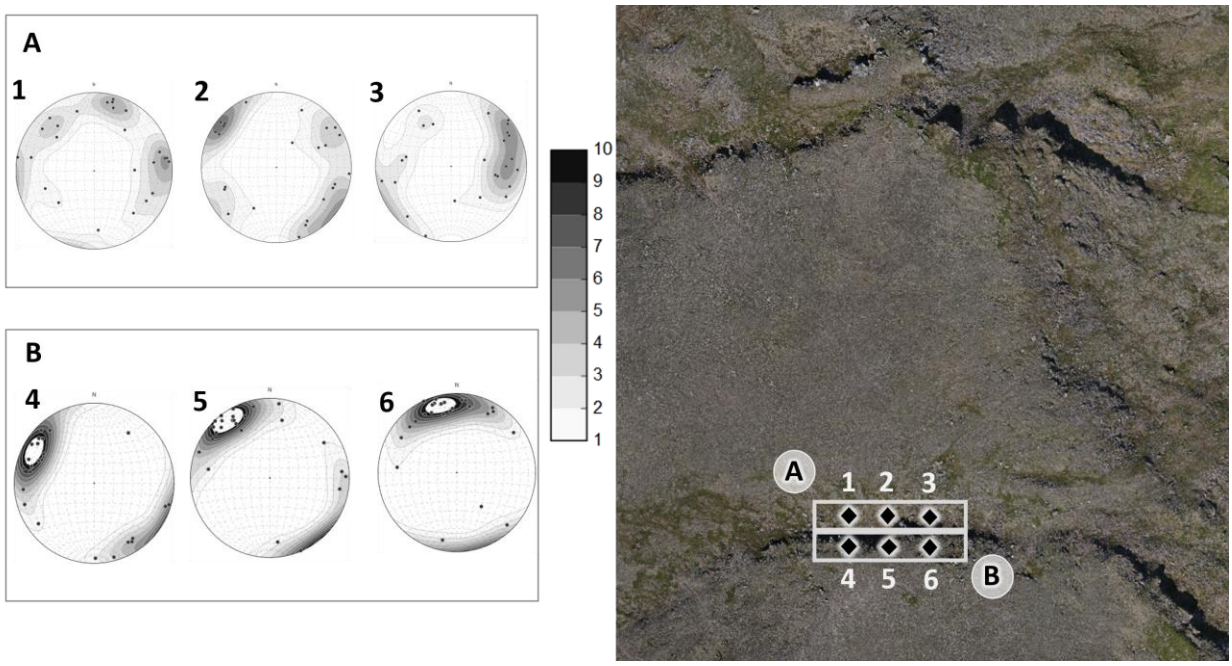

Figure 13. Scarp facet macrofabric Schmidt Net. *(A) Macrofabrics sampled from the base of the scarp and (B) from the upper area of the scarp. Note the strong orientation of fabric from areas at the top of the scarp versus the more chaotic fabrics sampled from the base of the scarp. Bright white areas of the Schmidt nets indicate clusters of n>10.*

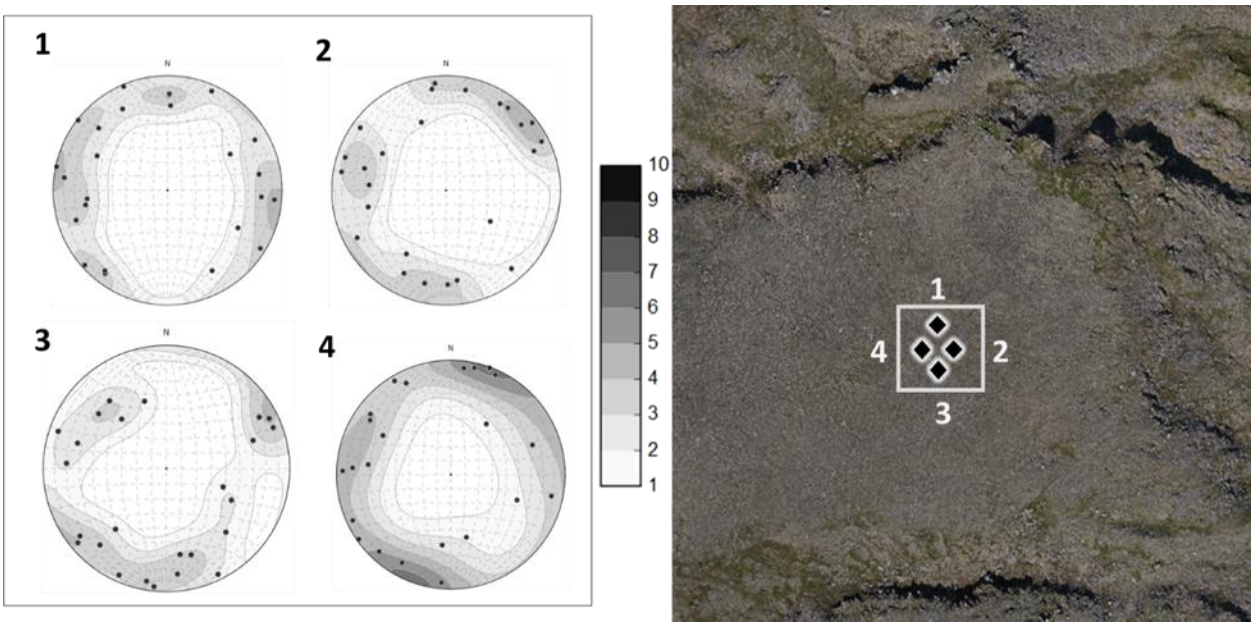

Figure 14. Tread macrofabric Schmidt nets. *Tread macrofabrics show girdle shapes.*

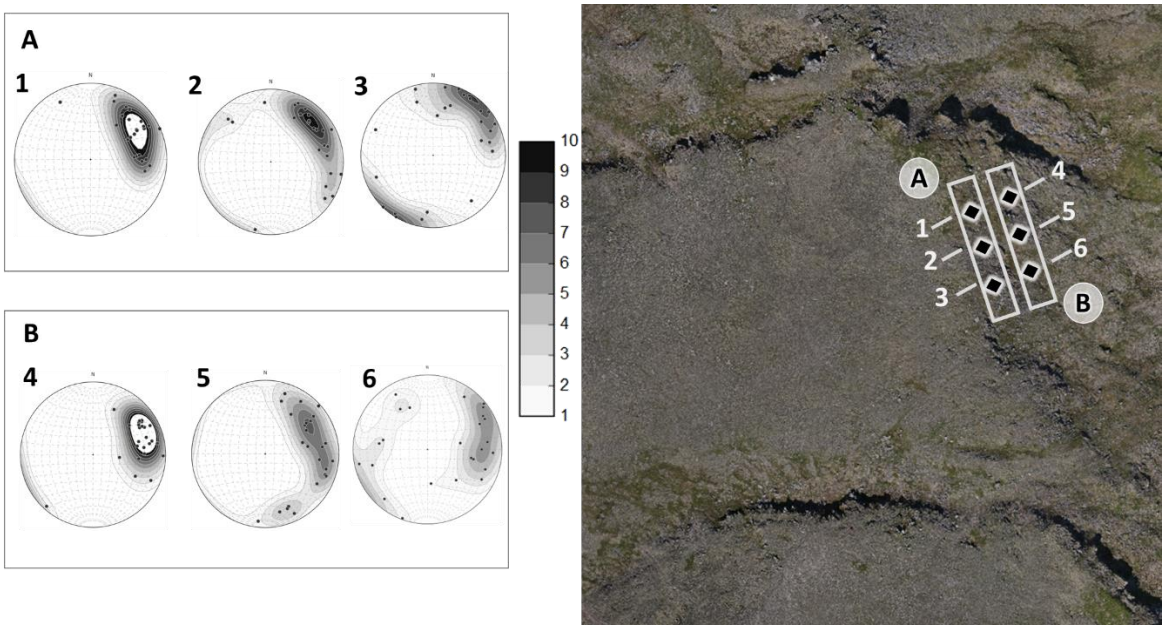

Figure 15. Upper side slope facet macrofabric Schmidt Net. *(A) Macrofabrics sampled from the top of the upper side slope and (B) from the lower area of the upper side slope. Note the strong orientation of fabrics across all samples, which aligns with the local slope. White areas of the Schmidt nets indicate clusters of n>10.*

Table 5. Facet sample Bingham's U statistical output. *Data are reported at the 0.01 significance level.*

Facet	$\bar{\tau}3$	$\bar{\tau}2$	$\bar{\tau}1$	U
Scarp	0.58	0.24	0.19	0.67*
Scarp	0.48	0.39	0.13	0.49
Scarp	0.54	0.33	0.12	0.66*
Scarp	0.75	0.20	0.05	2.04*
Scarp	0.75	0.21	0.04	2.09*
Scarp	0.75	0.19	0.06	2.04*
Upper side slope	0.79	0.17	0.04	2.41*
Upper side slope	0.62	0.34	0.04	1.28*
Upper side slope	0.86	0.10	0.04	3.16*
Upper side slope	0.68	0.24	0.08	1.49*
Upper side slope	0.67	0.31	0.03	1.53*
Upper side slope	0.82	0.15	0.03	2.71*
Tread	0.50	0.38	0.12	0.56*
Tread	0.53	0.38	0.10	0.71*
Tread	0.44	0.39	0.17	0.31
Tread	0.49	0.39	0.12	0.55*

Macrofabric Schmidt nets for scarp and upper side slope facts show strong point cluster shapes aligned with the local slope. Conversely, samples derived from the base of the scarp and from the tread show girdle shapes and are indicative of rubble accumulation where clasts show very different orientation patterns. A similar result was encountered from a site near the study area where fabrics from upslope scarp positions showed strong alignment with the local slope while fabrics obtained from corresponding locations at the base of the scarp showed "jumbled" fabrics indicative of rubble accumulations at the scarp base (F. Nelson, personal communication, 2022). Girdle fabrics from the tread reflect the relatively flat slopes characteristic of the CT treads. Overall, facet fabrics show good agreement with those obtained from the grid sample sites, indicating that sampling of fabric data both indicate CT facet sedimentological signals, and that CT fabric sampling is informative at both small-scale intensive sampling and larger scale systematic sampling. Previous work reporting periglacial colluvium

macrofabrics shows that periglacial deposits are characterized by strong fabrics related to depositional environment (Mills, 1990).

The results from this work showing strong bipolar cluster shapes provide insight into the quantitative characterization of periglacial surface facets and support the assertion that sedimentological data may be used to detect distinctive periglacial fabrics. A similar result was achieved in a comparison study where solifluction deposits were found to be distinctive when compared to deposits emplaced by other mass movement properties (Nelson, 1985), although Millar (2006) was less sanguine about the ability of fabric to distinguish between depositional environments. This discrepancy may be related to differences in clast shape (Millar and Nelson, 2003). Future work on other CT facets is needed to fully outline the range of CT surface fabrics.

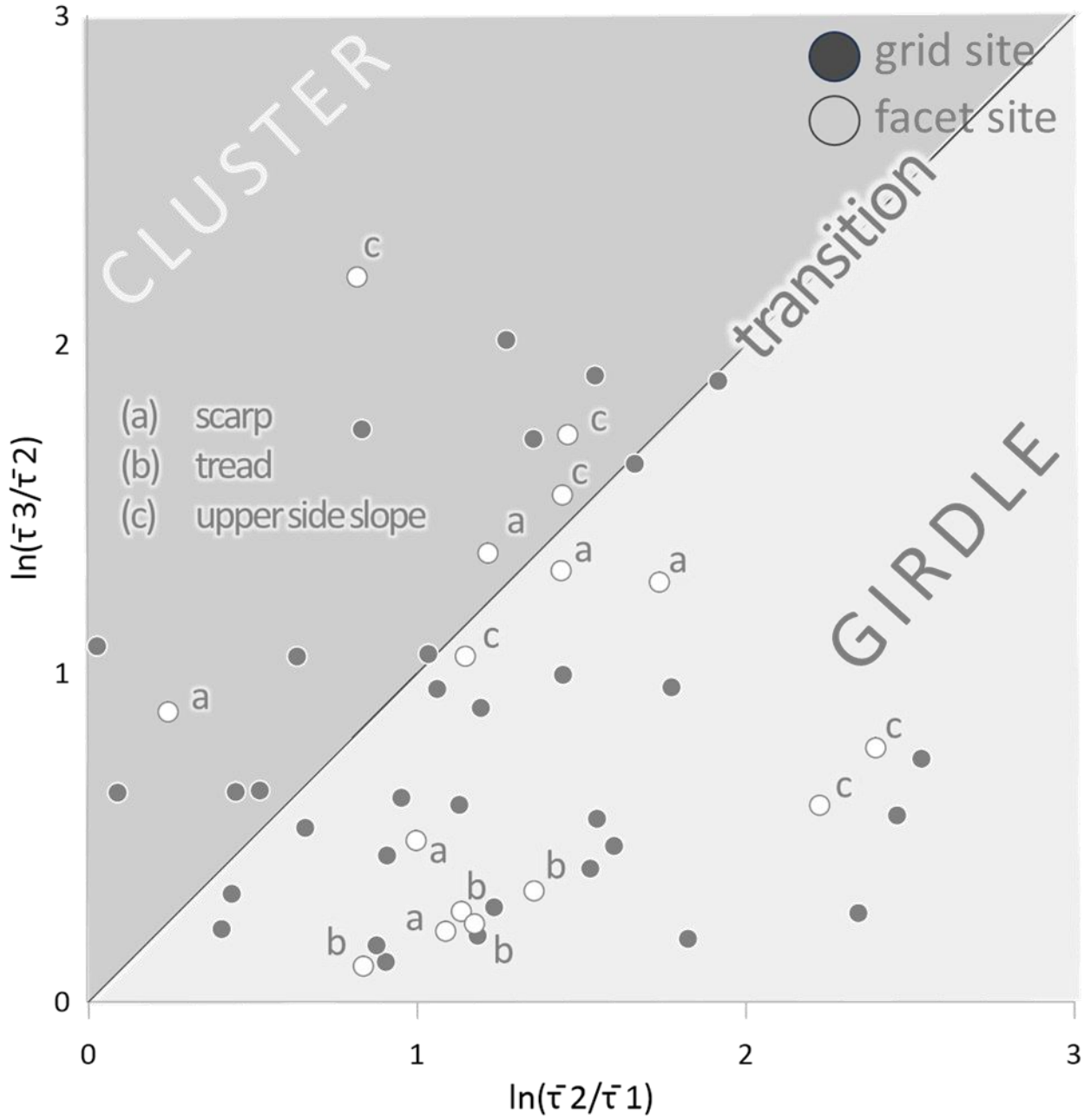

Figure 16. Woodcock Plot showing facet and grid sampled macrofabric shapes.

Macrofabric shape

The Woodcock plot above summarizes fabric data from both the grid and facet sampling procedures and characterizes CT facet microfabric shapes. Distance from the graph origin represents increasing fabric strength while weaker fabrics plot closer to the origin. Notable

findings include that samples from the upper scarp and the upper side slope are stronger than fabrics obtained from the tread, and tend to be clusetered, with a few deviations derived from the upper side slope. Fabrics obtained from the base of the scarp are much weaker than those obtained upslope and are characterized by girdle shapes. Fabrics obtained from the NES site are similar in shape and strength to those obtained from an area of periglacial flow deposits near the NES, published in outside studies (Mills, 1990; Millar, 2005).

Conclusion

Periglacial (cold but non glacial) environments affect at least 25% of the Earth's surface (Ballantyne, 2018, p. xi). Although studies focusing on periglacial processes and landforms date back to the early 1900s (von Łoziński, 1909) with a Quaternary focus, recent investigations focus on these environments under current climatic conditions (French, 2016). The periglacial facies concept was coined in the early 1900s (von Łoziński, 1909) and has been applied to describe the mountain-top detritus of alpine features in periglacial environments (French, 2017). The periglacial facies concept has been deemphasized in contemporary literature but due to the implications of this term highlighting the association between microclimate, topography, and landscape evolution, the term is used here to guide sampling methodology in an exploration of a characteristic periglacial environment in eastern Beringia.

Cryoplanation terraces are large, landscape-scale periglacial features, and their areal distribution has been used to delineate the extent of periglacial conditions (Nelson & Nyland, 2017). As such, cryoplanation terraces are exemplars of long-term periglacial landscape modification. The periglacial facies concept was used as a conceptual underpinning to guide the central hypothesis that cryoplanation terraces are comprised of facets, as posited by

Brunnschweiler & Nelson (2022) and are recognizable and are indicative of depositional environment. The results of this work indicate that sedimentological characteristics reveal the "signals" representing CT slope facets; scarps, treads, and upper side slopes and are in alignment with previous work highlighting the time-transgressive nature of CT development. The subsampling approach employed here revealed that these hypothesized periglacial facies are evident and mid and micro scales as evidenced by sedimentological characteristics observed at the facet and CT unit scales. Notable differences in clast microfabrics detected on a scale <20m indicate that CT surfaces are affected by micro-scale processes reflecting local slope and microclimate.

The NES CT surface shows observable differences based on location, evidenced by the close alignment in trends in relative weathering indices in the sample grid points. Relative weathering indices showed that CTs are variable when it comes to the surface but that ultimately, based on what we know about relative weathering indices and macro fabric, the hypothesized facets fit: scarps and upper side slopes are composed of larger clasts and are less flat with strong clast orientation. Treads show strong evidence of clast weathering based on rebound, size, and flatness. Macrofabrics from treads are much less clustered than those obtained from other facets. This information can be used as a quantitative basis by which to explore and potentially help identify relict CT surfaces in other regions of the world.

Identifiable trends in indices from the scarp toward the distal end of the CT tread show increases in weathering from the scarp to the middle of the tread followed by indications of dampened clast weathering near the scarp of the subsequent CT unit downslope. This trend highlights the primary components of the CT surface, the scarp and tread, which are easily

identified by the compilation of relative weathering indices. The results of this work provide quantitative support for the assertion that CTs are faceted environments and, in addition to morphological criteria (Matthews et al. 2019), can be conceptualized in terms of sedimentological characteristics.

Based on background understanding of clast macrofabric and relative weathering indices, CT surface facets appear to be the geomorphic culmination of topography, micro-climate, and time, all of which all contribute to the shaping of this upland periglacial environment. Findings from this work provide a quantitative foundation for future work aimed at characterizing periglacial faceted environments. The periglacial facies concept was expanded in this study by findings indicating that the horizontal distribution and characterization of periglacial surfaces can be used to work towards models of periglacial landscape evolution and used to make sense of the expansive rubble deposits (Madole, 1972).

Findings from this work are used to better inform processes related to landscape evolution in the periglacial realm and to provide suggestions on the standardization of research methods as they are applied to the periglacial facies literature. The advancement of research on periglacial facies is not only relevant for studies aimed at better understanding of hillslope processes in cold environments, but also to planetary studies given that hypothesized periglacial features have been identified on Mars (Farmer & Doms, 1979). On Mars, as on Earth, periglacial features such as sorted patterned ground, have been used to indicate frozen water and as such, periglacial studies are vital to work aimed at predicting the viability of life on Mars (Balme et al., 2013).

CHAPTER 4. PERIGLACIAL FACIES IN THE APPALACHIAN HIGHLANDS

Introduction

The Appalachian region of the eastern United States is a mountainous belt, the northern reaches of which were glaciated periodically during the Pleistocene epoch (French & Millar, 2014). Lowered temperatures and proximity to the Laurentide Ice Sheet facilitated the formation of permafrost, and periglacial conditions were widespread in at high elevations in the Appalachian Highlands (Clark & Hedges, 1992; Ivester et al., 2001). Today, the periglacial influence on the Appalachians is evidenced by relict periglacial features, which include block accumulations, patterned ground, and ice wedge casts (Middlekauff, 1987; French & Millar, 2014).

The geomorphic history of the Appalachian region of the U.S. has been subject to rigorous research since the late 1800s (Davis, 1899) and although the origin and evolution of this landscape is much better understood today than it was at the opening of the twentieth century, the extent of periglacial landscape modification remains largely undetermined (Braun, 1989; Denn et al., 2018). Specifically, the origin and formation of accordant, broad, upland ridgetops found throughout the Central Appalachian region remain unknown (Clark & Hedges, 1992). Researchers have noted the striking morphological similarities between these puzzling uplands and cryoplanation terraces (CTs), such as those found in periglacial environments in Alaska (Clark & Hedges, 1992), but no comparative study aimed at clarifying the genesis of Appalachian uplands that involves a comparison of these features with cryoplanation terraces has been conducted.

The occurrence of cryoplanated terrain in the Alaskan interior provides an opportunity to compare morphology and test the periglacial affinities of similar features in the Appalachian Highlands. Using the facies analysis methodology established in the previous chapter of this dissertation, this chapter investigates the surface morphology of a hypothesized cryoplanation terrace in the central Appalachian Mountains (Clark & Hedges, 1992). The previous chapter of this dissertation employed a rigorous sampling regime, relative weathering, clast macrofabric analysis, and remotely sensed data to characterize CT slope facets in known cryoplanated terrain. That study serves as a foundation for comparative efforts aimed at identifying and characterizing hypothesized periglacial terrain, and to test the hypothesis proposed by and Clark and Hedges (1992), that alternating steep and gentle slope segments in the Appalachian Highlands are cryoplanation terraces. This comparison is achieved through quantitative characterization, supported by analysis of sedimentological relative weathering indices and clast marcrofabrics, of the surface morphology of Spruce Knob, a hypothesized cryoplanation feature in West Virginia. Quantitative characterization of the Spruce Knob site will inform the climatic and depositional history of this feature and will add to the growing body of literature focused on the periglacial imprint on the Appalachian Highlands (Braun, 1989; Del Vecchio et al., 2020, 2022).

Background

Appalachian Highlands

The Appalachian Highlands is a mountainous region in the eastern U.S. in which summits achieve elevations exceeding 2000 m.a.s.l. (Fenneman, 1946; Leffler, 1981). The temperature depression triggering Pleistocene glaciations promoted formation of periglacial features,

including blockfields, patterned ground, and block streams, all of which are abundant in the Appalachian Highlands (Clark, 1993; Orme, 2001, pp. 295-296; French & Millar, 2014). Virtually all periglacial features in the region are relict, except for those at higher elevations in the mountains of northern New England (Orme, 2001, p. 296). The geomorphology of the Appalachian region has been the subject of investigation for over a century (Guyot, 1861; Davis, 1899) and previous trends in geomorphological research, rooted in the Davisian cycle of erosion, have been applied to explain the origin and formation of broad upland summits in the Appalachian Highlands as peneplain remnants.

The Davisian cycle of erosion in geomorphology in the Appalachian region

The Davisian cycle of erosion (“*the geographical cycle”)* is a theory of landscape evolution first proposed in the late 1800s by geomorphologist William Morris Davis (Davis, 1899). The *geographical cycle* or *cycle of erosion,* outlines the pathway by which uplifted surfaces are gradually made flat through the erosive effect of fluvial dissection (Davis, 1899). Davis theorized that over time, landscapes proceeded through “young,” “mature,” and “old” stages, which were characterized based on the relative dissection of the ground surface via fluvial incision. Culmination of the cycle was evidenced by the occurrence of broad, flat, alluvium-capped surfaces of uniform elevation called *peneplains* (Davis, 1899). “Rejuvenation” of the cycle would occur following uplift of an area (Davis, 1899).

The cycle of erosion was the dominant paradigm of early 20th century Anglophone geomorphology. The central tenants of this landscape evolution pathway, e.g., the development of peneplains, have been applied to describe the topography of regions such as Appalachian Highlands (Davis, 1899). Progress in geomorphological research has led to the

rejection of the notion that all Appalachian topography, specifically the broad, flat uplands of the central Appalachians, were formed via Davis' cycle of erosion (Clark, 1993). In the absence of a prevailing formation hypothesis however, the origin and formation of some terrain in the Appalachian Highlands is speculative (Clark & Hedges, 1992; Clark, 1993).

Alternatives to the cycle of erosion and periglacial landscape evolution

Alternative perspectives of landscape evolution were proposed in the mid-1900s to recognize the impact of climate on landscape evolution (Peltier, 1950). Climatic geomorphology, arising as a European challenge to the dominance of the Davisian cycle of erosion in Anglo-American literature, outlined landscape evolution pathways dictated by the dominant climatic regime of a region (morphogenetic regions), thereby defining the climatic imprint on the landscape (e.g., Büdel 1977). Peltier (1950) in essence combined the two approaches, appending periglacial morphogenetic regions to Davis's list of "climatic accidents" responsible for deviations from fluvial ("normal") erosion. According to Peltier's (1950) scheme, stages of erosion proceed through the effects of frost weathering and periglacial mass-movement processes, resulting in extensive areas of flattened summits and low relief. Climatic geomorphology provided an alternative way to interpret and explain landscape evolution in areas subjected to climates that deviated from the temperate, humid conditions commonly encountered in the mid-latitudes.

Cryoplanation

The term" cryoplanation" (Bryan 1946) describes long-term landscape modification through scarp retreat in cold regions (Ballantyne, 2018). The term was used by Peltier (1950) to describe landscape evolution in periglacial environments and, more specifically, was applied to

characterize the peneplain analogues in periglacial regions, which are characterized by step-like sequences known as cryoplanation terraces (Demek 1969; Reger 1975). Cryoplanation terraces (CTs) give rise to entire landscapes in periglacial realms and their upland surfaces support the formation of periglacial feature assemblages comprised of sorted patterned ground, block deposits, and solifluction terraces (Brunnschweiler & Nelson, 2022; Queen & Nelson, 2022). Similar distinctive step-like CT morphology has been observed in the upland terrain of the Appalachians and in addition to the occurrence of periglacial features in the Appalachians and due to past glacial cycles, some have likened upland Appalachian terrain to cryoplanation features (Clark & Hedges, 1992).

"High-elevation local broad uplands in the Central Appalachians"

The broad, flat ridge crests that occur in the central Appalachians are pervasive in the region and feature morphological sequences of tors, summit flats, and tread/riser morphology that are often occupied by patterned ground (Clark, 1993; Clark & Hedges, 1992). These rubble-mantled surfaces have perplexed geomorphologists who initially attempted to explain this aspect of Appalachian topography in terms of the Davisian cycle of erosion (Clark & Hedges, 1992). Subsequent research established that the widely-adhered-to Davisian cycle was not necessary for the explanation of Appalachian topography in its entirety and that instead, Appalachian topography could largely be explained by fold regularity, thinness of resistant sandstones, and the spacing of sandstones in the geologic column and as such, topographic accordance is the result of the uniform properties of resistant rock units (Clark & Hedges, 1992 and references therein).

Observation-based work focusing on the upland surfaces of the Appalachian Highlands contains descriptions of the terrain highlighting the "…wide and 'flat' summit areas (Clark, 1993 p. 65). Clark and Hedges (1992) provide elaborations of hypothesized cryoplanation landforms in the Central Appalachians, writing "…relatively flat uplands locally truncate lithology and structure and break abruptly at their edges into block slopes. Short horizontal and vertical distances downslope from these risers are one or more terraces" (Clark, 1993, p. 66). As many as twelve such upland regions of unknown origin have been identified and these areas have been characterized as being periglacial in origin (Clark & Hedges, 1992). Adjacent areas of research in the Appalachian Highlands featuring investigations on the erosional history of the area outlined the efficacy of periglacial erosion in the Appalachians (Braun, 1989), which is in line with assertions of high weathering and erosion rates encountered in periglacial regions (Braun, 1989; Clark, 1993; Del Vecchio et al., 2018, 2022). Research in the Appalachians has also focused on the comparison between rubble deposits in the mid-Atlantic regions and modern periglacial landscapes.

A paleoperiglacial interpretation

The origin and formation of the broad uplands in the central Appalachians remains enigmatic, although a periglacial interpretation has been applied to describe this topography (Clark, 1993). Morphological similarities between Appalachian ridge sequences and cryoplanation terraces such as those encountered in Alaska have been identified, lending support to the interpretation that Appalachian uplands were modified by periglacial processes during past glacial intervals (Clark & Hedges, 1992). Addition support for a periglacial origin hypothesis is the occurrence of sorted patterned ground and angular blocky material occupying

Appalachian upland surfaces (e.g., Clark 1968), as opposed to surface cover of alluvium, as would be the case with surfaces representing long term peneplanation (Davis, 1899). Periglacial processes no longer dominate in the Appalachian Highlands and as such, periglacial features in the region are relict (Merrits & Rahnis, 2022) although contemporary permafrost is known to affect Mt. Washington and other high-elevation areas of limited extent in the northern Appalachians (Walegur & Nelson, 2003).

Despite the record of work in the Appalachians extending back to the late 19th century and based on the morphological similarities of this terrain to cryoplanated terrain, no comparative studies featuring known and hypothesized periglacial terrain have been conducted for the Appalachian upland areas described by Clark and Hedges (1992). This study centers on the hypothesis that the broad uplands of central Appalachia are genetically related to cryoplanation terraces. Interrogation of this hypothesis is achieved through the quantitative characterization of surface morphology of Spruce Knob, a site of hypothesized periglacial origin. The precise identification of features of hypothesized periglacial origin is of importance for paleoclimatic reconstruction of the area. The relict periglacial terrain of the Appalachian Highlands provides an opportunity to establish and characterize the periglacial imprint on the region (Clark, 1993).

Study Area

Spruce Knob (38.70°N, 79.53°W, ~1480 m.a.s.l.) is the highest point on Spruce Mountain (Robison, 1960). Located in the Allegheny Mountains and Monongahela National Forest of West Virginia, Spruce Mountain is a long (26 km), slightly domed, northeast/southwest trending synclinal ridge (Fenneman, 1946). Spruce Knob is a terrace/plateau-like feature capped with

resistant Sharon Conglomerate (mostly sandstone) of the Pottsville Series (Tilton et al., 1927), which is exposed at the surface in masses of broken stones (Core, 1926; Tilton et al., 1927; LaBarbara, 2017 and references therein). The flanks of Spruce Mountain and Spruce Knob area are predominantly the Mauch Chunk group, a grayish-red shale sandstone of Upper Mississippian age (Tilton et al., 1927; Cardwell et al., 1968). Spruce Knob stands above what has been described as the Schooley Peneplain (Sevon, 1983), and as such Spruce Knob has been hypothesized as representing a monadnock erosional feature (Tilton et al., 1927)

Descriptions of the Spruce Knob site note that the scene encountered at the summit is "…almost a reminder of the Subarctic landscape near Hudson Bay". (Fosberg, 1960, p. 120), characterized by "…cold barren knobs on the summit" (Tilton et al., 1927, p. 36) and "seamed and broken fragments of sandstone" (LaBarbara, 2017 and references therein). Meso-scale sorted patterned ground occupying large areas on Spruce Knob has also been documented (Clark & Ciolkosz, 1988). Spruce Knob soils are classified as frigid, based on the USDA classification system (Walegur, 2001).

Spruce Knob was chosen for analysis in this study because the site features classic periglacial features and terrain, and because of the morphological similarities between Spruce Knob and CTs observed in the interior of Alaska (Figure 17). The occurrence of patterned ground, angular rock mantled surfaces reminiscent of von Lozinski's periglacial facies, and boulder fields at Spruce Knob in addition to the fact that West Virginia was never glaciated during the Pleistocene, either by continental ice sheets or alpine glaciers (Cremeens et al., 2005), are all factors indicating that the site was affected by periglacial conditions. Similar sites

in West Viginia have been analyzed in periglacial studies and have been attributed to cryoplanation during the Pleistocene epoch (Clark & Hedges, 1992).

Figure 17. Broad-topped upland in West Virginia and cryoplanated terrain in Alaska. *Left: Spruce Mountain and Spruce Knob, indicated by a circle in WV. Photo taken by drone, V. Tolmanov May 2023. Right: Cryoplanated terrain in the interior of Alaska. Photo taken by drone, V. Tolmanov July 2022.*

Methodology

Quantitative characterization of the Spruce Knob rubble deposit was supported through collection and analysis of relative weathering data. Clast sphericity, flatness, rebound, volume, and macrofabric were used to infer past geomorphological processes (Benn & Ballantyne, 1993; Evans & Benn, 2014) and as data inputs to assess the hypothesis that broad uplands bear genetic similarities to cryoplanation terraces in periglacial regions. The area analyzed at the Spruce Knob site, a transverse (parallel with the contour) rubble deposit, was chosen based on morphology, which is like upper side slopes in cryoplanated terrain observed at the North Eagle Summit site serving as a basis for comparison and based on the availability of clasts at the surface for sampling.

Sampling design

A series of four east-west oriented sampling transects were established along the west-facing rubble exposure at Spruce Knob (Figure 18). Sampling transects were arranged semi-

perpendicular to the primary axis of the widest portion of the rubble deposit to maximize sampling coverage of the total exposed area. Areas with thick forest cover were avoided to eliminate the influence of vegetation on feature morphology and clast surface characteristics. Elevation plots establishing the relief along sample transects are shown in Figure 18. Individual sampling transects were spaced 16 m apart to encompass an area of approximately 60 meters across the long axis of the rubble exposure. Individual sampling transect lengths ranged from 25-30 m, based on the varying width of the rubble exposure. Individual sampling locations along the transects were spaced nine meters apart.

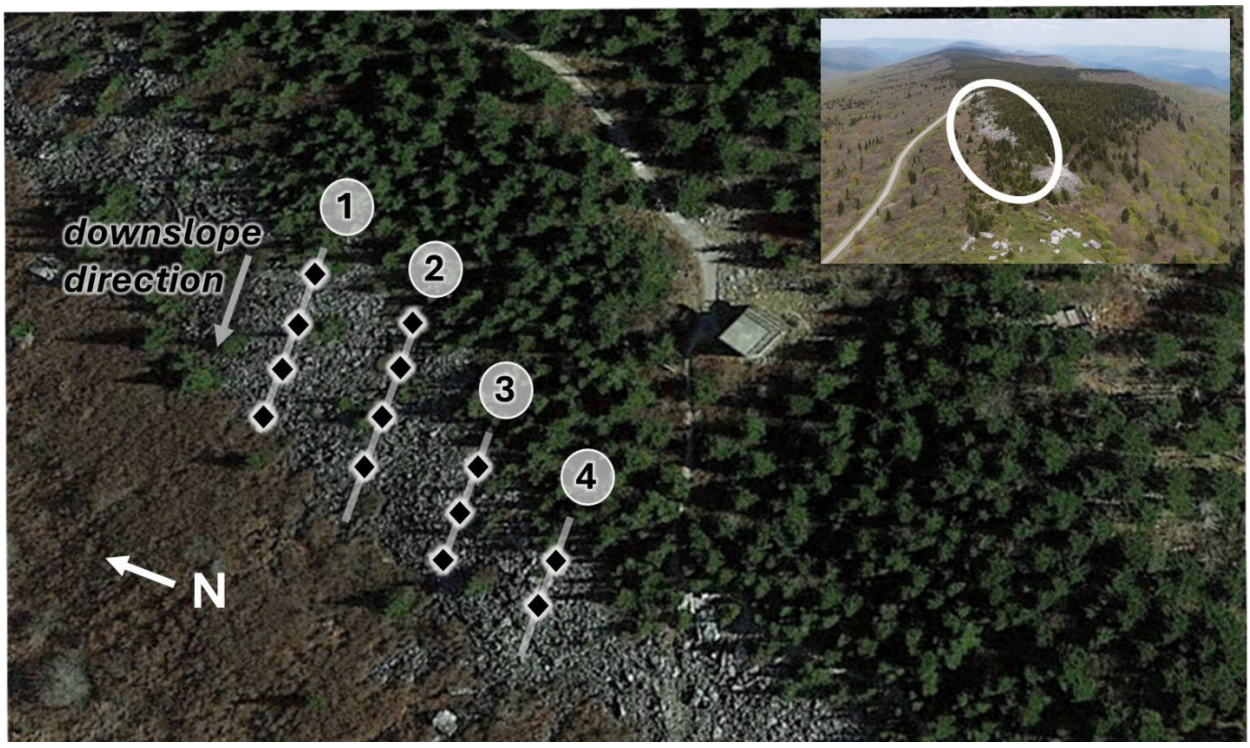

Figure 18. Sampling transects along the Spruce Knob rubble exposure. *The sampling site location is indicated by the white oval in the oblique photo of Spruce Mountain in the upper right-hand corner.*

Field data

Relative weathering data (clast sphericity, flatness, volume, and rebound) in addition to clast long axis macrofabric were collected from 25 clasts at each sampling location and were used to support the investigation of terrain characteristics of hypothesized cryoplanated terrain. The relative weathering indices employed here are common in periglacial studies (e.g., King, 1966; Nyland & Nelson, 2019), and allow for future comparisons between Spruce Knob and other regions. The number of samples taken resulted in n=325, which is within the limitations of acceptable accuracy of up to 90% confidence and was deemed acceptable for this study (Thompson, 2012, p. 54). Sample interval spacing falls within the bound of acceptable resolution provided in the literature (Lohr, 1999). Explanations for the calculations of relative weathering indices can be found in Table 2 of this dissertation.

Remotely sensed data

A DJI Mavic Air 2 drone[10] captured aerial imagery of the site. Pix4D[11] mapper software was used to generate an orthomosaic, a geo-referenced mosaic of photos (Hengl & Reuter, 2008), and digital surface elevation model rasters of the Spruce Knob sample area. The resulting orthomosaic and elevation rasters achieved a resolution of ~3cm and were used to support the spatial analysis of trends in relative weathering data across the Spruce Knob sampling area.

[10] DJI Mavic Air 2 Drone. https://store.dji.com/product/mavic-air-2?vid=91071.
[11] PIX4Dmapper version 4.7.5 software. https://support.pix4d.com/hc/en-us/categories/360001503192

Analytical Methods

Surface visualization

The spline interpolation method for interpolating surface values of physical data (Franke, 1982; Mitáš & Mitášová, 1999) was used to generate continuous prediction surfaces representing sampled sphericity, flatness, rebound, and volume data. The resulting prediction surfaces aid visual interpretation of morphological surface trends at Spruce Knob and support the quantitative characterization of the terrain. The Spruce Knob rubble exposure provides an opportunity to study the continuous surface trends of relative weathering indices, which can serve as a visual aid in the interpretation of the site's geomorphic character (Dobesch et al., 2013). Spatial interpolation techniques such as the spline method, which uses a mathematical equation and sampled data points to estimate unsampled areas, can be implemented in GIS software citation (Mitášová et al., 1996). The spline interpolation method was used here to depict the Spruce Knob rubble surface based on sampled relative weathering indices. Relative weathering data were first georeferenced by tabulating sample coordinates and corresponding sample data. Tabulated data were input into ArcGIS pro version 3.2.1 software[12] to generate interpolated prediction surfaces. Using the Spline Spatial Analyst tool in ArcGIS Pro software, interpolation surfaces were generated using the following parameters: regularized spline type with a weight of 0.1, using five points. Parameter inputs follow the "typical" values used with this interpolation method (*Spline (Spatial Analyst)—ArcGIS Pro | Documentation*, n.d.).

[12] ArcGIS Pro Software version 3.2.1. https://www.esri.com/en-us/arcgis/products/arcgis-pro/overview.

Decisions regarding spline input parameters were guided by the desired goal of the output surfaces generating a smooth surface representative of spatial variation of the sampled data.

Clast macrofabric analysis

Clast long axis macrofabric has been used to interpret past depositional characteristics in glacial and periglacial research contexts (Millar, 1995; Benn & Evans, 2014) and was used here to support the characterization of the surface morphology of the rubble deposit at Spruce Knob. The resulting clast macrofabrics showing the three-dimensional orientation of samples were plotted on Schmidt Equal-area projection nets (Nelson, 1982; Millar, 2006; Benn & Evans, 2014). Contouring of Schmidt net plots was implemented at two standard deviation intervals using the Kamb Exponential method (Kamb, 1959; Vollmer, 1995). Schmidt nets were generated using InnStereo geological data plotting software[13].

Clast macrofabric data were analyzed with Bingham's U test of uniformity (Equation 1) to statistically evaluate the hypothesis of uniformity for fabric shapes (Bingham, 1974). Rejection of uniformity was used here to indicate significant fabric shapes representative of past depositional characteristics (Nelson, 1985). The null hypothesis of uniformity is rejected based on critical values of Bingham's U statistic (Bingham, 1974; Mardia, 1975). Fabric data must first be resolved into three primary axes, eigenvectors, the eigenvalues of which characterize the lengths of the axes. The normalized eigenvalues can be used to characterize the shape of the macrofabric (Bingham, 1974; Mardia, 1975).

[13] InnStero Stereographic projections for structural geology: https://innstereo.github.io/.

The strength and shape of clast macrofabric can be used to interpret past depositional characteristics (Woodcock, 1977; Benn & Evans, 2014). Comparison of fabric shape and strength across sites is important to interpret past depositional properties but such comparisons can be complicated by the fact that fabric shapes are represented by three values, thus making traditional representations on a two-axis graph difficult (Woodcock, 1977). Woodcock plots are a common way to depict clast fabric data and resolve the three-variable issue by collapsing the eigenvalues into natural log ratios, which can then be plotted on a standard x-y axis graph (Woodcock, 1977). Spruce Knob fabric data were plotted on a Woodcock diagram to support the visual interpretation of clast fabric shapes.

Results

Relative weathering indices

Relative weathering data were organized and plotted graphically to reveal surface dynamics along the sampling transects oriented in the downslope-trending direction of the rubble exposure (Figure 19). The graphical representation of the average values of each data type was organized to facilitate comparison between the surface morphologies of the Spruce Knob site and the North Eagle Summit site analyzed in the previous chapter of this dissertation, and to simplify interpretation of the voluminous dataset. Interpretation of sphericity data should follow information regarding this index, which states that on a scale of 0-1, values near unity indicate a perfectly spherical pebble, and in theory, represent a highly weathered specimen (Krumbein, 1941) Flatness is a related measure, and output values can be interpreted with the understanding that values of 100 represent a perfectly equant clast whereas values > 100 represent increasingly flatter specimens (Cailleux, 1947). In terms of clast rebound (R),

studies establishing expected rebound for various lithologies exist (Goudie, 2006) and provide an R value of 50.8 for Devea sandstone for Ohio, which was the closest lithology and geographical location to compare against the Spruce Knob Sharon sandstone conglomerate. This R value provided by Goudie (2006) should serve only as a point of reference for rebound data derived from Spruce Knob as the relative differences between rebound of clasts of the same lithology is the relationship studied here and in other studies employing this methodology (e.g., Nyland & Nelson, 2019).

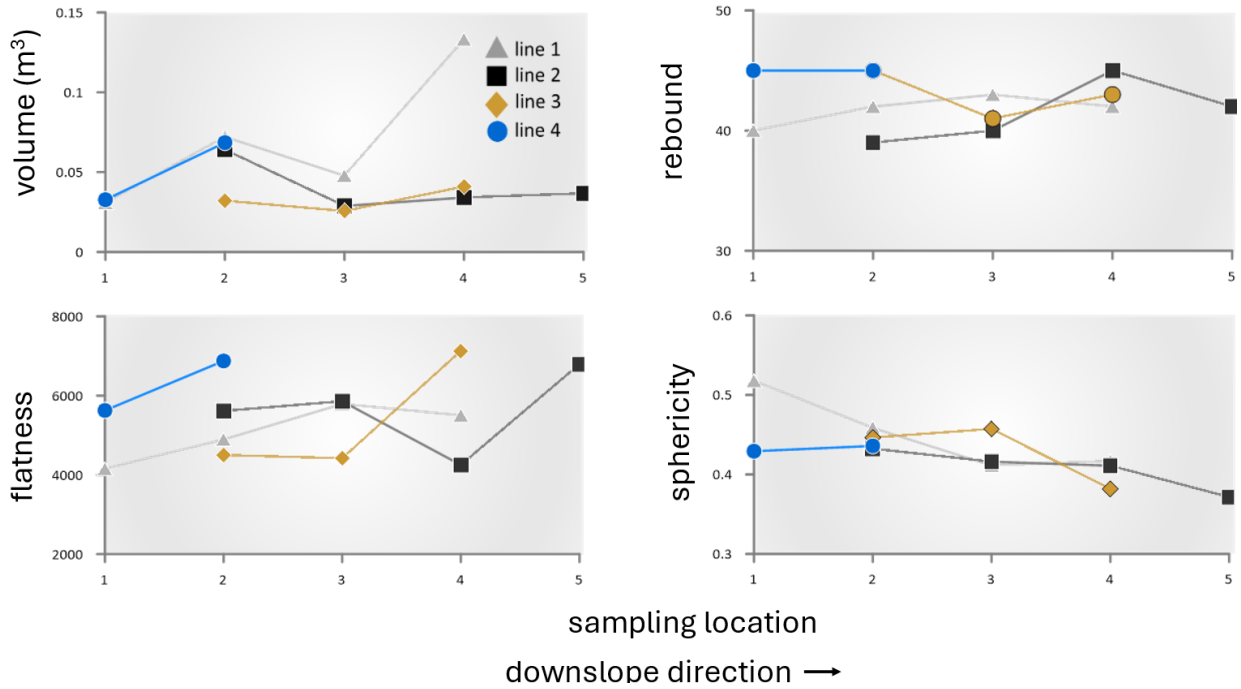

Figure 19. Relative weathering indices plotted by transect. *Data are plotted in the downslope direction.*

Graphical representation of relative weathering data shows that individual weathering index trends are consistent across the primary axis of the rubble exposure. Trends in relative weathering at this site are characterized by decreases in volume and sphericity with distance in the downslope direction, which is approximately due west. Flatness and rebound tended to

increase with distance along the sampling transects. Variability in weathering trends of the intermediate axis of the rubble exposure, although not diagnostic of formation, indicate complex weathering histories consistent with emplacement (e.g., Nyland & Nelson, 2019). Elevation profiles spanning each sampling transect (Figure 20) show that in some areas, the Spruce Knob rubble deposit appears to be slightly notched, which may be indicative of past nivation impacts via the cryoplanation pathway as hypothesized by Clark & Hedges (1992). Other transects display slightly convex profiles.

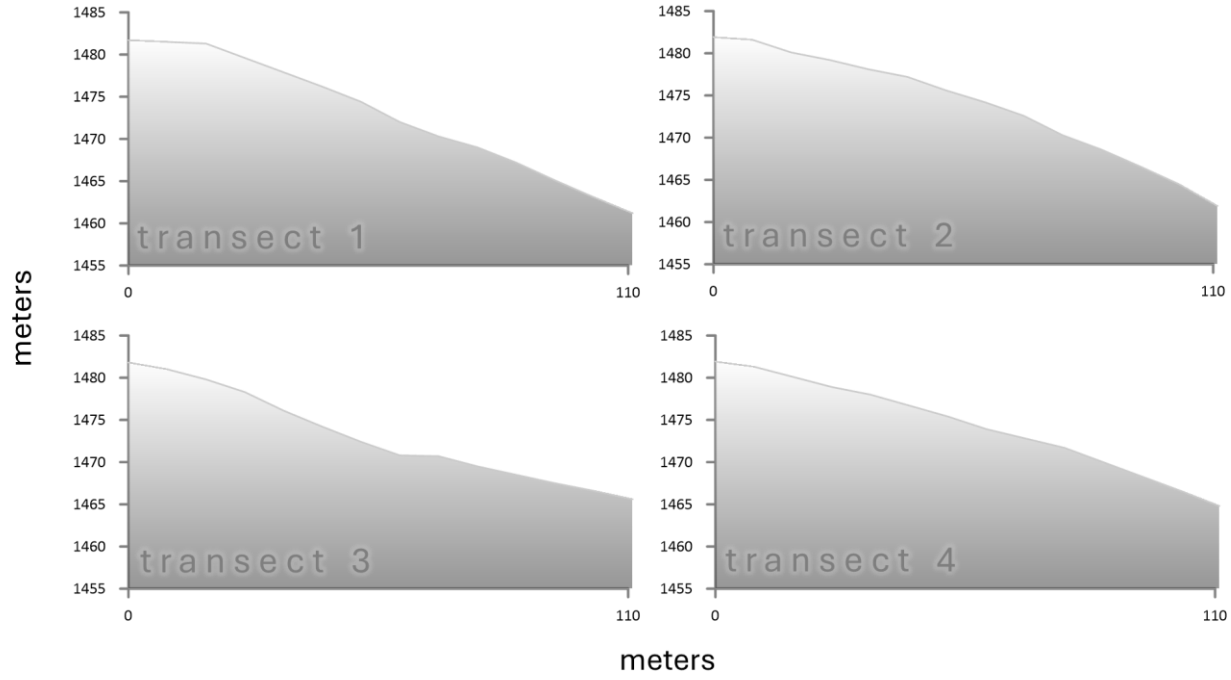

Figure 20. Elevation plots of sample transects.

Relative weathering prediction surfaces

Prediction surfaces showing the interpolated relative weathering data are shown in Figure 21 and are used here to interpret the spatial variability of surface weathering. The prediction surfaces indicate that relative weathering indices vary by location across the rubble exposure and more specifically, that relative weathering indices all show clustering patterns as

opposed to diffuse trends in weathering. These results can be interpreted as indicators of weathering patterns that vary spatially, and which indicate this deposit may have been emplaced over time and that weathering affected areas based on the time clasts were exposed at the surface. This interpretation is in line with the hypothesis that Spruce Knob is a bolvan (a monadnock-type periglacial feature) (Demek 1969; Reger 1975) formed through cryoplanation like the other broad-topped uplands in the central Appalachians (Clark & Hedges, 1992).

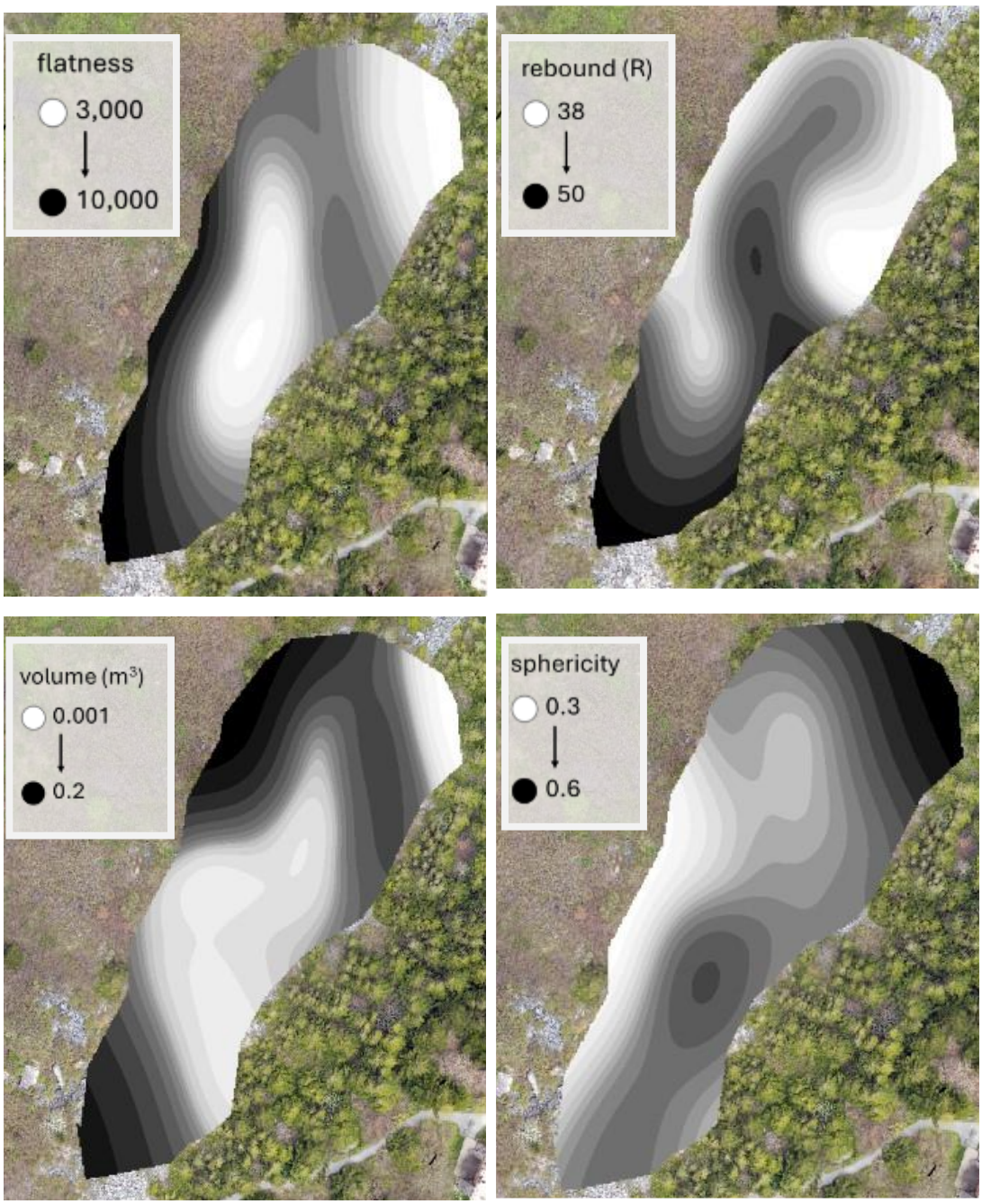

Figure 21. Relative weathering indices prediction surfaces. *All graphics are oriented with the north direction at the top.*

Clast macrofabric analysis

Clast macro fabric data Schmidt nets are shown in Figure 22. Bingham's U uniformity testing output is summarized in Table 6. A Woodock plot is provided (Figure 23) to support commentary on the fabric signatures revealed from clast macrofabric data at Spruce Knob.

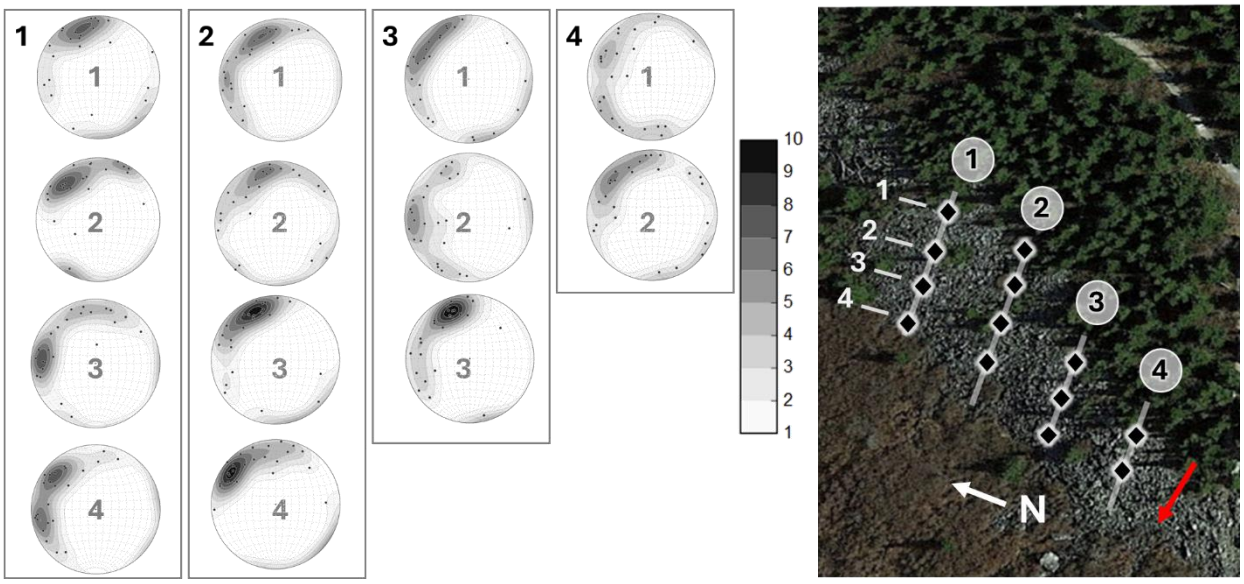

Figure 22. Equal Area Schmidt Nets. *Schmidt nets were contoured at the 2σ interval following the Kamb method (Kamb, 1959). A scale bar indicating the point density of fabrics is provided. Clast macrofabric data are shown for all samples along the sampling transects and are numbered in the downslope direction, as is shown for Transect 1. The downslope direction faces approximately due west and is indicated by a red arrow in the bottom right corner of the areal image.*

Table 6. Eigenvalue and Bingham's U testing output. *Site naming convention indicates the transect line and site number along the transect. The hypothesis of uniformity was rejected for all samples, which were tested at the 0.05 level.*

Site	$\bar{\tau}3$	$\bar{\tau}2$	$\bar{\tau}1$	U
t1.1	0.623	0.291	0.086	1.102
t1.2	0.624	0.316	0.06	1.196
t1.3	0.534	0.417	0.049	0.961
t1.4	0.633	0.334	0.033	1.350
t2.2	0.569	0.407	0.024	1.175
t2.3	0.578	0.356	0.066	0.989
t2.4	0.684	0.263	0.053	1.549
t2.5	0.68	0.279	0.042	1.560
t3.2	0.615	0.342	0.043	1.228
t3.3	0.547	0.358	0.095	0.773
t3.4	0.632	0.322	0.045	1.293
t4.1	0.632	0.322	0.045	1.293
t4.2	0.598	0.335	0.067	1.057

Clast macrofabric Schmidt nets and Bingham's U uniformity testing indicate moderately strong fabrics for all areas sampled at the Spruce Knob site. The hypothesis of uniformity was rejected for all samples and fabric nets show north-westerly oriented girdle shapes but containing strong concentrations. Girdle shapes are represented by points spread semi-evenly around a great circle, as opposed to clustered fabrics where the a-axes point in the same direction (Woodcock, 1977). Isotropic fabrics show no primary direction among fabrics (Woodcock, 1977).

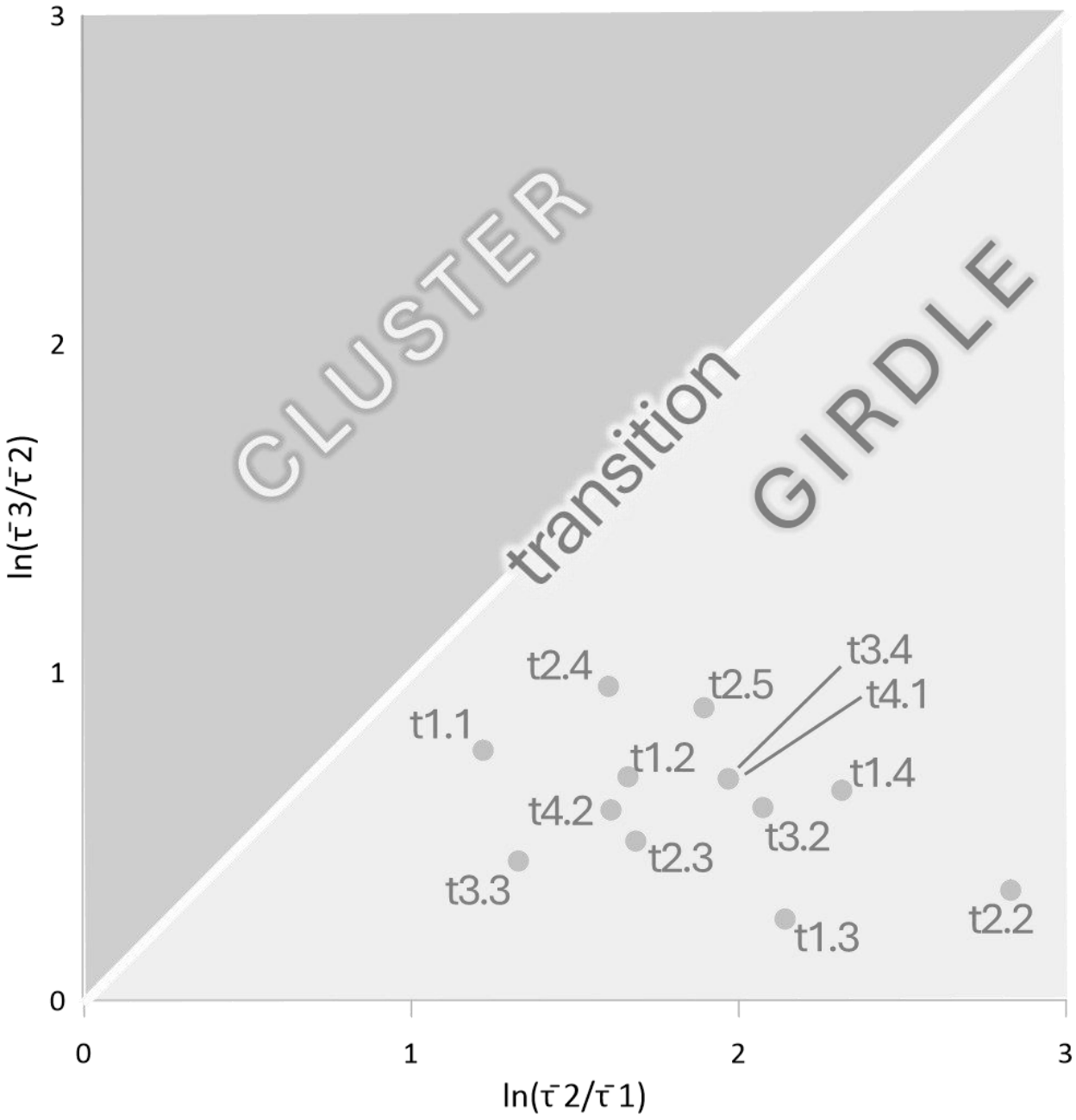

***Figure 23. Woodcock Plot showing facet and grid sampled macrofabric shapes*.**

The Woodcock plot of fabric data above shows that all samples fall within the same shape category and are of a similar strength to one another. Partial girdle shapes observed are like the upper side slope and scarp facets sampled from the North Eagle Summit site in Chapter 3 of this dissertation. The results here lend support for the interpretation that the Spruce Knob

rubble deposit comprises one facet of a larger matrix of cryoplanated terrain, as was observed in the different facets analyzed at the North Eagle Summit site.

Conclusions

The Spruce Knob rubble deposit comprises an area of hypothesized cryoplanated terrain. This study used relative weathering indices and clast macrofabric analysis to quantitatively characterize the surface and to support comparison of this site to a known periglacial site. Clast macrofabric analysis uniformity testing shows that clast fabrics are not uniform but instead show weakly north-west orientations that loosely comport with the dominant downslope direction at the site. This type of fabric shape may be explained by the nature of clasts at Spruce Knob, which are angular and somewhat imbricated. Previous work on fabric shapes of various slope deposits, including rockfalls, solifluction deposits, and debris flows, showed that in cases where clasts roll downslope, resulting orientations are perpendicular to the orientation of the downslope direction (Bertran et al., 1997). Additional examples characterizing debris slopes in periglacial settings describe the influence of drag forces imposed by structural obstacles and clast shapes that can result in clast a-axis alignment perpendicular to the local slope (Giardino & Vitek, 1985). A Woodcock plot was used to specify fabric shape and showed that fabrics are of strength and shape like upper side slope and scarp facet shapes sampled from the North Eagle Summit site.

Comparison between the Spruce Knob and North Eagle Summit sites via spatial patterns in relative weathering indices and clast macrofabric offer insight into the characterization of the Spruce Knob cryoplanated terrain. CTs possess characteristics that have been outlined in the literature, which include strong poleward orientation, elevations that follow the climatic

snowline, and terraced morphology supporting periglacial feature assemblages (Nelson, 1989; Queen & Nelson, 2022). Analysis of the Spruce Knob morphology in the context of surface trends and in the context of the area, which was subjected to periglacial conditions, the Spruce Knob rubble deposit appears to align with the morphological characteristics reminiscent of the upper slope facet observed at North Eagle Summit (Figure 24). Key factors linking the Spruce Knob Rubble deposit include the downslope orientation of microfabric, and the accumulation of boulders similar to the transportation slopes observed at the site in Alaska. The Spruce Knob rubble deposit does not conform with the flat erosional surfaces typical of CT treads, nor do surface transects follow a typical riser-tread sequence. Conversely, the north-facing tread like feature capped with patterned ground and boulders is backed by an area reminiscent of a scarp. Taken together, the series of morphological units at the Spruce Knob site appear to represent classic cryoplanated terrain comprised of scarp-rise, tread, and upper side slope components.

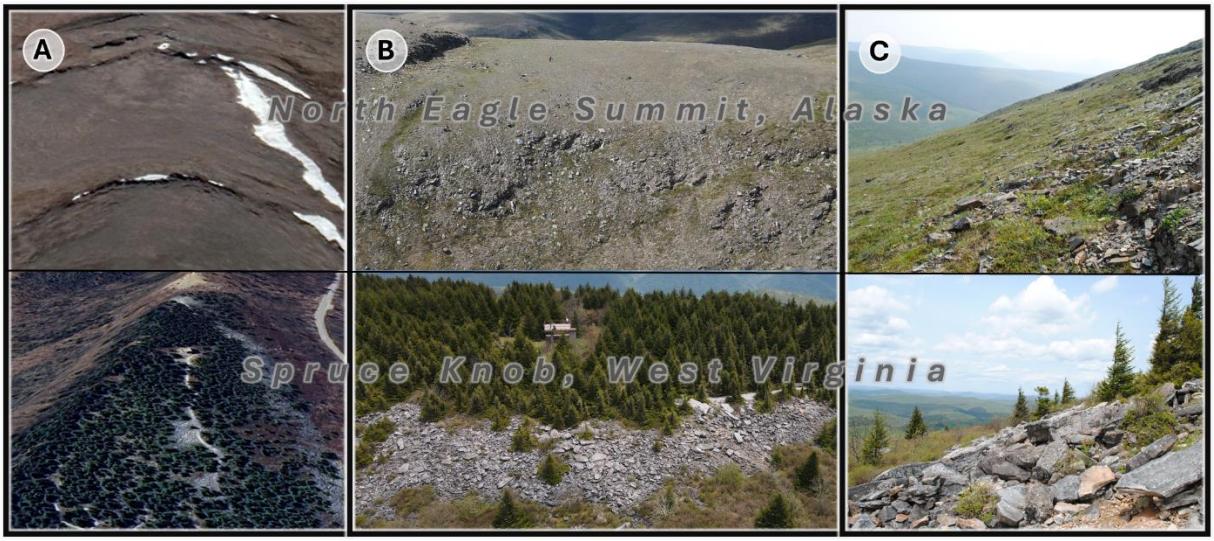

Figure 24. Morphological Comparison of North Eagle Summit and Spruce Knob. *(A) Aerial view of the North Eagle Summit site (top) and aerial view of the Spruce Knob site. Photos are oriented in with north facing up. (B) Photos show rubble exposures at the Eagle Summit and Spruce Knob areas. (C) East-facing Eagle Summit and Spruce Knob side slope areas.*

Taken with the known periglacial activity in the area and the morphological similarities to scarp and upper side slope facets observed in cryoplanated terrain, this study provides new insight to the erosional history of the Spruce Knob site. Although not diagnostic of origin and formation, the results here lend support for the interpretation that Spruce Knob was sculpted by periglacial processes, which contributed to the present-day morphology of the site, a result in line with previous hypotheses of landscape evolution in the area (Clark & Hedges, 1992).

Future work employing analysis of adjacent ridges could help to clarify the erosional characteristics of the uplands in West Virginia. Due to the thick vegetation in these regions analysis of surface morphology is difficult. LiDAR (light detecting and ranging) derived surface models could be used as data inputs to integrate into analysis of a larger area of the Spruce Knob site. Future work should also focus on the surface exposure histories of sorted patterned

ground and block fields on Spruce Mountain to better constrain the potential influence of past periglacial processes in this region.

CHAPTER 5. THE HICKORY RUN BOULDER FIELD, REVISITED

Introduction

The Hickory Run Boulder Field (HRBF), located in Carbon County, Pennsylvania (41.05°N, 75.64°W, ~500 m.a.s.l.) is the most impressive feature of its type in the eastern U.S.A. and is among one of the most expansive periglacial features in the Appalachian Highlands region (Sevon, 1987). Open to the public and designated as a National Natural Landmark and as a State Park Natural area (*Hickory Run State Park Boulder Field*, 2020) HRBF is easily identified by its ~6.5 ha expanse of sandstone conglomerate clasts nearly devoid of vegetation except for the thick forest delimiting the feature (Figure 25). HRBF is almost flat (~1°), and clasts near the surface lack interstitial fines, imparting a jagged appearance to the surface. Large voids within HRBF reveal increasingly smaller clasts with depth that during periods of high precipitation are inundated by flowing water (Geyer, 1969; F. Nelson, personal communication 2021).

Figure 25. Ground-Level Photo of the Hickory Run Boulder Field. *Photo taken near the upslope head of the boulder field, facing southwest (downslope). Photo: R. Mitchell, May 2021.*

HRBF has attracted the attention of earth scientists for more than seven decades (Smith, 1953) and research on the feature has employed absolute dating, remote sensing, and some field-based measurements in attempts to discern its formation (Helmke et al., 2007; Potter & Helmke, 2007; Denn et al., 2015, 2018). Major findings from recent studies conform with the generally accepted interpretation that HRBF formed during times of intense periglacial activity existing during the Pleistocene and, more specifically, that HRBF formed as large, frost-weathered rock fragments suspended in a matrix of fine material emplaced via slow downslope movement over permafrost (solifluction) (Smith, 1953; Geyer, 1969; Sevon, 1987; Reese, 2016). Despite the lengthy record of research, previous studies have been unable to determine the origin and formation of HRBF unambiguously. Contention within the literature centers on

determining whether HRBF was formed in-situ or if it is instead a time-transgressive surface formed under the influence of periglacial mass wasting (Merritts & Rahnis, 2022).

The identification of processes responsible for HRBF is important for paleoclimatic reconstruction in the Appalachian Highlands. HRBF lies within 2 km of the late-glacial maximum's (LGM) Laurentide Ice-Sheet margin (Merritts & Rahnis, 2022) and as such, has potential to clarify the glacial history and geomorphic evolution of the region. Insight into the formation of allochthonous boulder fields is relevant to the broader periglacial literature because these features are pervasive in relict periglacial regions (e.g., other locales in the Appalachian Highlands) as well as in areas that are presently undergoing alterations in response to global climate change such as unglaciated Beringia in Alaska (Selby, 1966; Sevon, 1967; Caine, 1972; Boelhouwers, 1999; Goodfellow et al., 2014; Wilson et al., 2017; Ballantyne, 2018; Chigira & Hirata, 2021).

This study revisits the HRBF enigma and is focused on quantitative characterization of the feature. This aim is achieved through evaluation of the central research question: are there identifiable trends in clast weathering across HRBF and, if so, are such trends associated with formation under periglacial environmental conditions, as suggested by Smith (1953)? Clast macrofabrics and relative weathering index data collected from the HRBF are used in this study as input to test the hypothesis that the HRBF is allochthonous, and that clast weathering increases along the primary axis of the feature. The status of HRBF as a National Natural Landmark and as a major component of the Hickory Run State Park serves as a testament to the cultural and geological significance of this relic. Efforts to clarify its origin and formation are

relevant to both the research literature and to the continued conservation and preservation efforts involving HRBF.

Background

Boulder fields in the Eastern U.S.

The Laurentide Ice Sheet covered northern portions of the continental U.S. episodically during the Pleistocene, facilitating periglacial conditions near its margin through disruption of climate and wind patterns (Delcourt & Delcourt, 1988). Near the LGM margin in areas that escaped glaciation in the eastern USA, periglacial features such as solifluction lobes, patterned ground, boulder fields and streams, and cryoplanation terraces are abundant (Clark & Schmidlin 1992; Merritts & Rahnis, 2022). Although most of these forms are presently relict, many investigators regard them as evidence of the operation of periglacial processes in the past (Delcourt & Delcourt, 1988; Park Nelson et al. 2007; Merritts & Rahnis, 2022).

Boulder fields are open-work clast accumulations occupying low-gradient slopes (Van Everdingen, 2005; Ballantyne, 2018). They are nearly devoid of vegetation (except lichens and mosses) and have continuous spatial extents of several hundred to many thousands of square meters (Park Nelson et al., 2007). Boulder fields are among the best geomorphic expressions of long-term periglacial weathering and are found globally in periglacial regions that escaped glaciation, including Scandinavia, Scotland, Svalbard, Greenland, Arctic Canada, Tasmania, the Falkland Islands, the United States, and Antarctica (Ballantyne, 2018).

Boulder fields occur in two forms: autochthonous (formed in situ) or allochthonous (formed by boulder emplacement) (Park Nelson et al., 2007). Although the term “block field” has also been employed (Ballantyne, 2018, p. 185), “boulder field” has been used regionally in

the eastern USA (Smith, 1953; Park Nelson et al., 2007) and is retained here to describe these deposits. Nearly one hundred boulder fields have been identified in the eastern USA (Park Nelson et al., 2007) and although the occurrence of these features has been used to indicate paleoperiglacial environments there is contention surrounding the climates/processes responsible for boulder field formation (Ballantyne, 2018).

One hypothesis of boulder field formation states that the features formed during the warmer, wetter conditions of the Neogene period and were only subtly modified by subsequent periglacial conditions (French & Millar, 2014). An opposing hypothesis states that boulder fields are solely the result of periglacial processes operating during Pleistocene cold intervals (Ballantyne, 2018). These diverging hypotheses highlight recent contention surrounding the ability of periglacial processes to generate characteristic terrain (e.g., Queen and Nelson 2022), a topic that for the eastern U.S. has garnered both attention and scrutiny (Braun, 1989). Contemporary evidence favoring the periglacial interpretation of boulder field formation includes spatial-analytic work showing the parallel relationship between boulder field and permafrost elevation during the LGM (Park Nelson et al., 2007) along with the general distribution of boulder fields, which cluster in areas affected by permafrost either presently or in the past (Merritts & Rahnis, 2022).

The Hickory Run Boulder Field

The periglacial origin of HRBF proposed by Smith (1953) is generally accepted today by many geomorphologists and is included in Hickory Run State Park informational pamphlets (*Hickory Run State Park Boulder Field*, 2020), which attribute HRBF to periglacial environments that existed during the Pleistocene. Smith's (1953) hypothesis emphasizes bedrock weathering

and slow movement of weathered material over an impermeable permafrost table during Pleistocene glacial intervals and states that greater weathering of clasts farthest from the bedrock source area would be expected owing to longer exposure of the clasts to weathering processes. Elaborations of this hypothesis propose that the present-day form of the HRBF was achieved as clasts moving within a fine-textured medium via solifluction and frost creep were subsequently eluviated following deglaciation of the area as the climate warmed (Merritts & Rahnis, 2022). Critics of this hypothesis question the ability of material to move across HRBFs shallow slope and whether periglacial processes could give rise to a feature as large as HRBF (cf. Merritts & Rahnis, 2022).

Other hypotheses of HRBF genesis suggested by Smith (1953) include 1) glacial/glaciofluvial deposition; 2) residual weathering products (i.e., autochthonous formation); and 3) accumulation from adjacent valley walls. Using field observations and visual interpretation, Smith (1953) rejected these hypotheses because 1) clasts within the boulder field appear to be locally sourced from nearby bedrock outcrops; 2) the lack of topographic relief on HRBF does not conform with expected moranic deposits; 3) irregular joint spacing indicates processes outside of weathering in place; and 4) spatially controlled clast roundness is greatest at the toe of the boulder field. Smith (1953) also noted the apparently anomalous nature of HRBF relative to present climate conditions and wrote that “It is believed to represent a special, local facies of a more extensive rubble deposit, formed by accelerated mechanical weathering and mass movement related to intensified frost action, probably with perennially frozen subsoil.” Proximity of the HRBF to the LGM margin has been cited as additional evidence

for the periglacial interpretation of formation (Figure 26) due to the periglacial conditions that occurred near the boulder field (French & Millar, 2014; Merritts & Rahnis, 2022).

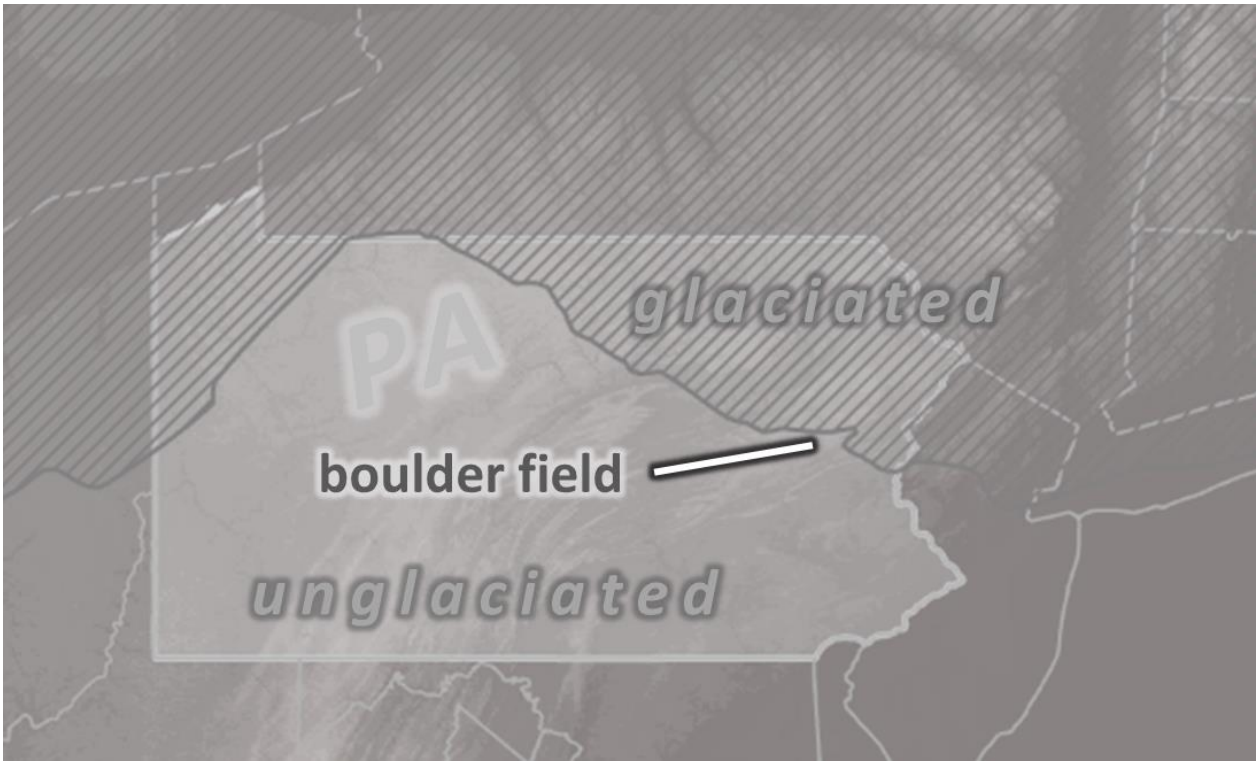

Figure 26. Proximity of the Hickory Run Boulder Field to the Last Glacial Maximum Glacial Margin.

Remotely sensed imagery of HRBF has been used to analyze surface-level clast morphology (Helmke et al., 2007; Potter & Helmke, 2007; Denn et al., 2015). Studies found increased clast roundness in the downslope direction of HRBF, which is consistent with an allochthonous formation pathway. These studies established the utility of remote sensing and automated feature identification software in geomorphic applications, but the overall findings were not diagnostic of feature origin and evolution. Visual observation of HRBF by Sevon (1987) also confirms the decrease in clast size and an increase in clast roundness in the downfield direction of the boulder field. In 1974 students from Lehigh University made sparse clast orientation measurements from multiple locations along the primary axis of HRBF (Sevon,

1987) and visual interpretation of these measurements show that clast long-axes align with the downslope direction of HRBF, which conforms with the interpretation that clasts flowed downslope over time (Lundqvist, 1949). A similar finding of increased clast roundness, indicative of increased weathering with distances, was observed by Wedo (2005).

Using cosmogenic nuclides, Denn et al. (2018) confirmed increased weathering in the downslope direction of the boulder field, which is in alignment with the hypothesis of allochthonous formation. Based on exposure dates indicating surface exposure histories between 70-600ka, Denn et al. (2018) asserted HRBF has a long and complex history of which a climatic (periglacial) explanation is likely an "oversimplification" and thus applications of HRBF in climatic reconstruction studies is precarious. Absolute dating using cosmogenic nuclides is an effective method in periglacial contexts to discern past geomorphic histories (e.g., Nyland et al., 2020) but this methodology is limited because as a direct measure of clast surface exposure, it cannot determine when clasts were integrated as part of the boulder field itself and therefore dates obtained provide limited information about HRBF formation.

The studies mentioned above are generally supportive of the periglacial interpretation of HRBF formation and Smith's (1953) writings ruled out alternate formation hypotheses, but no study has been conducted that explicitly tests Smith's (1953) periglacial-allochthonous hypothesis. In the absence of studies to test this hypothesis, and, due to the presently contentious literature surrounding HRBF, this study is aimed at quantitative characterization of HRBF sedimentological properties. Recent studies have confirmed the operation of "periglacial form communities," groups of micro-meso-scale periglacial features that work to sculpt periglacial terrain over long timescales, in the generation of characteristic periglacial terrain

(Poser 1977; Karte 1979; Queen 2018; Brunnschweiler and Nelson 2022; Mitchell et al. 2023). Such studies provide additional support for the interpretation that an expansive feature such as HRBF was generated during peak periglacial activity. Another element that remains unexplored is the smaller adjacent limb of the boulder field. Several studies (e.g., Sevon, 1987; Denn et al., 2018) have noted that this component exists but very few include this smaller area in analysis. An investigation of all areas of HRBF is necessary for a holistic and thorough analysis of the feature.

Study Area

The Appalachian Highlands region is mountainous belt including the Blue Ridge, Ridge and Valley, and Appalachian Plateaus provinces extending in the USA from New England to Alabama (Fenneman, 1946; Thornbury, 1965). HRBF, located in the Pocono Plateau region of northeastern PA, (Figure 27) lies approximately 2 km south of the LGM margin (Smith, 1953; Denn et al., 2018; Merritts & Rahnis, 2022). Glacial erratics found south of the boulder field indicate that it may have been overridden or skirted by ice at least once (Denn et al., 2018).

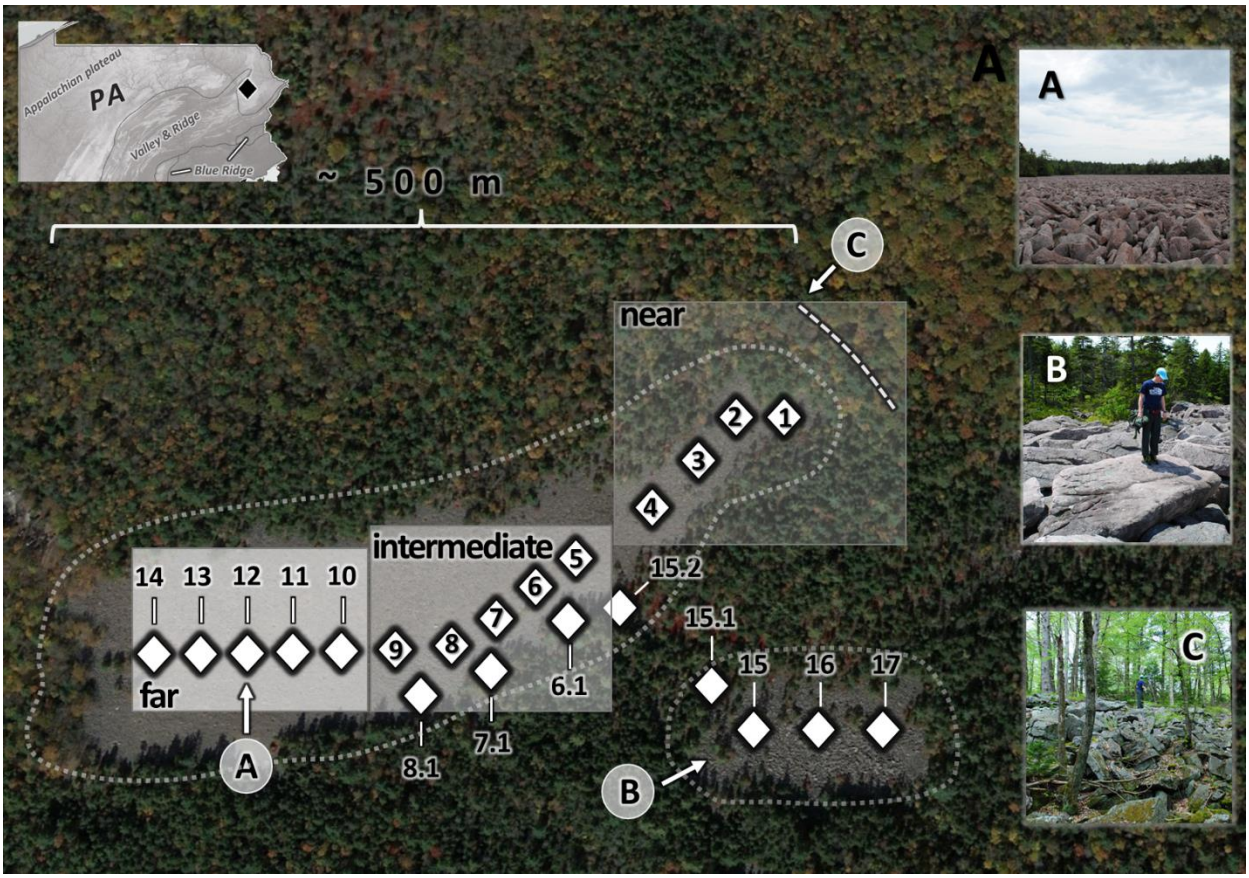

Figure 27. Aerial Imagery of the Hickory Run Boulder Field with site locations and on the ground characteristics. *The main extent of the primary and secondary (smaller) boulder fields are delineated by gray dashed lines. The long axis of the main field is ~500m, the axis of the smaller field is ~150m. Site locations are indicated by white diamonds. An inset map in the upper left corner of the figure shows the location of the Hickory Run Boulder Field in Pennsylvania, which is indicated by a black diamond. White shaded boxes delineate site groupings used for statistical analysis. (A) Ground view of the boulder field. Note the flatness of the field and lack of vegetation. (B) Typical boulder sizes in the smaller ancillary field, person for scale. Boulders in the minor field are generally larger than those found in the major field. (C) Parent bedrock outcrop, delimited by a white dashed line.*

HRBF occupies a flat (~1°) ~6.5 ha (550 x 120 m) area situated in a valley with gently sloping (~20°) walls (Smith, 1953). An eastern limb of the main boulder field section is separated by a strip of vegetation (Figure 27B). Surface clasts are covered with lichens and mosses, and vegetation in the form of forest is found only at the boulder field margins and a few "tree islands." Many of the boulders here are loosely packed and lack interstitial fines,

which are absent at shallow depths. The boulder field is surrounded by coniferous forest (*Web Soil Survey*, n.d.).

The surficial geology of HRBF is mapped as the Devonian age Duncannon Member of the Catskill Formation, which is an interbedded sandstone, siltstone, mudstone, and shale up to 30 meters thick (Smith, 1953; Geyer, 1969; Sevon, 1987; Reese, 2016; Denn et al., 2018). Boulders within the field are dominantly reddish-gray, medium-grained quarzitic sandstone conglomerate (Smith, 1953; Geyer, 1969; Sevon, 1987; Reese, 2016; Denn et al., 2018;) that is easily traceable upslope as lithology trails extending from the lower reaches of the boulder field upslope to the bedrock source area and surrounding valley walls (Smith, 1953). HRBF is underlain by gently folded, resistant Paleozoic sandstone and conglomerate (Denn et al., 2018). HRBF clasts achieve sizes of up to 6 meters with the largest clasts found in the smaller ancillary field (Figure 27B). Clast surfaces exhibit signs of chemical and physical weathering in place (e.g., lichen growth, pitting), which serves as an indication of the relict nature of the boulder field (Smith, 1953). The average thickness of HRBF is estimated to be between 3.0 to 3.5 meters (Sevon, 1987).

Methodology

Relative weathering indices

Sedimentological relative weathering indices and clast macrofabric data were collected from 22 locations in the boulder field (Figure 27) and are used to evaluate the hypothesis that frost-shattered rocks were carried downslope under the influence of periglacial mass movement, as posited by Smith (1953). Clast volume, shape, and rebound (hardness) relative weathering indices (Equations 2-4) have been used as sources of information to inform past

transport and depositional environments in glacial and periglacial contexts (King & Buckley, 1968; Barrett, 1980; Benn & Ballantyne, 1993; Evans & Benn, 2014, p. 78;). The relative weathering indices implemented here are based on clast volume, which is the foundation for calculations used to reflect clast shape; Cailleux flatness (Cailleux, 1947) and Krumbein sphericity (Krumbein, 1941). Indices were calculated as follows:

Volume $$a * b * c \quad (2)$$

Cailleux Flatness $$1000\left(\frac{a+b}{2c}\right) \quad (3)$$

Krumbein Sphericity $$\sqrt[3]{\frac{bc}{a^2}} \quad (4)$$

Where "a", "b", "c" refers to clast long, intermediate, and short axes, respectively.

Sampling sites were arranged to capture weathering trends 1) along the primary axis of the major boulder field; and 2) along the primary axis of the minor boulder field. Additional sites were established in the intervening areas between the major and minor boulder fields and along the main boulder field transect to investigate potential depositional and/or movement signals between the major and minor boulder fields. Multiple relative weathering indices were used to increase the interpretation strength of the indices and to facilitate comparison between data collected here and those published in the periglacial literature (King, 1966; Benn & Ballantyne, 1993; Evans & Benn, 2014). Sampling locations were spaced at 35 m intervals. Twenty-five clasts were measured at each of the sampling sites (Figure 27). Only the reddish-gray Catskill sandstone conglomerate clasts (the dominant lithology in the boulder field) were sampled. The HRBF is part of the Hickory Run State Park, which attracts tourists throughout the

year. Although modification, stacking, or defiling of clasts within the boulder is strictly prohibited, only the visibly largest clasts devoid of graffiti and/or other signs of human modification were measured from each sampling location to minimize the impacts of human interaction.

Relative weathering indices were analyzed, and descriptive statistics calculated. Data distributions for each of the indices were analyzed for normality for each individual site using the Shapiro-Wilk (Shapiro & Wilk, 1965) and Kolmogorov-Smirnov tests (with Lilliefors significance correction) (Lilliefors, 1967), both of which indicated non-normality for all indices across most of the sampling sites. A Humboldt Schmidt N-type hammer was used to measure clast rebound and, following the guidelines outlined in the rebound hammer user manual,[14] median hardness values (of the five taken for each clast across all sampling locations) were chosen for analysis to avoid the impact of large ranges of values that occur in some of the sampled data. This sampling procedure has been undertaken in other periglacial studies and is retained here as to facilitate comparison within the literature (Nyland & Nelson, 2019).

Ordinary least squares (OLS) regression analysis is used to model the relationships between an independent and dependent variable (Ostertagová, 2012) and was applied here to identify the relationship between relative weathering index median values and distance from the source outcrop Sites 1-14 along the main axis of HRBF. OLS is widely used and is performed by generating a “best fit” line that minimizes the error sum of squares (Ostertagová, 2012). The

[14] Humboldt Concrete Rebound Hammer (https://www.humboldtmfg.com/humboldt-concrete-rebound-hammer.html) model number H-2987H. Humboldt Construction Materials Testing Equipment, Humboldt Scientific Service Center 2525 Atlantic Ave., Raleigh, NC 27604.

regression analysis was performed in Google Colaboratory[15] using the 'scripy.stats module in Python, the 'np.polyfit()' function to identify the best-fit polynomial regression. Criteria used to identify the highest performing curvilinear regression model have been proposed (e.g., r-squared, adjusted r-squared, root mean squared error) (Gelman, 2007). The best-fit model code applied here identified the final regression model with the highest r-squared value that also minimized the number of constants to avoid overfitting the regression models (Gelman, 2007). Model residuals, the differences between the observed and predicted values (Gelman, 2007) were used to further assess model performance and to investigate underlying dynamics in weathering trends along the boulder field.

As an exploratory investigation of general weathering patterns across the main axis of the major boulder field, sites were split into near, intermediate, and far groups (Figure 27) to represent weathering patterns at increasing distances from the parent outcrop. Site groupings contained equal numbers of sites and relative weathering indices were treated with the Kruskal-Wallis test, the non-parametric alternative to the one-way analysis of variance test[16] (Kruskal & Wallis, 1952). Once this hypothesis testing was completed, groups with significantly different sample medians were treated with the Dunn test, a non-parametric multiple pairwise comparison procedure (Dunn, 1961). To complement statistical treatments, weathering index data were plotted for visual interpretation.

Clast macrofabric

[15] Google Colaboratory online coding console platform: https://colab.google/.

[16] Normality testing was performed using IBM SPSS software 23. https://www.ibm.com/spss.

Clast macrofabric analysis, the directional properties of particles that are visible to the unaided eye, has been used in Quaternary studies to yield information about former or present depositional processes and environments (Evans & Benn, 2014). Specifically, the orientation of the long (a) axes have been applied to reconstruct past ice flow directions and to identify features emplaced by periglacial processes in the geological past (Nelson, 1985; Mills, 1990; Evans & Benn, 2014). Clast macrofabrics can be analyzed in two dimensions (clast orientation about a compass dial) and in three dimensions (the intersection between clast dip relative to a horizontal plane and clast azimuth) (Evans & Benn, 2014).

Two-dimensional fabrics

Rose diagrams are commonly employed to aid the visual interpretation of two-dimensional (azimuthal) circular data (Hewitt et al., 2018) and are used here to assess clast orientation across sampled sites. Two-dimensional fabric data are axial, consisting of an undirected line with two possible values, e.g., both 90˚/270˚ (*Oriana Version 4 Users' Manual*, 2011), thus the application of statistical methods necessitates transformation of the data into directed form with only one possible value (Vollmer, 1995; *Oriana Version 4 Users' Manual*, 2011; NCSS Statistical Software, 2024). It is standard practice to transform the data by doubling the angles (modulo 360˚) to restrict the domain to half of the unit circle (e.g., 1˚-180˚) (Mardia, 1975; Mardia & Jupp, 1999; *Oriana Version 4 Users' Manual*, 2011; NCSS Statistical Software, 2024). This procedure preserves the direction of the data in a semi-circular space while also enabling the application of statistical tests of uniformity (*Oriana Version 4 Users' Manual*, 2011; Birch, 2018). After this transformation the HRBF data are restricted to the interval [1,180]. To

enhance the interpretation of uniformity test outputs, data can be normalized by then dividing the transformed data by 180, thus restricting the data to the interval [0,1] (Birch, 2018).

Three-dimensional fabrics

Three-dimensional fabric data representing clast a-axis orientation about a 360-degree compass dial (azimuth) and angle in relation to a horizontal plane (dip) were plotted graphically and treated statistically. Equal area projections (nets), also referred to as Schmidt nets, are diagrams used to represent clast macrofabric data, where each data point is represented as a point on the projections (Evans & Benn, 2014). Visual interpretation of Schmidt nets generated using HRBF data was augmented by employing the Kamb contour line method labeled in two standard deviation units that indicate the statistical significance of point clusters (Kamb, 1959; Vollmer, 1995; Cardozo & Allmendinger, 2013; Evans & Benn, 2014).

Statistical analysis of HRBF clast three-dimensional macrofabrics included implementation of the eigenvalue method (e.g., Mardia, 1972), whereby observations are resolved into three orthogonal, normalized eigenvectors that represent the primary axes of data clustering (Millar & Nelson, 2001; Evans & Benn, 2014). As such, eigenvalues indicate macrofabric shape, a parameter that can be used to compare datasets across different environmental settings (Woodcock, 1977; Millar & Nelson, 2001). Eigenvalues were analyzed statistically using Bingham's U tests statistic a test of uniformity for axial data where the uniformity hypothesis is rejected if the sample eigenvalue scatter matrix displays departures from the expected value (Bingham, 1974; Mardia 1975; Mardia et al., 2000). Bingham's U has been applied in periglacial settings to analyze the hypothesis that clast orientation of periglacial patterned ground display significantly departures from uniformity (Nelson, 1982a, 1982b) and is

used here to assess departures from uniformity in samples taken from HRBF. Bingham's U (Equation 1).

The eigenvalue method used to evaluate clast shape and strength is useful for hypothesis testing but is limited in the sense that interpretation of statistical results and raw values can be difficult in the context of comparison with findings from other environments. The limitation is introduced because graphical representation is difficult where three variables must be displayed (Woodcock, 1977). Woodcock log ratio plots are two-axis representations of eigenvalues generated by taking the natural log ratios of the three principal eigenvalues derived from clast a-axis macrofabric data (Woodcock, 1977). Woodcock plots facilitate fast interpretation of clast orientation and strength and provide a graphical space to plot data from different environments for comparison (Millar & Nelson, 2001). Woodcock plots are used here to support visual interpretation of clast fabric strength and shape.

Results

Relative weathering indices

Relative weathering indices plotted by site with increasing distance from the traceable local bedrock outcrop, are summarized in Figure 28. Graphics were generated using Grapher 22 software[17]. Polynomial regression statistics used to summarize trends in relative weathering indices along the main field are provided in Table 7. Regression residuals are summarized in Figure 29. Relative weathering indices for sites not included in the polynomial regression analysis are summarized in Table 8.

[17] Golden Software, Grapher: https://www.goldensoftware.com/products/grapher/.

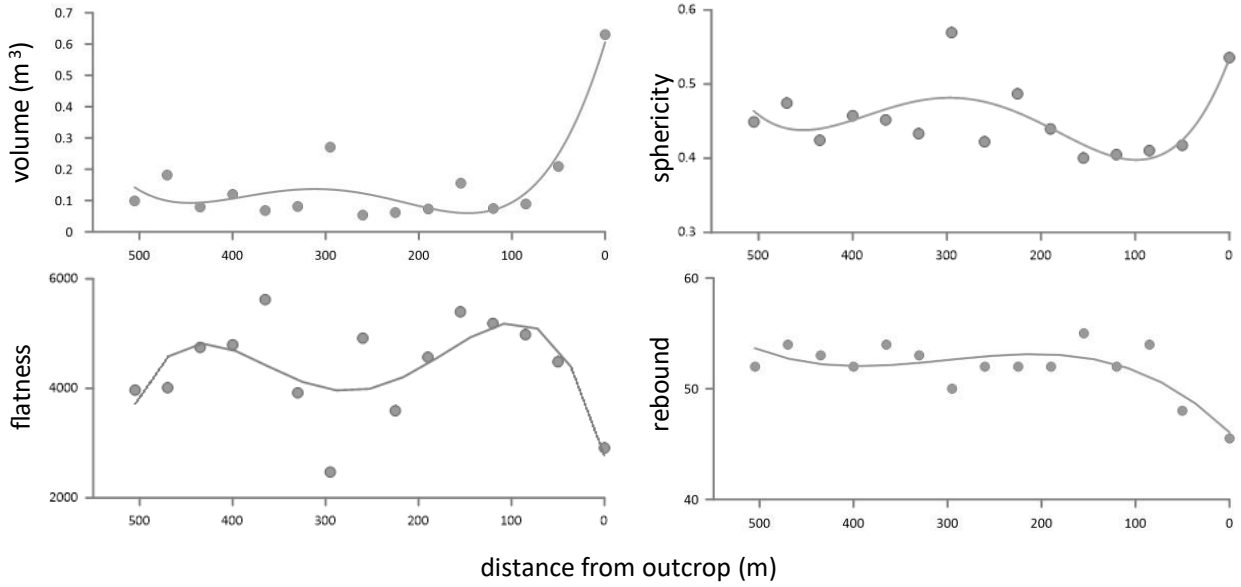

Figure 28. Relative weathering indices from sites 1-14 and distance from local outcrop. *The "0" distance from outcrop indicated data sampled from the local bedrock outcrop. Gray lines represent polynomial regression fit, details in Table 7.*

Table 7. Statistical output of polynomial regression fits for each relative weathering index.

Index	Polynomial Fit Degree	p-value	r-squared
volume	4	<0.0001	0.828
flatness	4	0.0042	0.480
rebound	3	0.0008	0.726
sphericity	4	0.0024	0.521

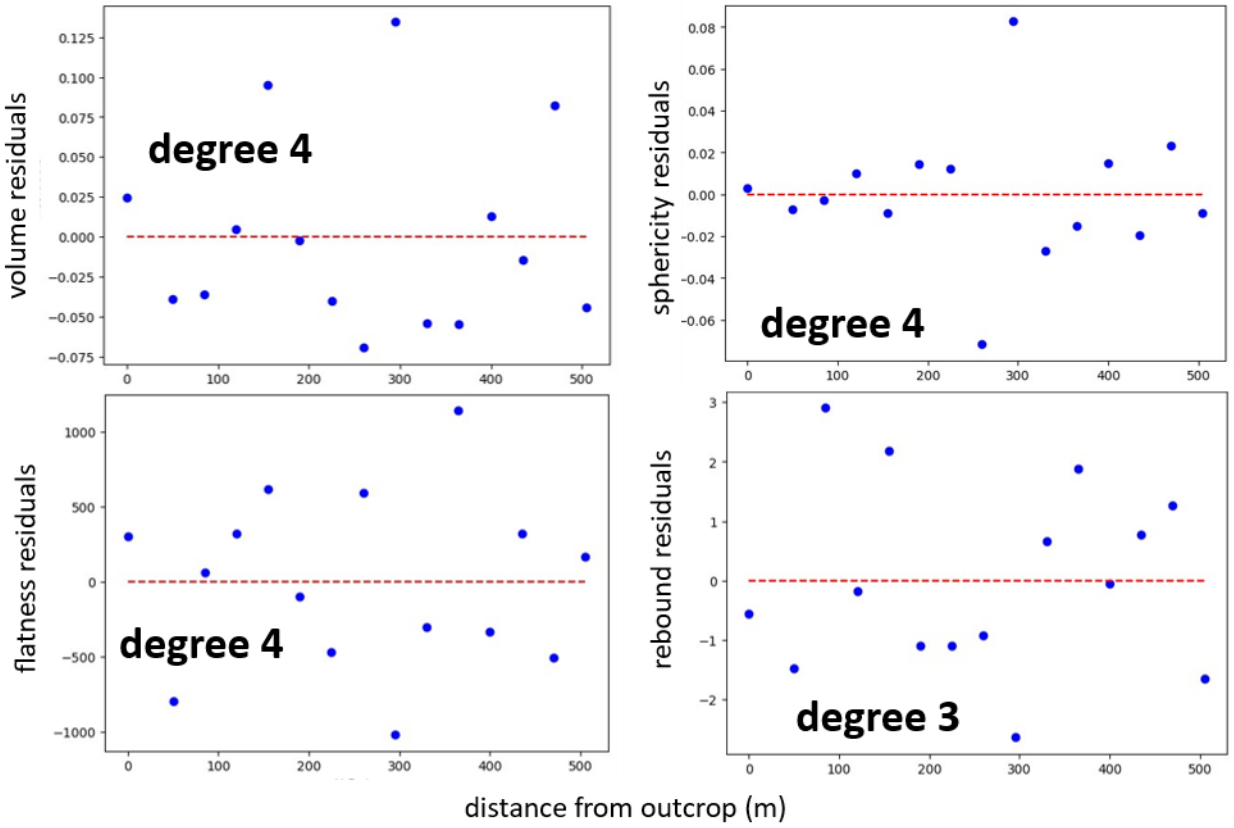

Figure 29. Relative weathering regression residuals. *Residuals were plotted using the Google Colaboratory platform. The degree of each regression model is indicated on the graphs.*

Most of the relative weathering indices show good agreement with one another, and polynomial regression of relative weathering indices reveal dynamic trends in clast weathering with distance along the major axis of the boulder field. Polynomial regression curves indicate that the nonlinearity of weathering trends with distance from the local outcrop. Although weathering appears to be greater at the distal end of the boulder field, relative weathering indices show disturbances in the patterns near intermediate sites, i.e., Sites 6, 7, and 8. Assessment of model residuals show departures from model prediction power near intermediate sites, especially near site 8, which has much larger, more spherical, less flat, and slightly softer clasts relative to clasts sampled from other sites. This outcome may reflect the integration of clasts from the minor field by way of "tributary-like" movement of clasts from the minor field. Table 8 summarizes relative weathering indices from Sites 15-17 in the smaller field. Comparison between data from these sites and values obtained from the intermediate

sample sites in the main boulder field confirm similarities in clast characteristics between Sites 15-17 and Sites 6-8.

Table 8. Median relative weathering data from sites 6.1-17.

Site	Volume (m^3)	Sphericity	Flatness	Rebound
6.1	0.0070	0.5152	3111	50
7.1	0.0395	0.5048	3028	48
8.1	0.0114	0.4919	2909	50
15.1	0.1059	0.5500	2125	52
15.2	0.0100	0.4994	2278	51
15	1.2375	0.5196	2944	50
16	2.7585	0.5566	3379	48
17	1.9944	0.4804	3163	46

Clasts in the minor field are much larger than those encountered in the main field. Sites closer to the minor field but in the major field are also larger than clasts encountered at other sites along the primary axis of the field. Table 8 also shows that clasts are of similar sphericity to those sampled from the minor field, indicating that clasts may have been derived from the minor boulder field area.

Statistical output from pairwise Kruskal-Wallis testing is summarized in Table 9 Statistical comparison of areas in HRBF show the significant differences between clast weathering depending on location within the boulder field. Specifically, differences in clast weathering are encountered between the near and intermediate areas of the boulder field where clasts may have been incorporated from the minor boulder field area.

Table 9. Results of HRBF relative weathering indices pairwise Kruskal-Wallis testing procedures. *The results of post-hoc pair-wise testing are shown below. Only those indices with significant differences between median population values were treated with post-hoc analyses.*

Site Comparison	Test Statistic	Significance	Adjusted Significance	Reject/Fail to H_o[†]
Volume				
Intermediate - Far	-25.5	.054	0.16	Fail to reject
Intermediate - Near	58.6	<.001	0.000	Reject
Far - Near	33.1	.015	.044	Reject
Sphericity				
Intermediate - Far	22.7	.086	.258	Fail to reject
Intermediate - Near	-48.5	<.001	.001	Reject
Far - Near	-25.7	.059	.176	Fail to reject
Flatness				
Intermediate - Far	-43.4	.001	.003	Reject
Intermediate - Near	47.3	<.001	.003	Reject
Far - Near	3.82	.779	1.00	Fail to reject

Clast macrofabric

Two- and three-dimensional clast macrofabric data are summarized graphically in Figures 30-34. Rose diagrams generated using Grapher software with a bin width of 10˚ were chosen to visualize the two-dimensional data. Schmidt nets were generated in InnStereo[18] and contoured using the Exponential Kamb Method to aid assist visual impression of the nets (Kamb, 1959; Vollmer, 1995; Evans & Benn, 2014). Contours were plotted at two standard deviation intervals and serve as an indication of point density statistical significance (Evans & Benn, 2014). Uniformity testing 3-D (Bingham's U) were performed using Oriana software[19] and are summarized in Table 10. A Woodcock log-ratio plot generated using Grapher software is shown in Figure 35.

[18] InnStereo Software stereographic projections for structural geology: https://innstereo.github.io/.

[19] Oriana circular statistics software version 4: https://www.kovcomp.co.uk/oriana/.

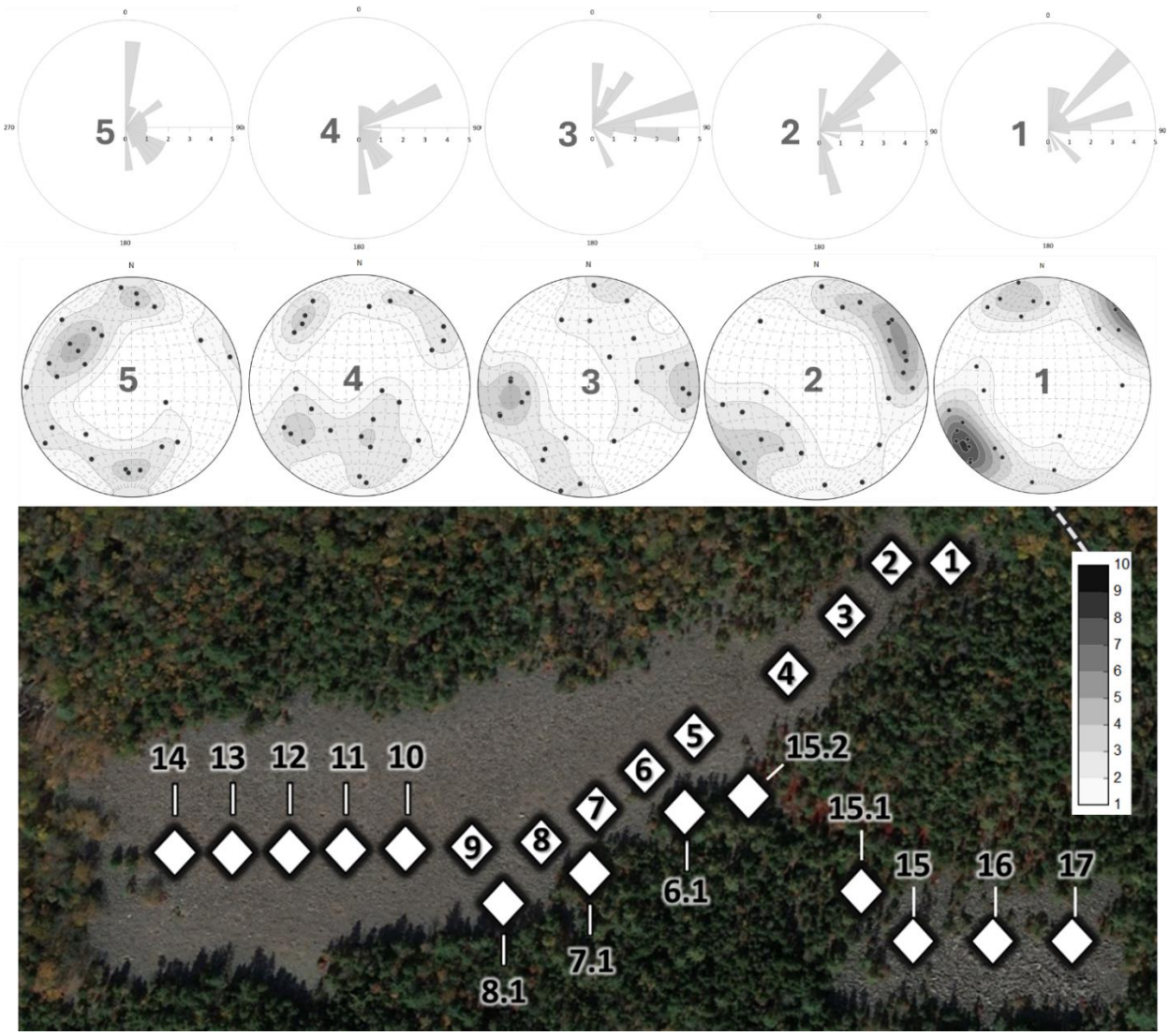

Figure 30. Rose Diagrams and Equal-area Schmidt nets show 2 and 3-dimensional fabric, respectively, for sites 1-5. *Two-dimensional data are shown in rose diagrams with bins set at 10˚ intervals. Clast three-dimensional data are plotted on Lambert Equal-Area projections. Isotropic fabrics are displayed as an even distribution of points across the Schmidt net, in girdles points are concentrated in bands following great circles of the projection, and clusters are points confined to discrete locations in the sphere (Evans & Benn, 2014). Schmidt net contours were generated using the Exponential Kamb method (Kamb, 1959; Vollmer, 1995) and were plotted at 2σ intervals.*

The surface of HRBF near Sites 1-5 has a gentle northeast-southwest orientation (Sevon, 1987). Fabrics obtained from these sites, especially Sites 1 and 2, show strong bipolar alignment with the local alignment of HRBF, which would be expected under the interpretation of clast

liberation from the local bedrock outcrop and flow downslope. Two-dimensional fabrics from Sites 3-5 display a progressively developed alignment orthogonal to the local slope. In three dimensions, Samples 3-5 show a progressively developing girdle tendency, which transitions to a more chaotic pattern near Sites 7 and 8.

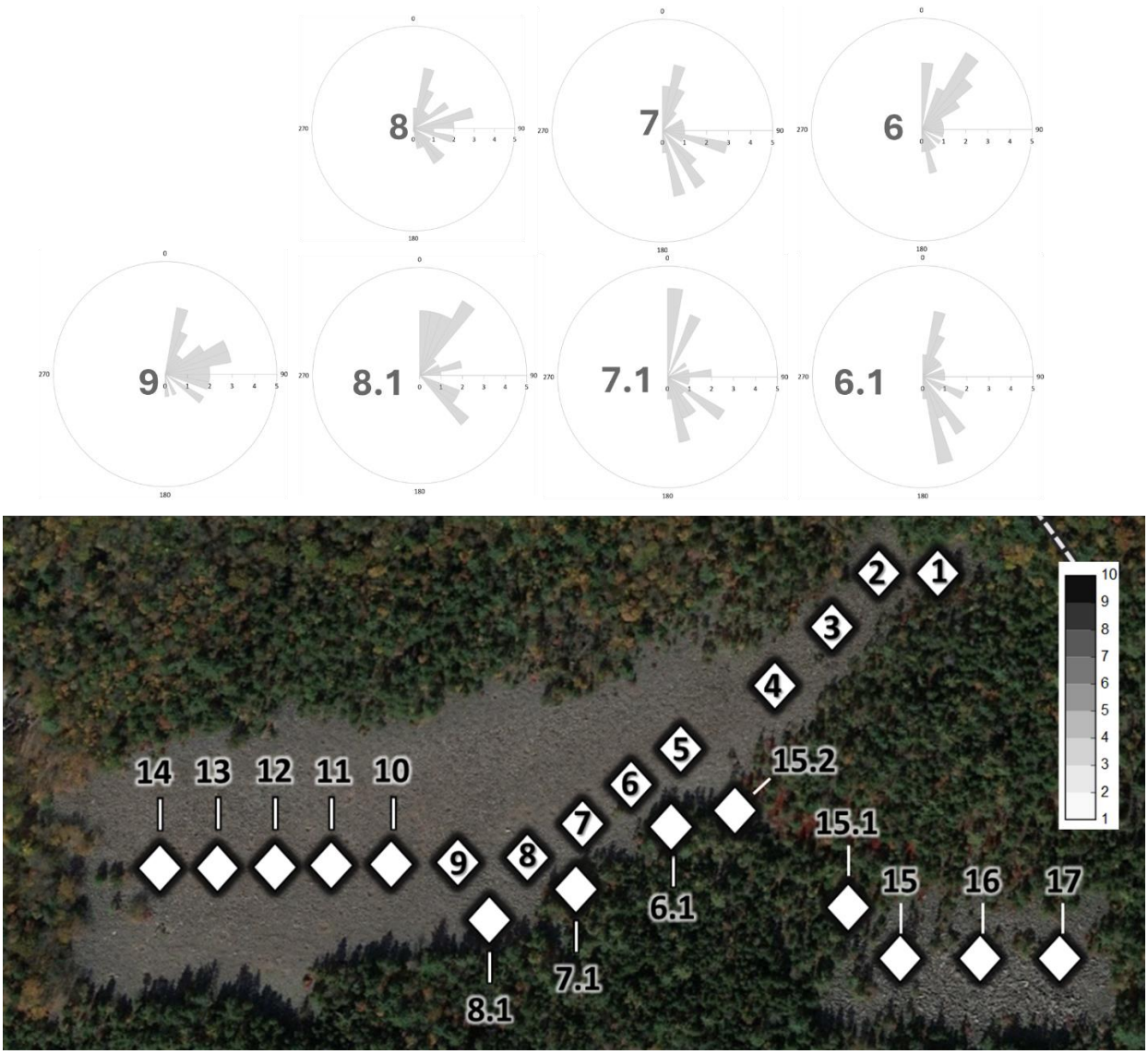

Figure 31. Rose diagrams showing 2-dimensional fabric for sites 6-9. *Two-dimensional data are shown in rose diagrams with bins set at 10˚intervals.*

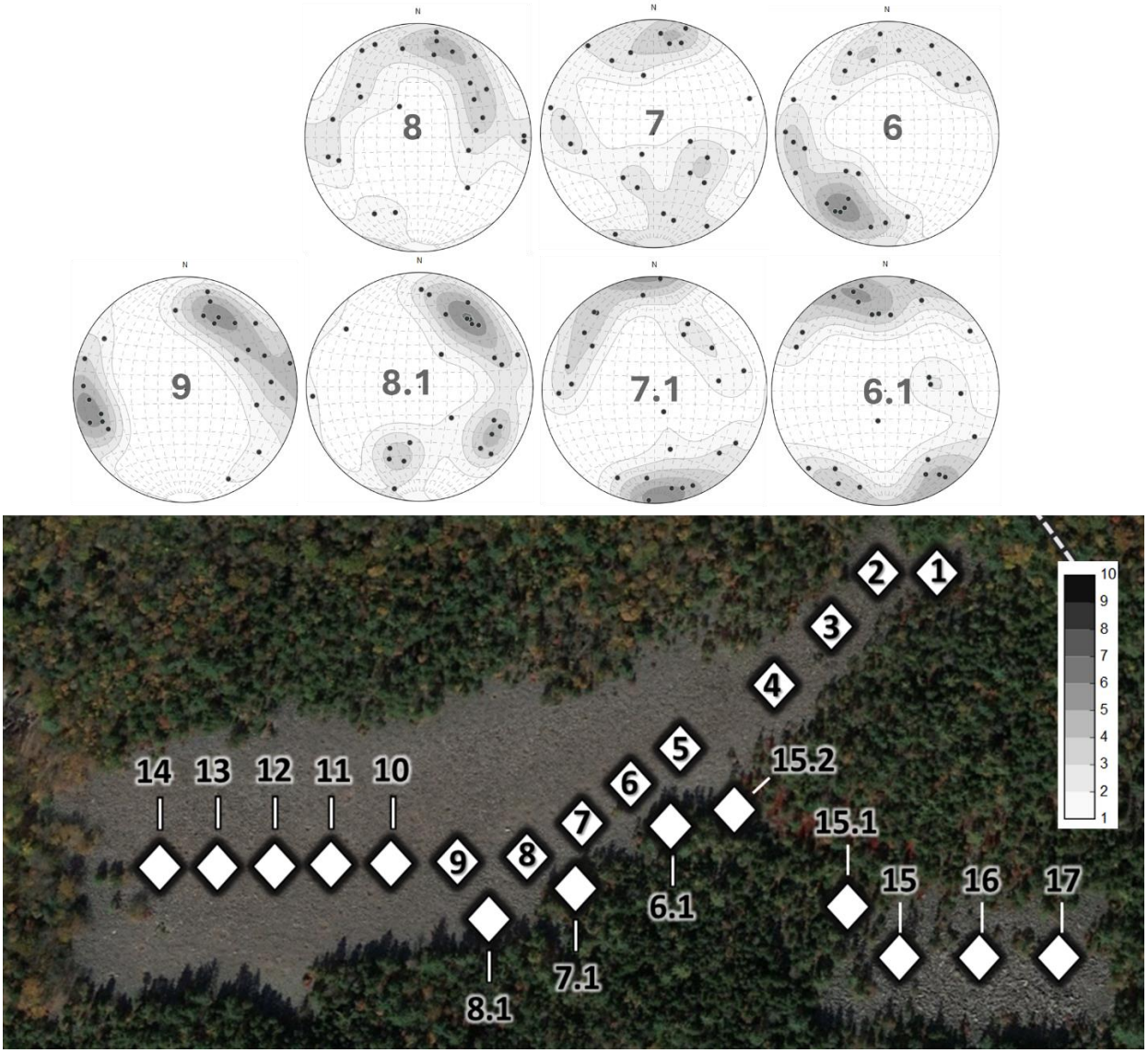

Figure 32. Equal-area Schmidt nets showing 3-dimensional fabric for sites 6-9. *Two-dimensional data are shown in rose diagrams with bins set at 10˚ intervals. Clast three-dimensional data are plotted on Lambert Equal-Area projections. Isotropic fabrics are displayed as an even distribution of points across the Schmidt net, girdle shapes are characterized by an even distribution of points on the outside of the sphere, and clusters are points confined to discrete locations in the sphere (Evans & Benn, 2014). Schmidt net contours were generated using the Exponential Kamb method (Kamb, 1959; Vollmer, 1995) and were plotted at 2σ intervals.*

Site 6 continues the girdle pattern but has a strong secondary mode aligned with the local slope. Conversely, Sites 7 and 8 display less defined clusters and appear to have very little dominant orientation in both two and three dimensions. Sites 6.1, 7.1, 8.1, and 15.2, taken

parallel to Sites 6-8, but lying closer to the minor boulder field, show girdle tendencies but with some modes aligned orthogonal to the margin of the boulder field and to fabrics obtained upslope. These fabrics reflect progressive entrainment of clasts from the smaller field into the main field. Fabrics from sites closest to the minor field are observably different from those obtained upslope along the main axis of the boulder field, suggestive of a disturbance in the intermediate area of the boulder field. This finding agrees with relative weathering indices, which also indicate disruption to general trends near the middle of the major boulder field, which becomes a major feature of the HRBF data in the vicinity of Sample 8. Fabric data from Site 9 appear to "re-form" the bipolar pattern and show alignment with the local orientation of the major field.

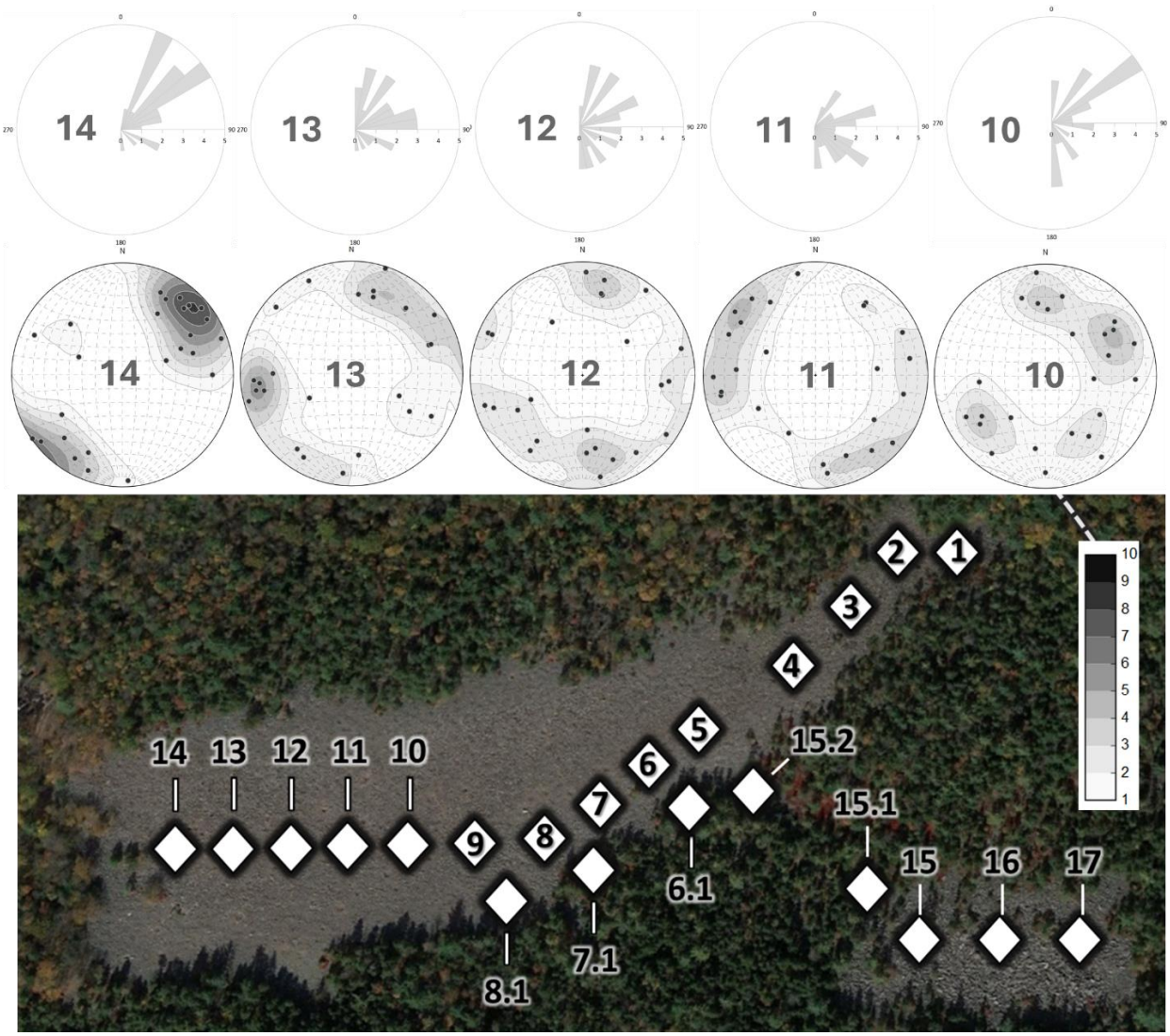

Figure 33. Rose diagrams Equal-area Schmidt nets showing 2 and 3-dimensional fabric for sites 10-14. *Two-dimensional data are shown in rose diagrams with bins set at 10˚intervales. Two-dimensional data are shown in rose diagrams with bins set at 10˚ intervals. Clast three-dimensional data are plotted on Lambert Equal-Area projections. Isotropic fabrics are displayed as an even distribution of points across the Schmidt net, girdle shapes are characterized by an even distribution of points on the outside of the sphere, and clusters are points confined to discrete locations in the sphere (Evans & Benn, 2014). Schmidt net contours were generated using the Exponential Kamb method (Kamb, 1959; Vollmer, 1995) and were plotted at 2σ intervals.*

Clast fabric from Site 10 degenerates into a multimodal distribution, indicating an impediment to flow or other disturbance in the immediate vicinity; note that clasts from this sample dip more steeply than in surrounding samples. Weak horizontal girdles are apparent at

Sites 11 and 12, reflecting the continuing but diminishing effects of the impediment near Site 10 Fabrics from Sites 13 and 14 re-aligne with boulder field local orientation. Sevon (1987) reported fabric data from some locations in the HRBF. Fabrics obtained from a site near Site 12 here, also appear unorganized, and depart from samples obtained from fabrics upslope (Sevon, 1987), indicating the presence of another impediment to flow.

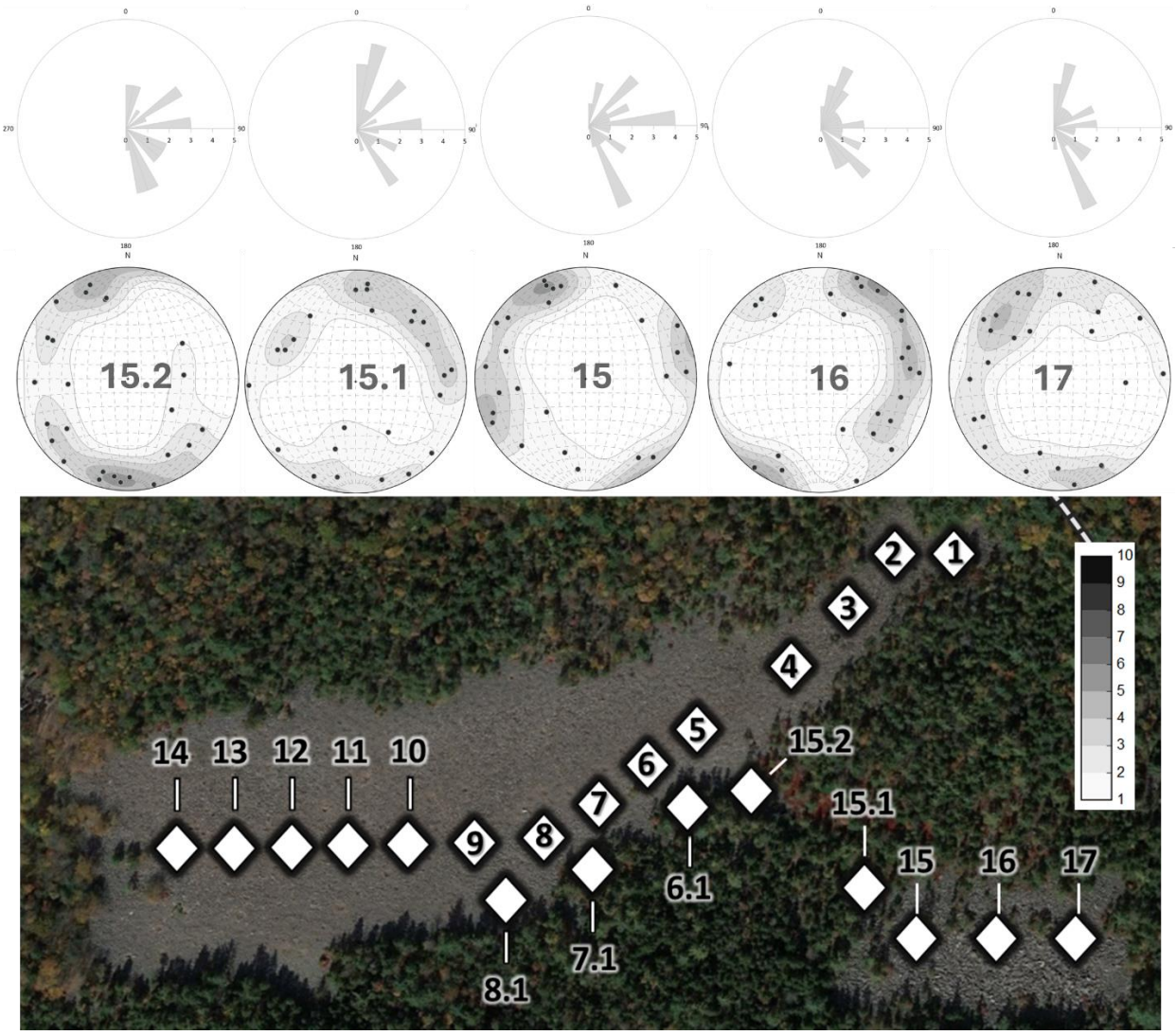

Figure 34. Equal-area Schmidt nets showing 2 and 3-dimensional fabric for sites 15-17. *Two-dimensional data are shown in rose diagrams with bins set at 10˚intervales. Two-dimensional data are shown in rose diagrams with bins set at 10˚ intervals. Clast three-dimensional data are plotted on Lambert Equal-Area projections. Isotropic fabrics are displayed as an even distribution of points across the Schmidt net, girdle shapes are characterized by an even distribution of points on the outside of the sphere, and clusters are points confined to discrete locations in the sphere (Evans & Benn, 2014). Schmidt net contours were generated using the Exponential Kamb method (Kamb, 1959; Vollmer, 1995) and were plotted at 2σ intervals.*

Three-dimensional fabrics obtained from Sites 15-17 in the small field form weak girdles, but with statistically significant departures from uniformity. Clasts here are much larger than those in the main field and may have been resistant to strong clast alignment with the local orientation of the field. Girdle patterns from clasts sampled in the minor field indicate that

clast orientation is roughly parallel to the ground surface (e.g., approaching lying flat relative to a horizontal plane) and may indicate a "settling" of clast depositional signal. Settling could have occurred following deglaciation and permafrost as ground ice melted and interstitial material was flushed from the boulder field, as suggested by Smith (1953).

Table 10. Macrofabric eigenvalue data and results of Bingham U Statistical testing.
Eigenvalues were calculated using InnStereo stereographic projection programming software. Bingham's U test was used to test the null hypothesis that clast macrofabric were drawn from a uniform distribution at the 0.05 alpha level. Values with an asterisk indicate statistically significant fabrics in which the hypothesis of uniformity may be rejected.

Site	$\bar{\tau}3$	$\bar{\tau}2$	$\bar{\tau}1$	Bingham's U
1	0.555	0.263	0.182	0.577*
2	0.594	0.288	0.118	0.872*
3	0.468	0.274	0.258	0.205
4	0.454	0.291	0.255	0.169
5	0.428	0.381	0.191	0.236
6	0.558	0.316	0.126	0.703*
6.1	0.559	0.286	0.155	0.637*
7	0.451	0.281	0.268	0.156
7.1	0.531	0.282	0.187	0.473*
8	0.47	0.344	0.186	0.304
8.1	0.488	0.37	0.142	0.464*
9	0.595	0.302	0.103	0.919*
10	0.453	0.328	0.218	0.207
11	0.522	0.309	0.169	0.474*
12	0.453	0.359	0.189	0.269
13	0.525	0.304	0.171	0.480*
14	0.674	0.176	0.15	1.308*
15	0.494	0.396	0.109	0.600*
15.1	0.471	0.368	0.161	0.374
15.2	0.523	0.329	0.147	0.530*
16	0.478	0.413	0.109	0.582*
17	0.488	0.37	0.142	0.464*

Statistical treatment of the 3-dimensional data summarized in Table 10 highlight areas in the field where clast samples depart significantly from uniformity, the hypothesis that points are distributed equally about a unit circle (Bingham, 1974). Statistically significant fabrics were

obtained from upslope areas of the main field near Site 1, within the minor field, and from downslope areas of the major field. Significant U values represent departure from uniformity and lend support for the interpretation that clast macrofabrics may be attributable to paleodepositional processes. Significant fabrics from the upslope and downslope areas in the major field are characterized by clusters showing the dominant flow direction of clasts while girdle and random fabrics from intermediate areas in the main field indicate a strong disturbance to clast orientation, likely due to an obstruction imposed by the much larger clasts moving from the minor to the main field. The results of the Woodcock plot highlight this pattern of variation in fabric shape for areas in the main and minor boulder field (Figure 35).

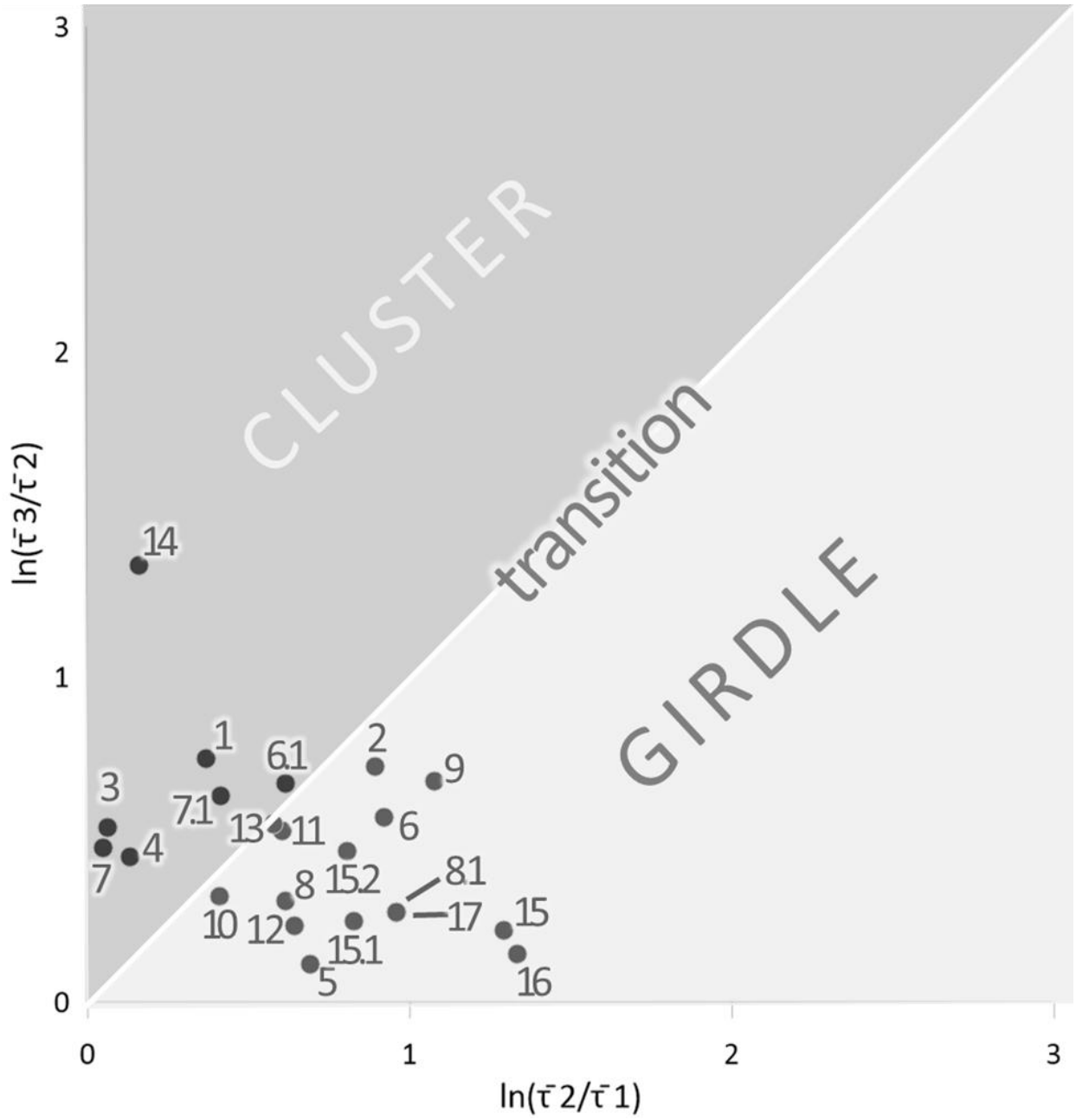

Figure 35. Woodcock Plot (Woodcock, 1977) showing clast macrofabric shape. *Data are shown as two-axis logarithmic plot of ratios of normalized eigenvalues τ3, τ2, τ1. Individual data points are labeled. The transition line, labeled, indicates the region in eigenvalue space where clast fabrics above and below the transition line represent cluster or girdle shapes, respectively. The distance from the graph origin is directly proportional to fabric strength; uniform distributions plot at the graph origin whereas progressively stronger preferred clast orientations plot further from the origin (Woodcock, 1977).*

Woodcock plots facilitate quick comparison of clast macrofabrics (Woodcock, 1977). The plot generated using HRBF data shows that upslope and downslope fabrics tend to be cluster and cluster/transition shapes. Fabrics from the minor field and from the intermediate area of the main field tend towards girdle shapes. The spatial dichotomy of the two dominant patterns observed in the HRBF area provide strong support for the interpretation that clasts moved downslope (strong cluster shapes) and that this downslope activity was disrupted by clasts mixing and "backing up" because of clast integration from the minor field.

Discussion

Relative weathering indices and fabric data collected for this study were analyzed statistically to test the allochthonous formation hypothesis. All the relative weathering indices show good agreement with one another, and polynomial regression of relative weathering indices reveal dynamic trends in clast weathering with distance along the major axis of the boulder field. Anomalous values from samples in the intermediate portion of the field are in line with relative weathering values obtained from the minor boulder field. These trends are evidence for the contribution of clasts from the minor to the major field. The integration of clasts from the minor field appears to have been accomplished via "tributary" flow during the height of periglacial conditions in the Last Glacial Maximum. Three-dimensional clast macrofabric data reveal that clast orientation tends to align with the major axis of the field, although statistically significant two-dimensional fabrics were found primarily in data obtained from the head and tail of the boulder field, with bimodal and more chaotic patterns in the area where the two components of the field merge. The integration of clasts from the smaller field into the primary boulder indicates piling up of clasts near the middle of the sampled site

transects. Fabrics show strongly clustered patterns, with the primary modes parallel to the boulder field's major axis in sites near the upper reaches of the field. Toward the middle of the main field fabrics disassemble or "smear," forming girdle patterns. From Sites 9 onward, clustered fabrics appear to "re-form" again in alignment with the primary axis of the field. Statistical analysis of three-dimensional data conforms with the hypothesis that sampled clasts do not display uniformity, thus indicating the effects of mass-movement within the boulder field. Disrupted fabrics from the middle of the main boulder field were also found from samples taken by Lehigh University students in 1975 (Sevon, 1987).

The results of this work lend support to the assertion that HRBF is a time-transgressive surface, having been formed under the influence of periglacial weathering mass transportation processes. Relative weathering and fabric data reveal the physical characteristics of the boulder field, which are typified by strong clast orientation and increased weathering with distance from the boulder field. These findings are in alignment with absolute dating efforts that indicated increased weathering along the long axis of the boulder field and increased roundness with distance from the traceable bedrock outcrop (Smith, 1953; Sevon, 1987; Potter & Helmke, 2007; Denn et al., 2015, 2018).

The collective data representing the major and minor fields, including the areas intermediate between the major and minor fields are strong evidence for a "tributary-like" conjoining of the major and minor fields, and for HRBF having formed through mass movement. Further, the fine spatial resolution of data sampled reveals that the HRBF surface is a dynamic and resistant feature. The results of this work complement absolute dating efforts and qualitative observations of the boulder field by providing a quantitative basis for the assertion

that HRBF was formed through emplacement under periglacial conditions. This interpretation is in line with the allochthonous formation hypothesis first posited by Smith (1953). The results of this work also lend support for the reevaluation of other allochthonous boulder fields in the context of paleoclimatic interpretation in the eastern U.S. The results of this work are interpreted as supportive of the notion that during development, the HRBF formed under extreme periglacial and permafrost conditions achieved during the LGM. Due to proximity to the Laurentide Ice Sheet margin, shallow permafrost along with highly effective frost weathering would have provided the conditions necessary for HRBF formation by promoting slow flow of liberated clasts from upslope bedrock moving within a matrix of finer material. Similar conclusions have been drawn from active periglacial regions. Amelioration of the climate following the LGM would have provided an abundance of meltwater that could work to "flush" out the interstitial material. Clast macrofabrics obtained from the HRBF were not of the same strength as those obtained from active periglacial environments, although this is to be expected considering that HRBF is a relict feature and that clast fabric deteriorated (tilted) following permafrost thaw, melting of ground ice, and interstitial material flushing. Support for this interpretation is described by Delcourt & Delcourt (1988), who through a paleoecological study employing spatial analytic methods on periglacial feature elevations derived results indicating that solifluction and active colluvial movement of boulder streams were the predominant geomorphic processes through the late-glacial interval. Elaborations provided detail that a decreased frequency and intensity of freeze-thaw cycles resulted in the stabilization of slopes and inactivation of boulder streams and that both geomorphic and ecological thresholds were crossed following the amelioration of the climate (Delcourt &

Delcourt, 1988). Additional paleoclimatic information and understanding of regions adjacent to the LGM margin offer further support for a paleoperiglacial interpretation of HRBF formation because the location of the boulder field (within 2 km of the LGM margin) would have meant that intense katabatic winds flowing off the ice sheet (Merritts & Rahnis, 2022). These intense periglacial conditions that persisted throughout the Pleistocene would have contributed to periglacial mass movement even under the gentle slope that characterizes the HRBF. Boulder fields in other well-studied periglacial regions such as the Falkland Islands and other boulder fields in the Appalachian Highlands, occupy similarly shallow valley bottoms, and span areas of up to several kilometers (Potter & Moss, 1968; Merritts & Rahnis, 2022 and references therein).

Conclusions

The Hickory Run Boulder Field is the most impressive boulder (block) field in the contiguous United States and has been the subject of study since the 1950s (Smith, 1953). Most studies of HRBF have been qualitative and findings from recent studies are not diagnostic of formation (Sevon, 1987; Helmke et al., 2007; Potter & Helmke, 2007; Denn et al., 2018). Relative weathering indices employed here reveal dynamic clast weathering and gradual increases in weathering with distance from local outcrops. Relative weathering indices, complemented by clast macrofabric data, also indicate that the integration of clasts from the minor boulder field occurred, offering strong additional support for the interpretation of emplacement by mass movement. Macrofabrics show that clast orientation agrees with the local slope and boulder field orientation in parts of the field unaffected by merger of the main and secondary fields. Overall, relative weathering and macrofabric data lend support to the hypothesis that HRBF formed as an allochthonous feature.

The findings summarized here also align with constraints on hillslope evolution and erosion for areas south of the LGM margin in central PA that emphasize increases in erosion during Pleistocene shifting from interglacial to periglacial conditions (Delcourt & Delcourt, 1988). The results of this work on the HRBF indicate that periglacial conditions during the Pleistocene were attributable to intense erosive activity, leading to significant landscape modifications. These results agree with findings from active periglacial regions, where recent relative and absolute dating efforts indicate that periglacial mass-movement and frost-weathering processes are attributable to long-term erosion, giving rise to entire landscapes (Nyland & Nelson, 2020; Queen & Nelson, 2022). In addition to the untapped geomorphic information of the Hickory Run Boulder Field, HRBF is also an important component of the Hickory Run State Park. This state park, like many around the country, is an area of conservation, education, and recreational engagement. Efforts to better understand the constituent natural elements of this major park have vast implications for the continuing dedication to education and conservation efforts undertaken to preserve this historical landscape.

The research presented here represents an important contribution to research on HRBF but as with any field-based study, there were limitations to the work related to methods employed and assumptions about HRBF geomorphology. A potential source of error in this study stems from the fact that the HRBF is a relict feature and has presumably been inactive for at least 10ka. In addition to the fact that the boulder field is a public landmark, there may have been alterations to the boulder field coming from human interference or general dampening/settling out of clasts in the boulder field which could impact clast orientation.

Future research on the HRBF should focus on obtaining additional samples from the boulder field to investigate clast dynamics along the intermediate axis of the feature.

CHAPTER 6. CONCLUSIONS

Summary of Findings

This dissertation contributes to understanding the characteristics and origins of periglacial terrain. Chapter 2 showed that periglacial feature elevations follow trends outlined in the European literature, which are characterized by increased feature elevations with decreases in latitude. Results also showed that periglacial feature elevations generally follow the elevation of the 0˚ MAAT line, thus indicating a climatic interpretation of the archived features. Insight gained from Chapters 3 and 4 show that upland periglacial terrain can be conceptualized in terms of facies, which are surface deposits distinguishable on the basis of sedimentological data and associated closely with specific slope facets. Facies identified include the scarp, upper side slope, and tread components, and analyses of these regions showed good alignment with previous studies highlighting the time-transgressive nature of cryoplanated terrain. Methodology outlined in Chapters 3 applied to Chapter 4 showed how field data and periglacial facies conceptual background can be used to set up a study focused on a hypothesized relict feature. Although facies analysis and sedimentological data alone cannot be diagnostic of feature origin, the results here highlight the utility of relict-modern comparative studies to provide insight to the potential climatic background of a feature. These chapters contribute to the body of work underpinned by the postulations of von Łoziński (1909, 1912) who first outlined the occurrence and areal distribution of periglacial facies.

The penultimate chapter of this dissertation addresses the Hickory Run Boulder Field. Methodology used on Chapters 3 and 4 informed work at the HRBF because the sedimentological data proved useful in the study of hypothesized time-transgressive surfaces.

Results from Chapter 5 lend support for the original hypothesis from Smith (1953), who asserted that the HRBF likely formed during the most recent cold interval under periglacial influences and that later climate warming would have facilitated conditions favorable for the flushing of fine-textured material from the boulder field.

This dissertation highlights the utility of incorporating large temporal and spatial scale components into periglacial research. The large spatial scale of this study, which spanned from the eastern USA into the interior of Alaska, facilitated comparison of relict and periglacial environments not previously undertaken for upland cryoplanated terrain. Here, both the investigation of periglacial facies and geographical periglacial geomorphology concepts were effective in "linking" not only periglacial processes to landscape evolution, but both concepts provided frameworks for thinking about the ways in which process relates to scale and overall landscape evolution pathways. Temporally, this study utilized relict and modern climate features to reveal formation processes. In addition, the temporal span of this work creates a linkage from a century-old concept to contemporary research contexts. Findings from this work show how foundational geomorphological theory influences and can inform contemporary work.

Comments on Areas for Improvement and Future Research

Constraints on the research presented here surround limitations on the amount of data collected and the methodology employed. Specifically, as the macofrabric analysis method in periglacial contexts remains understudied, there are no widely accepted standards for sample sizes and field design that appear in the literature. This lack of standardization makes it difficult to compare results across studies and environments. More samples from additional

cryoplanated uplands are needed to add to the inventory of sedimentological data on these regions. Additional CT facets cited in the literature include lower side-slope areas (Brunnschweiler & Nelson, 2022), which should be subjected to similar methodological treatments to encompass entire CT sequences. More periglacial feature elevations and locations should be added to the database generated here and additional efforts might include field visits to ground truth features identified using aerial imagery. At the HRBF, additional sampling transects, or grid sampling of the main field may provide more insight into surface dynamics related to formation. Overall, the methodologies employed in this work should be applied to other periglacial areas to test the applicability of sedimentological data to identify periglacial terrain.

Future work should also focus on applications of clast macrofabric analysis in periglacial settings given the utility of this methodology in elucidating past depositional processes (e.g., Millar & Nelson, 2003; Millar, 2006; Nelson, 1982). Future analyses would also focus on other periglacial regions to initiate a formalized repository of periglacial macrofabrics. Finally, more work on the etymology of von Łoziński's periglacial facies concept is needed before the term can be widely implemented in periglacial studies. Advancing understanding of the periglacial facies terminology could be initiated through the translations of von Łoziński's work into English, among other languages, to make the work more accessible to the international scientific community.

Broader Impacts

Periglacial environments comprise approximately 25% percent of the Earth' surface. Recent studies have shown how upland periglacial terrain impacts hillslope hydrology,

sediment, and nutrient transport (Paquette et al., 2018, 2020). As such, efforts to better constrain how these environments are expected to change under warming temperatures are of importance to the global scientific community. In addition, field-based data will continue to be needed to validate large-scale modeling efforts focused on these difficult-to-access areas of the globe. Features of hypothesized periglacial origin have also been identified on Mars (Balme & Gallagher, 2009). Terrestrial studies are needed to constrain speculation about the formation of Martian features, which for now, can only be studied via remotely sensed data.

REFERENCES

Antevs, E. (1932). Alpine Zone of Mt. Washington Range. Merrill & Webber company.

Ballantyne, C. K. (2018). Periglacial Geomorphology (1st ed.). John Wiley & Sons.

Ballantyne, C. K., Black, N. M., & Finlay, D. P. (1989). Enhanced boulder weathering under late-lying snowpatches. Earth Surface Processes and Landforms, 14(8), 745–750. https://doi.org/10.1002/esp.3290140808

Balme, M. R., Gallagher, C. J., & Hauber, E. (2013). Morphological evidence for geologically young thaw of ice on Mars: A review of recent studies using high-resolution imaging data. Progress in Physical Geography: Earth and Environment, 37(3), 289–324. https://doi.org/10.1177/0309133313477123

Barrett, P. J. (1980). The shape of rock particles, a critical review. Sedimentology, 27(3), 291–303. https://doi.org/10.1111/j.1365-3091.1980.tb01179.x

Benn, D. I., & Ballantyne, C. K. (1993). The description and representation of particle shape. Earth Surface Processes and Landforms, 18(7), 665–672. https://doi.org/10.1002/esp.3290180709

Berkland, JO and Raymond, LA (1973). Pleistocene glaciation in the Blue Ridge Province, Appalachian Mountains, North Carolina. *Science*, 181(4100): 651-653.

Bertran, P., Hétu, B., Texier, J.-P., & Van Steijn, H. (1997). Fabric characteristics of subaerial slope deposits. *Sedimentology*, *44*(1), 1–16. https://doi.org/10.1111/j.1365-3091.1997.tb00421.x

Bierman, P. R., Davis, P. T., Corbett, L. B., Lifton, N. A., & Finkel, R. C. (2015). Cold-based Laurentide ice covered New England's highest summits during the Last Glacial Maximum. Geology, G37225.1. https://doi.org/10.1130/G37225.1

Bingham, C. (1974). An antipodally symmetric distribution on the sphere. The Annals of Statistics, 2(6), 1201–1225.

Boelhouwers, J. (1999). Block deposits in southern Africa and their significance to periglacial autochthonous blockfield development. Polar Geography, 23(1), 12–22. https://doi.org/10.1080/10889379909377662

Boggs, S. (2006). Principles of sedimentology and stratigraphy (4. ed). Pearson Prentice Hall.

Bovis, M. J. (1978). Soil loss in the Colorado Front Range: Sampling design and areal variation. *Zeitschrift fuer Geomorphologie Supplementband* 29, 10-21. doi:10.

Bovis, M.J. and Thorn, C.E. (1981). Soil loss variation within a Colorado alpine area. *Earth Surface Processes and Landforms*, 151-163. doi:10.1002/esp.3290060208.

Braun, D. D. (1989). Glacial and periglacial erosion of the Appalachians. Geomorphology, 2(1), 233–256. https://doi.org/10.1016/0169-555X(89)90014-7

Braun, D. D. (2011). Chapter 40—The Glaciation of Pennsylvania, USA. In J. Ehlers, P. L. Gibbard, & P. D. Hughes (Eds.), *Developments in Quaternary Sciences* (Vol. 15, pp. 521–529). Elsevier. https://doi.org/10.1016/B978-0-444-53447-7.00040-4

Brunnschweiler, D. H., & Nelson, F. E. (2022). The morphology of altiplanation in interior Alaska. Polar Geography, 45(1), 1–36. https://doi.org/10.1080/1088937X.2021.1995065

Bryant, I. D. (1983). The utilisation of Arctic River analogue studies in the interpretation of periglacial river sediments from southern Britain. In K. J. Gregory (Ed.), Background to Palaeohydrology: A Perspective (pp. 413–431). Wiley-Interscience.

Cailleux, A. (1947). L'indice d'emousse: Definition et premiere application. Compte Rendu Sommaire de La Société Géologique de France, 13(14), 251–252.

Caine, N. (1978). Climatic Geomorphology in Mid-Latitude Mountains. In J. L. Davies, M. A. J. Williams, & J. N. Jennings (Eds.), Landform evolution in Australasia (pp. 113–127). Australian National University Press.

Cardozo, N., & Allmendinger, R. W. (2013). Spherical projections with OSXStereonet. Computers & Geosciences, 51, 193–205. https://doi.org/10.1016/j.cageo.2012.07.021

Chigira, M., & Hirata, Y. (2021). The Kui boulder fields: Formation processes controlled by columnar joints of granodiorite. CATENA, 207, 105683. https://doi.org/10.1016/j.catena.2021.105683

Clark, M.G. (1993). Central Appalachian periglacial geomorphology: A field excursion guidebook, under the auspices of: 27th International Geographical Congress ... [Et al.] (1–248 p. :). Agronomy Dept., The Pennsylvania State University.

Clark, M. G., & Ciolkosz, E. J. (1988). Periglacial geomorphology of the Appalachian highlands and interior highlands south of the glacial border—A review. Geomorphology, 1(3), 191–220. https://doi.org/10.1016/0169-555X(88)90014-1

Clark, M. G., & Hedges, J. (1992). Origin of certain high-elevation local broad uplands in the central Appalachians south of the glacial border, U.S.A.—A paleoperiglacial hypothesis. In J. C. Dixon & A. D. Abrahams (Eds.), Periglacial Geomorphology (1st ed., pp. 31–61). Routledge. https://doi.org/10.4324/9781003028901-2

Chigira, M., & Hirata, Y. (2021). The Kui boulder fields: Formation processes controlled by columnar joints of granodiorite. CATENA, 207, 105683. https://doi.org/10.1016/j.catena.2021.105683

Clark, G. M., & Schmidlin, T. W. (1992). Alpine periglacial landforms of eastern North America: A review. Permafrost and Periglacial Processes, 3(3), 225–230. https://doi.org/10.1002/ppp.3430030309

Colman, R., & Soden, B. J. (2021). Water vapor and lapse rate feedbacks in the climate system. Reviews of Modern Physics, 93(4), 045002. https://doi.org/10.1103/RevModPhys.93.045002

Core, E. L. (1926). Ecological Studies on Spruce Mountain. Proceedings of the West Virginia Academy of Science, 1, 36–39.

Cremeens, D. L., Darmody, R. G., & George, S. E. (2005). Upper slope landforms and age of bedrock exposures in the St. Francois Mountains, Missouri: A comparison to relict periglacial features in the Appalachian Plateau of West Virginia. Geomorphology, 70(1), 71–84. https://doi.org/10.1016/j.geomorph.2005.04.001

Davis, W. M. (1899). The geographical cycle. The Geographical Journal, 14(5), 481–504. https://doi.org/10.2307/1774538

Davis, W. M. (1909). Geographical essays (D. W. Johnson, Ed.). Ginn.

Delcourt, H. R., & Delcourt, P. A. (1988). Quaternary landscape ecology: Relevant scales in space and time. Landscape Ecology, 2(1), 23–44.

Del Vecchio, J. (2021). Appalachian pasts, Arctic futures: Permafrost landscape response to warming.

Del Vecchio, J., DiBiase, R. A., Corbett, L. B., Bierman, P. R., Caffee, M., & Ivory, S. (2020). Erosion rates before and after the Mid-Pleistocene Transition in periglaciated central Appalachia. 2020, EP035-03.

Del Vecchio, J., DiBiase, R. A., Corbett, L. B., Bierman, P. R., Caffee, M. W., & Ivory, S. J. (2022). Increased Erosion Rates Following the Onset of Pleistocene Periglaciation at Bear Meadows, Pennsylvania, USA. Geophysical Research Letters, 49(4), e2021GL096739. https://doi.org/10.1029/2021GL096739

Del Vecchio, J., DiBiase, R. A., Denn, A. R., Bierman, P. R., Caffee, M. W., & Zimmerman, S. R. (2018). Record of coupled hillslope and channel response to Pleistocene erosion and deposition in a sandstone headwater valley, central Pennsylvania. GSA Bulletin, 130(11–12), 1903–1917. https://doi.org/10.1130/B31912.1

Denn, A. R., Bierman, P. R., Zimmerman, S. R. H., Caffee, M. W., Corbett, L. B., & Kirby, E. (2018). Cosmogenic nuclides indicate that boulder fields are dynamic, ancient, multigenerational features. GSA Today, 4–10. https://doi.org/10.1130/GSATG340A.1

Denn, A. R., Bierman, Paul R., & Kirby, Eric. (2015). Investigation of a relict periglacial feature: Hickory Run Boulder Filed, Hickory Run State Park, Pennsylvania. T57. Soil to Sediment and Channels--From Geologic to Modern Time Scales: A Session to Honor the Work of Milan Pavich, 47, 550.

Deprez, M., De Kock, T., De Schutter, G., & Cnudde, V. (2020). A review on freeze-thaw action and weathering of rocks. Earth-Science Reviews, 203, 103143. https://doi.org/10.1016/j.earscirev.2020.103143

Dixon, C. J., & Leach, B. (1976). Sampling methods for geographical research. Geo Abstracts.

Dobesch, H., Dumolard, P., & Dyras, I. (2013). Spatial Interpolation for Climate Data: The Use of GIS in Climatology and Meteorology. John Wiley & Sons.

Dobiński, W. (2024). Periglaciology: Review and Discussion of Modern Concepts and its Relation to the Research in Poland. *Quaestiones Geographicae*, *43*(1), 211–233. https://doi.org/10.14746/quageo-2024-0013

Eckelmann, S. (1988). Die Untergrenze der rezent-periglazialen Höhenstufe in den Kordilleren Nordamerikas [Doctoral Dissertation]. Universität zu Göttingen.

Eppes, M.-C., & Keanini, R. (2017). Mechanical weathering and rock erosion by climate-dependent subcritical cracking. Reviews of Geophysics, 55(2), 470–508. https://doi.org/10.1002/2017RG000557

Evans, D. J. A., & Benn, D. I. (2014). A Practical Guide to the Study of Glacial Sediments. Routledge.

Fagan, J. D., & Nelson, F. E. (2017). Spatial Sampling Design in the Circumpolar Active Layer Monitoring Programme. Permafrost and Periglacial Processes, 28(1), 42–51. https://doi.org/10.1002/ppp.1904

Fame, M. L., Chilton, K. D., Spotila, J. A., Kelly, M. A., & Caton, S. A. (2024). Periglacial resurfacing of hillslopes and channels with large boulders in the Virginia Appalachians. Earth Surface Processes and Landforms, 49(1), 432–450. https://doi.org/10.1002/esp.5713

Farmer, C. B., & Doms, P. E. (1979). Global seasonal variation of water vapor on Mars and the implications for permafrost. Journal of Geophysical Research: Solid Earth, 84(B6), 2881–2888. https://doi.org/10.1029/JB084iB06p02881

Fenneman, N. M. (1946). Physical divisions of the United States (USGS Unnumbered Series). U.S. Geological Survey; USGS Publications Warehouse. https://doi.org/10.3133/70207506

Fosberg, F. R. (1960). Notes on the Vegetation of Spruce Knob, West Virginia. Castanea, 25(4), 120–122.

Foster, H. L., Keith, T. E. C., & Menzie, W. D. (1994). Geology of the Yukon-Tanana area of east-central Alaska. In G. Plafker & H. C. Berg (Eds.), The Geology of Alaska (pp. 205–240). Geological Society of America. https://doi.org/10.1130/DNAG-GNA-G1.205

Foster, H. L., Weber, F. R., Forbes, R. B., & Brabb, E. E. (1973). Regional Geology of Yukon-Tanana Upland, Alaska1. In M. G. Pitcher, Arctic Geology. American Association of Petroleum Geologists. https://doi.org/10.1306/M19375C43

Fowler, B.K. (2010). Interim Surficial Geologic Map of Mt. Washington 7.5 Minute Quadrangle. *New Hampshire Geological Survey STATEMAP Program.*

https://www.des.nh.gov/sites/g/files/ehbemt341/files/documents/2020-01/Geo-047-024000-SMOF_MtWashington_LEGEND-Fowler.pdf

Fowler, B. K., Davis, P. T., Thompson, W. B., Eusden, J. D., & Dulin, I. T. (2012). *The Alpine Zone & Glacial Cirques of Mt. Washington & the Northern Presidential Range, New Hampshire* (75th Reunion of the Northeastern Friends of the Pleistocene). Bates College SCARAB (Scholarly Communication and Research at Bates).

https://scarab.bates.edu/?utm_source=scarab.bates.edu%2Ffaculty_publications%2F13&utm_medium=PDF&utm_campaign=PDFCoverPages

Franke, R. (1982). Smooth interpolation of scattered data by local thin plate splines. Computers & Mathematics with Applications, 8(4), 273–281. https://doi.org/10.1016/0898-1221(82)90009-8

French, H. M. (2000). Does Lozinski's periglacial realm exist today? A discussion relevant to modern usage of the term 'periglacial.' Permafrost and Periglacial Processes, 11(1), 35–42. https://doi.org/10.1002/(SICI)1099-1530(200001/03)11:1<35::AID-PPP334>3.0.CO;2-6

French, H. M., & Millar, S. (2014). Permafrost at the time of the Last Glacial Maximum (LGM) in North America. Boreas, 43(3), 667–677. https://doi.org/10.1111/bor.12036

French, H. M. (2016). Do periglacial landscapes exist? A discussion of the upland landscapes of Northern Interior Yukon, Canada. Permafrost and Periglacial Processes, 27(2), 219–228. https://doi.org/10.1002/ppp.1866

French, H. M. (2017). The Periglacial Environment (4th ed.). John Wiley & Sons.

Germain, D., & Milot, J. (2024). An overcooled coarse-grained talus slope at low elevation: New insights on air circulation and environmental impacts, Cannon Cliff, New Hampshire, USA. Earth Surface Processes and Landforms.

Goudie, A. S. (2006). The Schmidt Hammer in geomorphological research. Progress in Physical Geography: Earth and Environment, 30(6), 703–718. https://doi.org/10.1177/0309133306071954

Graf, K. (1973). Vergleichende Betrachtungen zur Solifluktion in verschiedenen Breitenlagen. Zeitschrift Für Geomorphologie, N.F.Supplementband, 16, 104–154.

Geyer, A. R. (1969). Hickory Run State Park—Boulder field (Supersedes Park Guide 2 16-002.0; Trail of Geology, p. 4). Pennsylvania Department of Conservation and Natural Resources Bureau of Topographic and Geologic Survey.

Giardino, J. R., & Vitek, J. D. (1985). A Statistical Interpretation of the Fabric of a Rock Glacier. *Arctic and Alpine Research*, *17*(2), 165–177. https://doi.org/10.2307/1550846

Goodfellow, B. W., Stroeven, A. P., Fabel, D., Fredin, O., Derron, M.-H., Bintanja, R., & Caffee, M. W. (2014). Arctic–alpine blockfields in the northern Swedish Scandes: Late Quaternary – not Neogene. Earth Surface Dynamics, 2(2), 383–401. https://doi.org/10.5194/esurf-2-383-2014

Guyot, A. (1861). On the Appalachian Mountain System ... E. Hayes.

Hambrey, M. J. (1994). Glacial Environments. University of British Columbia Press. https://press.uchicago.edu/ucp/books/book/distributed/G/bo70068889.html

Helmke, M. F., Coughlin, M. F., Potter, N., & Sevon, W. D. (2007). Hickory Run Boulder Field (2): Collecting high-resolution, low-altitude aerial photographs by UAV. Northeastern Section - 42nd Annual Meeting (12-14 March 2007), 39(1), 43. https://gsa.confex.com/gsa/2007NE/webprogram/Paper117968.html

Hengl, T., & Reuter, H. I. (2008). Geomorphometry: Concepts, Software, Applications. Newnes.

Hewitt, R. J., Parfitt, S. A., & Wenban-Smith, F. F. (2018). Rose diagrams and statistical tests for archaeological orientation data: A case applied to the Southfleet Road Elephant site, Ebbsfleet, UK [Preprint]. SocArXiv. https://doi.org/10.31235/osf.io/f2vzs

Hickory Run State Park Boulder Field. (2020). Pennsylvania Department of Conservation and Natural Resources. http://elibrary.dcnr.pa.gov/GetDocument?docId=1737635&DocName=HICK_BoulderFieldBrochure.pdf#

Ivester, A. H., Leigh, D. S., & Godfrey-Smith, D. I. (2001). Chronology of Inland Eolian Dunes on the Coastal Plain of Georgia, USA. Quaternary Research, 55(3), 293–302. https://doi.org/10.1006/qres.2001.2230

Jones, S. J. (2015). Introducing Sedimentology. Dunedin Academic Press; eBook Collection (EBSCOhost). https://ezproxy.msu.edu/login?url=https://search.ebscohost.com/login.aspx?direct=true&db=nlebk&AN=1018575&site=ehost-live&scope=site

Jorgenson, M., Yoshikawa, K., Kanevskiy, M., Shur, Y., Romanovsky, V., Marchenko, S., Grosse, G., Brown, J., & Jones, B. (2008). Permafrost characteristics of Alaska + Map. *Proceedings of the Ninth International Conference on Permafrost*, *3*, 121–122.

Kamb, W. B. (1959). Ice petrofabric observations from Blue Glacier, Washington, in relation to theory and experiment. Journal of Geophysical Research (1896-1977), 64(11), 1891–1909. https://doi.org/10.1029/JZ064i011p01891

Karte, J. (1979). Räumliche Abgrenzung und regionale Differenzierung des Periglaziärs. Bochumer Geographische Arbieten, 35(35), 211.

King, C. A. M. (1966). Techniques in geomorphology (First Edition). St Martin's Press.

King, C. A. M., & Buckley, J. T. (1968). The analysis of stone size and shape in arctic environments. Journal of Sedimentary Research, 38(1), 200–214. https://doi.org/10.1306/74D7191A-2B21-11D7-8648000102C1865D

Koester, A. J., Shakun, J. D., Bierman, P. R., Davis, P. T., Corbett, L. B., Goehring, B. M., Vickers, A. C., & Zimmerman, S. R. (2021). Laurentide ice sheet thinning and erosive regimes at Mount Washington, New Hampshire, inferred from multiple cosmogenic nuclides. In R. B. Waitt, G. D. Thackray, & A. R. Gillespie (Eds.), Untangling the Quaternary Period—A Legacy of Stephen C. Porter (Vol. 548, p. 0). Geological Society of America. https://doi.org/10.1130/2020.2548(15)

Kottek, M., Grieser, J., Beck, C., Rudolf, B., & Rubel, F. (2006). World Map of the Köppen-Geiger climate classification updated. Meteorologische Zeitschrift, 15(3), 259–263. https://doi.org/10.1127/0941-2948/2006/0130

Krumbein, W. C. (1941). Measurement and geological significance of shape and roundness of sedimentary particles. Journal of Sedimentary Research, 11(2), 64–72. https://doi.org/10.1306/D42690F3-2B26-11D7-8648000102C1865D

Kruskal, W. H., & Wallis, W. A. (1952). Use of Ranks in One-Criterion Variance Analysis. Journal of the American Statistical Association, 47(260), 583–621.

Kuiper, N. H. (1960). Tests concerning random points on a circle. Indagationes Mathematicae (Proceedings), 63, 38–47. https://doi.org/10.1016/S1385-7258(60)50006-0

LaBarbara, J. M. (2017, August 14). Looking Back (and Up) at Spruce Knob [West Virginia University Libraries]. https://news.lib.wvu.edu/2017/08/14/looking-back-and-up-at-spruce-knob/

Leffler, R. J. (1981). Estimating Average Temperatures on Appalachian Summits. Journal of Applied Meteorology and Climatology, 20(6), 637–642. https://doi.org/10.1175/1520-0450(1981)020<0637:EATOAS>2.0.CO;2

Lohr, S. L. (1999). Sampling: Design and analysis. Duxbury Press,.

Lundqvist, G. (1949). The orientation of the block material in certain species of flow Earth: Points of view on method. Geografiska Annaler, 31(1–4), 335–347. https://doi.org/10.1080/20014422.1949.11880817

Madole, R. F. (1972). Neoglacial Facies in the Colorado Front Range. Arctic and Alpine Research, 4(2), 119. https://doi.org/10.2307/1550395

Mardia, K. V. (1975). Statistics of Directional Data. Journal of the Royal Statistical Society, 37(3), 349–371. https://doi-org.proxy1.cl.msu.edu/10.1111/j.2517-6161.1975.tb01550.x

Mardia, K. V., Jupp, P. E., & Mardia, K. (2000). Directional statistics (Vol. 2). Wiley Online Library.

Marsh, B. (1987). Pleistocene pingo scars in Pennsylvania. Geology, 15(10), 945–947.

Martini, I. P., French, H. M., & Alberti, A. P. (2011). Ice-marginal and periglacial processes and sediments: An introduction. Geological Society, London, Special Publications, 354(1), 1–13. https://doi.org/10.1144/SP354.1

Matthews, J. A., Wilson, P., Winkler, S., Mourne, R. W., Hill, J. L., Owen, G., Hiemstra, J. F., Hallang, H., & Geary, A. P. (2019). Age and development of active cryoplanation terraces in the alpine permafrost zone at Svartkampan, Jotunheimen, southern Norway. Quaternary Research, 92(3), 641–664. https://doi.org/10.1017/qua.2019.41

McKeon, JB, Hack, JT, Newell, WL, Berkland, JO, Raymond, LA (1974). North Carolina glacier: evidence disputed. Science, 184(4132) 88-91.

Merritts, D. J., & Rahnis, M. A. (2022). Pleistocene Periglacial Processes and Landforms, Mid-Atlantic Region, Eastern United States. Annual Review of Earth and Planetary Sciences, 50(1), 541–592. https://doi.org/10.1146/annurev-earth-032320-102849

Middlekauff, B. D. (1987). Relict periglacial morphosequences in the northern Blue Ridge [Ph.D., Michigan State University]. https://www.proquest.com/docview/303578719/abstract/FFE0E73ADB53453FPQ/1

Millar, S. (1995). Clast fabric in periglacial mass-movement deposits [Ph.D., Rutgers The State University of New Jersey, School of Graduate Studies]. In ProQuest Dissertations and

Theses (304247080). ProQuest Dissertations & Theses Global. https://ezproxy.msu.edu/login?url=https://www.proquest.com/dissertations-theses/clast-fabric-periglacial-mass-movement-deposits/docview/304247080/se-2?accountid=12598

Millar, S., & Nelson, F. E. (2001). Sampling-surface orientation and clast macrofabric in periglacial colluvium. Earth Surface Processes and Landforms, 26(5), 523–529. https://doi.org/10.1002/esp.200

Millar, S.W.S. and Nelson, F.E. (2003). Influence of clast axial ratio on macrofabric strength in periglacial colluvium. *Journal of Sedimentary Research* 73(5): 720-724.

Millar, S. (2005). Fabric variability associated with periglacial mass-wasting at Eagle Summit, Alaska. Geomorphology, 72(1), 222–237. https://doi.org/10.1016/j.geomorph.2005.05.012

Mills, H. H. (1990). Three-dimensional clast orientation in glacial and mass-movement sediments: A compilation and preliminary analysis (Report 90–128; Open-File Report). USGS Publications Warehouse. https://doi.org/10.3133/ofr90128

Mitáš, L., & Mitášová, H. (1988). General variational approach to the interpolation problem. Computers & Mathematics with Applications, 16(12), 983–992. https://doi.org/10.1016/0898-1221(88)90255-6

Mitáš, L., & Mitášová, H. (1999). Spatial interpolation. In Longley, P, Goodchild, M.F., Maguire, D.J., & D.W. Rhind (Eds.), Geographical information systems: Principles, techniques, management and applications (Vol. 1, pp. 481–492). Wiley.

Mitchell, R. J., Nelson, F. E., & Nyland, K. E. (2023). Little tools, big job: The periglacial conveyor system in cryoplanated uplands. *Permafrost and Periglacial Processes*, *34*(3), 384–398. https://doi.org/10.1002/ppp.2193

Monongahela National Forest—Spruce Knob and Spruce Knob Observation Tower. (n.d.). Retrieved December 27, 2023, from https://www.fs.usda.gov/wps/portal/fsinternet3/cs/recarea/mnf/recreation/recarea/

Murton, J. B. (2021). What and where are periglacial landscapes? Permafrost and Periglacial Processes, 32(2), 186–212. https://doi.org/10.1002/ppp.2102

Nelson, F. E. (1979). *Patterned ground in the Juneau Icefield region, Alaska-British Columbia* [M.S. Thesis, Michigan State University]. https://doi.org/10.25335/M5251FT98

Nelson, F.E. (1982a). Sorted-Circle Macrofabrics. Polarforschung, 52(1/2), 43–53.

Nelson, F.E. (1982b). Sorted-Stripe Macrofabrics. Geografiska Annaler. Series A, Physical Geography, 64(1/2), 25–33. https://doi.org/10.2307/520493

Nelson, F. E. (1985). A preliminary investigation of solifluction macrofabrics. CATENA, 12(1), 23–33. https://doi.org/10.1016/S0341-8162(85)80002-3

Nelson, F. E., & Nyland, K. E. (2017). Periglacial cirque analogs: Elevation trends of cryoplanation terraces in eastern Beringia. Geomorphology, 293, 305–317. https://doi.org/10.1016/j.geomorph.2017.05.005

Nyland, K. E., & Nelson, F. E. (2019). Time-transgressive cryoplanation terrace development through nivation-driven scarp retreat. Earth Surface Processes and Landforms, 45(3), 526–534. https://doi.org/10.1002/esp.4751

Nyland, K. E., & Nelson, F. E. (2020). Long-term nivation rates, Cathedral Massif, northwestern British Columbia. Canadian Journal of Earth Sciences, 57(11), 1305–1311. https://doi.org/10.1139/cjes-2019-0176

Nyland, K. E., Nelson, F. E., & Figueiredo, P. M. (2020). Cosmogenic 10 Be and 36 Cl geochronology of cryoplanation terraces in the Alaskan Yukon-Tanana Upland. Quaternary Research, 97, 157–166. https://doi.org/10.1017/qua.2020.25

Nyland, K. E., Nelson, F. E., & Higgins, D. (2024). The trajectory of contemporary cryoplanation literature: A bibliometric assessment. Permafrost and Periglacial Processes, n/a(n/a). https://doi.org/10.1002/ppp.2214

Nyland, K. E., Vandenberghe, J., & Nelson, F. E. (2023). Cryoplanation terraces and cryopediments. In *Reference Module in Earth Systems and Environmental Sciences* (p. B9780323999311001112). Elsevier. https://doi.org/10.1016/B978-0-323-99931-1.00111-2

Ostertagová, E. (2012). Modelling using Polynomial Regression. Procedia Engineering, 48, 500–506. https://doi.org/10.1016/j.proeng.2012.09.545

Olyphant, G. A. (1985). Topoclimate and the Distribution of Neoglacial Facies in the Indian Peaks Section of the Front Range, Colorado, U.S.A. Arctic and Alpine Research, 17(1), 69. https://doi.org/10.2307/1550962

Orme, A. (Ed.). (2001). Appalachia and the Eastern Cordillera. In *Physical Geography of North America* (First Edition, pp. 291–306). Oxford University Press.

Park Nelson, K. J., Nelson, F. E., & Walegur, M. T. (2007). Periglacial Appalachia: Palaeoclimatic significance of blockfield elevation gradients, eastern USA. Permafrost and Periglacial Processes, 18(1), 61–73. https://doi.org/10.1002/ppp.574

Peltier, L. C. (1950). The Geographic Cycle in Periglacial Regions as it is Related to Climatic Geomorphology. Annals of the Association of American Geographers, 40(3), 214–236. https://doi.org/10.1080/00045605009352070

Poser, H. (Ed.). (197). Formen, Formengesellschaften und Untergrenzen in den heutigen periglazialen Höhenstufen der Hochgebirge Europas und Afrikas zwischen Arktis und Äquator von Hans Poser (kartoniertes Buch). https://www.sutmoeller.de/shop/item/9783525821053/formen-formengesellschaften-und-untergrenzen-in-den-heutigen-periglazialen-hohenstufen-der-hochgebirge-europas-und-afrikas-zwischen-arktis-und-aquator-von-hans-poser-kartoniertes-buch

Péwé, T. L., Burbank, L., & Mayo, L. R. (1967). Multiple glaciation of the Yukon-Tanana Upland, Alaska. IMAP, Article 507. https://doi.org/10.3133/i507

Potter, N., & Helmke, M. (2007). Hickory Run Boulder Field 3: More Observations and New Interpretations. *2007 GSA Annual Meeting & Exposition*, *53*, 30. https://gsa.confex.com/gsa/2007AM/webprogram/Paper127016.html

Potter, N., & Moss, J. H. (1968). Origin of the Blue Rocks Block Field and Adjacent Deposits, Berks County, Pennsylvania. *Geological Society of America Bulletin*, *79*(2), 255. https://doi.org/10.1130/0016-7606(1968)79[255:ootbrb]2.0.co;2

Queen, C. W. (2018). Large-scale mapping and geomorphometry of upland periglacial landscapes in eastern Beringia [M.S. Thesis, Michigan State University]. MSU Libraries Digital Repository. https://d.lib.msu.edu/etd/19379

Queen, C. W., & Nelson, F. E. (2022). Characteristic periglacial topography: Multi-scale hypsometric analysis of cryoplanated uplands in eastern Beringia. Permafrost and Periglacial Processes, 33(3), 241–263. https://doi.org/10.1002/ppp.2148

Queen, C. W., Nelson, F. E., Gunn, G. E., & Nyland, K. E. (2021). A characteristic periglacial landform: Automated recognition and delineation of cryoplanation terraces in eastern Beringia. Permafrost and Periglacial Processes, 32(1), 35–46. https://doi.org/10.1002/ppp.2083

Reger, R. D. (1975). Cryoplanation Terraces of Interior and Western Alaska [Doctoral Dissertation, Arizona State University]. Proquest Dissertations & Theses Global.

Robison, W. C. (1960). Spruce Knob Revisited: A Half-Century of Vegetation Change. Castanea, 25(1), 53–61.

Selby, M. J. (1966). Some slumps and boulder fields near Whitehall. Journal of Hydrology (New Zealand), 5(2), 35–44.

Sevon, W. D. (1967). The Bowmanstown boulder field, Carbon County, Pennsylvania. Proceedings of the Pennsylvania Academy of Science, 40(2), 90–94.

Sevon, W. D. (1983). Appalachian peneplains: An historical review. Earth Sciences History, 2(2), 156–164.

Sevon, W. D. (1987). The Hickory Run boulder field, a periglacial relict, Carbon County, Pennsylvania. In North-Eastern Section of the Geological Society of America: Decade of North American Geology, Centennial Field Guides Volume 5 (Vol. 5, pp. 75–76). Geological Society of America.

Smith, H. T. U. (1953). The Hickory Run boulder field, Carbon County, Pennsylvania. American Journal of Science, 251(9), 625–642. https://doi.org/10.2475/ajs.251.9.625

Stewart, K. (2014). Subsampling. In A. C. Michalos (Ed.), Encyclopedia of Quality of Life and Well-Being Research (pp. 6462–6464). Springer Netherlands. https://doi.org/10.1007/978-94-007-0753-5_2909

Sumner, P., Nel, W., Holness, S., & Boelhouwers, J. (2002). Rock Weathering Characteristics as Relative-Age Indicators for Glacial and Post-Glacial Landforms on Marion Island. South African Geographical Journal, 84(2), 153–157. https://doi.org/10.1080/03736245.2002.9713766

Thompson, S. K. (2012). Sampling (3rd ed). Wiley.

Tilton, J. L., Prouty, W. F., & Price, P. H. (1927). Pendleton County (Vol. 1). Wheeling news litho. Company.

Troll, C. (1944). Strukturboden, Solifluktion und Frostklimate der Erde: Geol. Rundschau. Bd, 34.

U.S. E.P.A., O. (2016, July 1). Climate Change Indicators: Snow and Ice [Reports and Assessments]. EPA, United States Environmental Protection Agency. https://www.epa.gov/climate-indicators/snow-ice

Uxa, T., & Mida, P. (2017). Rock glaciers in the Western and High Tatra Mountains, Western Carpathians. *Journal of Maps*, *13*(2), 844–857. https://doi.org/10.1080/17445647.2017.1378136

Van Everdingen, R. (2005). Multi-language glossary of permafrost and related ground-ice terms in Chinese, English, French, German, Icelandic, Italian Norwegian, Polish, Romanian, Russian, Spanish, and Swedish (p. 159). The Arctic Institute of North America.

Vollmer, F. W. (1995). C program for automatic contouring of spherical orientation data using a modified Kamb method. Computers & Geosciences, 21(1), 31–49. https://doi.org/10.1016/0098-3004(94)00058-3

von Łoziński, W. (1909). Über die mechanische Verwitterung der Sandsteine im gemässigten Klima.

von Łoziński, W. (1912). Die periglaziale Fazies der mechanischen Verwitterung. PA Norstedt & Söner.

Wahrhaftig, C. (1965). Physiographic Divisions of Alaska (Geological Survey Professional Paper 482; p. 52). U.S. Department of the Interior. https://dggs.alaska.gov/webpubs/usgs/p/text/p0482.pdf

Walegur, M. T. (2001). Spatial Trends of Air and Soil Temperature at High Elevations in the Appalachian Mountain Range. University at Albany, State University of New York.

Walegur, M. T., Nelson, F. E., & Phillips, M. (2003). Permafrost distribution in the Appalachian Highlands, northeastern USA. In *8th International Conference on Permafrost Proceedings* (pp. 1201-1206). Swets and Zeitlinger: Lisse, Zürich.

Washburn, A. L. (1980). *Geocryology: A Survey of Periglacial Processes and Environments*. Wiley.

Web Soil Survey. (n.d.). Retrieved April 2, 2024, from https://websoilsurvey.nrcs.usda.gov/app/WebSoilSurvey.aspx

Weber, F. R. (1986). Glacial geology of the Yukon-Tanana upland. In Hamilton, Thomas D., Reed Katherine M., & Thorson, Robert M. (Eds.), Glaciation in Alaska: The Geologic Record (First Edition, pp. 79–98). Alaska Geological Society. https://archives-datapages-com.proxy1.cl.msu.edu/data/alaska/data/017/017001/79_akgs0170079.htm

Wedo, A. (2005, April 7). Sedimentary Characteristics of the Hickory Run Boulder Field, Carbon County, Pennsylvania. The Association of American Geographers, Denver, Colorado.

Wieczorek, G. F., & Morgan, B. A. (2008). *Debris-Flow Hazards within the Appalachian Mountains of the Eastern United States* (Fact Sheet 2008–3070; Fact Sheet). U.S. Department of the Interior.

Wilson, F. H., Hults, C. P., Mull, C. G., & Karl, S. M. (2015). Geologic map of Alaska: U.S. Geological Survey Scientific Investigations Map 3340 [Scientific Investigations Map]. http://dx.doi.org/10.3133/sim3340

Woodcock, N. H. (1977). Specification of fabric shapes using an eigenvalue method. GSA Bulletin, 88(9), 1231–1236. https://doi.org/10.1130/0016-7606(1977)88<1231:SOFSUA>2.0.CO;2

Woodcock, D. W., & Wells, P. V. (1990). Full-glacial summer temperatures in eastern North America as inferred from Wisconsinan vegetational zonation. Palaeogeography, Palaeoclimatology, Palaeoecology, 79(3–4), 305–312. https://doi.org/10.1016/0031-0182(90)90024-2

APPENDIX

CHAPTER 2 SUPPLEMENTARY MATERIAL

Table 11. Periglacial feature type, location, elevation, and source.

Feature	Latitude	Longitude	Elevation (m.a.s.l)	Source
Subsummit terraces	40.24611	-78.1278	695-701	Clark & Hedges (1992)
Summit with tors	40.06806	-77.2417	428-463	Clark & Hedges (1992)
Summit with tor remnant	39.83417	-77.4917	616-622	Clark & Hedges (1992)
Summit plain	39.78583	-79.1772	969-979	Clark & Hedges (1992)
Summit area	39.72889	-77.4897	512-516	Clark & Hedges (1992)
Riser, terrace	39.69556	-77.5133	646-652	Clark & Hedges (1992)
Summit tor crest	39.66056	-77.5389	475-481	Clark & Hedges (1992)
Tors, subsummit flat	39.61611	-77.4483	463-476	Clark & Hedges (1992)
Tor, risers	39.51	-77.4753	488-494	Clark & Hedges (1992)
Risers, terraces	39.41694	-77.6386	402-433	Clark & Hedges (1992)
Tors, riser, terrace	39.06472	-79.3003	1183-1189	Clark & Hedges (1992)
Risers, terraces	38.97778	-79.3356	1183-1195	Clark & Hedges (1992)
Blockfield	41.0403	-75.6092	566.5	Park Nelson et al. (2007)
Blockfield	41.0494	-75.6394	563.5	Park Nelson et al. (2007)
Blockfield	41.0508	-75.6425	561.5	Park Nelson et al. (2007)
Blockfield	40.8056	-75.5342	369	Park Nelson et al. (2007)
Blockfield	40.8006	-75.5328	234	Park Nelson et al. (2007)
Blockfield	40.8022	-75.5361	295.5	Park Nelson et al. (2007)

Table 11 (cont'd).

Blockfield	40.7961	-75.5856	436	Park Nelson et al. (2007)
Blockfield	40.7869	-75.6186	395	Park Nelson et al. (2007)
Blockfield	40.6925	-75.8094	187	Park Nelson et al. (2007)
Blockfield	40.6925	-75.8122	185	Park Nelson et al. (2007)
Blockfield	40.6939	-75.8631	448.5	Park Nelson et al. (2007)
Blockfield	40.6561	-75.9092	210	Park Nelson et al. (2007)
Blockfield	40.6611	-75.9292	471.5	Park Nelson et al. (2007)
Blockfield	40.6	-75.9194	316.5	Park Nelson et al. (2007)
Blockfield	40.5931	-75.9172	218.5	Park Nelson et al. (2007)
Blockfield	40.6	-75.9214	315	Park Nelson et al. (2007)
Blockfield	40.62	-75.9342	275	Park Nelson et al. (2007)
Blockfield	40.6386	-75.9675	237	Park Nelson et al. (2007)
Blockfield	40.6258	-75.9739	436	Park Nelson et al. (2007)
Blockfield	40.6342	-75.9781	308.5	Park Nelson et al. (2007)
Blockfield	40.6372	-75.9794	287.5	Park Nelson et al. (2007)
Blockfield	40.5469	-75.1414	188	Park Nelson et al. (2007)
Blockfield	40.5869	-75.1458	186	Park Nelson et al. (2007)
Blockfield	40.5472	-75.1289	178.5	Park Nelson et al. (2007)
Blockfield	40.4858	-76.6444	417.5	Park Nelson et al. (2007)
Blockfield	40.4792	-76.6417	429.5	Park Nelson et al. (2007)
Blockfield	40.4967	-76.6556	247.5	Park Nelson et al. (2007)

Table 11 (cont'd).

Blockfield	40.4908	-76.6569	338	Park Nelson et al. (2007)
Blockfield	40.4936	-76.6631	232	Park Nelson et al. (2007)
Blockfield	40.4886	-76.6742	229.5	Park Nelson et al. (2007)
Blockfield	40.4586	-76.7033	473.5	Park Nelson et al. (2007)
Blockfield	40.4561	-76.7083	473.5	Park Nelson et al. (2007)
Blockfield	40.4433	-76.7403	412	Park Nelson et al. (2007)
Blockfield	40.4414	-76.745	444.5	Park Nelson et al. (2007)
Blockfield	40.4428	-76.7531	511.5	Park Nelson et al. (2007)
Blockfield	40.4317	-76.7514	352	Park Nelson et al. (2007)
Blockfield	40.4375	-76.7556	466.5	Park Nelson et al. (2007)
Blockfield	40.4303	-76.7556	358.5	Park Nelson et al. (2007)
Blockfield	40.4283	-76.7594	359.5	Park Nelson et al. (2007)
Blockfield	40.4244	-76.7736	360.5	Park Nelson et al. (2007)
Blockfield	40.4389	-76.7894	233.5	Park Nelson et al. (2007)
Blockfield	40.4375	-76.8067	171	Park Nelson et al. (2007)
Blockfield	41.1914	-76.9583	305.5	Park Nelson et al. (2007)
Blockfield	41.2044	-77.0219	241.0968	Park Nelson et al. (2007)
Blockfield	41.1614	-77.0428	498	Park Nelson et al. (2007)
Blockfield	41.1342	-77.0631	249.5	Park Nelson et al. (2007)
Blockfield	41.1225	-77.1033	512	Park Nelson et al. (2007)
Blockfield	41.1208	-77.1078	535	Park Nelson et al. (2007)

Table 11 (cont'd).

Blockfield	41.1169	-77.1133	480	Park Nelson et al. (2007)
Blockfield	39.7658	-77.4161	332	Park Nelson et al. (2007)
Blockfield	39.7633	-77.4208	346	Park Nelson et al. (2007)
Blockfield	39.6944	-77.3961	297.5	Park Nelson et al. (2007)
Blockfield	39.7233	-77.4094	432	Park Nelson et al. (2007)
Blockfield	39.6931	-77.4322	445	Park Nelson et al. (2007)
Blockfield	39.6936	-77.4361	382.5	Park Nelson et al. (2007)
Blockfield	39.6736	-77.4422	356.5	Park Nelson et al. (2007)
Blockfield	39.6756	-77.4439	384	Park Nelson et al. (2007)
Blockfield	39.6617	-77.4633	442	Park Nelson et al. (2007)
Blockfield	39.5878	-77.4406	265.176	Park Nelson et al. (2007)
Blockfield	39.6722	-77.5222	330	Park Nelson et al. (2007)
Blockfield	39.6719	-77.5225	442	Park Nelson et al. (2007)
Blockfield	39.4989	-77.4853	374.904	Park Nelson et al. (2007)
Blockfield	39.6081	-77.5644	374.904	Park Nelson et al. (2007)
Blockfield	38.2281	-78.75	905.256	Park Nelson et al. (2007)
Blockfield	38.2267	-78.75	859.536	Park Nelson et al. (2007)
Blockfield	38.2272	-78.7522	920.496	Park Nelson et al. (2007)
Blockfield	38.2189	-78.7497	908.304	Park Nelson et al. (2007)
Blockfield	38.2172	-78.7542	734.568	Park Nelson et al. (2007)
Blockfield	38.215	-78.7567	731.52	Park Nelson et al. (2007)

Table 11 (cont'd).

Blockfield	38.2	-78.75	646.176	Park Nelson et al. (2007)
Blockfield	38.2206	-78.7756	627.888	Park Nelson et al. (2007)
Blockfield	37.4536	-80.6008	899.16	Park Nelson et al. (2007)
Blockfield	37.3783	-80.5772	960.12	Park Nelson et al. (2007)
Blockfield	37.3758	-80.6058	1123.95	Park Nelson et al. (2007)
Blockfield	36.1667	-81.6944	1152.144	Park Nelson et al. (2007)
Blockfield	36.1664	-81.6964	1200.912	Park Nelson et al. (2007)
Blockfield	36.1719	-81.7078	1170.432	Park Nelson et al. (2007)
Blockfield	36.0408	-81.7469	798.576	Park Nelson et al. (2007)
Blockfield	36.0386	-81.7497	786.384	Park Nelson et al. (2007)
Blockfield	36.0358	-81.7519	762	Park Nelson et al. (2007)
Blockfield	36.0275	-81.7586	725.424	Park Nelson et al. (2007)
Blockfield	36.1608	-81.8258	1316.736	Park Nelson et al. (2007)
Blockfield	36.0614	-81.7989	890.016	Park Nelson et al. (2007)
Blockfield	36.0347	-81.7892	737.616	Park Nelson et al. (2007)
Blockfield	36.0664	-81.8053	822.96	Park Nelson et al. (2007)
Blockfield	36.0617	-81.8092	920.496	Park Nelson et al. (2007)
Blockfield	36.0328	-81.7989	697.992	Park Nelson et al. (2007)
Blockfield	36.0064	-81.8019	704.088	Park Nelson et al. (2007)
Blockfield	36.0156	-81.8303	1132.332	Park Nelson et al. (2007)

Table 11 (cont'd).

Blockfield	35.6628	-83.3417	1784	Park Nelson et al. (2007)
Blockfield	35.6306	-83.4039	1621.536	Park Nelson et al. (2007)
Blockfield	35.6306	-83.4064	1682.496	Park Nelson et al. (2007)
Blockfield	35.6514	-83.4333	1834.5	Park Nelson et al. (2007)
Blockfield	35.6522	-83.4361	1935.06	Park Nelson et al. (2007)
Blockfield	35.6536	-83.4453	1965.96	Park Nelson et al. (2007)
Blockfield	35.6458	-83.4442	1530.096	Park Nelson et al. (2007)
Large-scale sorted patterned ground on Mt. Washington	44.25	-71.3	1550	Antevs (1932)
CT- like feature big lawn on Mt. Washington	44.25	-71.3	1600	Antevs (1932)
Upper inactive lobe	46.95	-68.8833	358	Putnam & putnam (2009)
Pingo scar	40.99445	-77.1808	500	Marsh (1987)
Pingo scar	40.8576	-77.0538	220	Marsh (1987)
Relict protalus rampart/embry-onic rock glacier	44.1565	-71.6984	677.5	Germain & Jean-François (2024)
Periglacial boulder deposit	37.27277	-80.4492	745	Fame et al. (2024)
Periglacial boulder deposit	37.27919	-80.4863	763	Fame et al. (2024)
Periglacial boulder deposit	37.35422	-80.5971	649	Fame et al. (2024)
Periglacial boulder deposit	37.58181	-79.4707	705	Fame et al. (2024)
Block stream	39.18	-79.29	1046	Cremeens et al. (2005)
Summit feature	39.14	-79.33	1158	Cremeens et al. (2005)

Table 11 (cont'd).

Block stream	37.66	-90.38	348	Cremeens et al. (2005)
Block stream	37.4	-90.39	350	Cremeens et al. (2005)
Block stream	37.25	-90.52	380	Cremeens et al. (2005)
Block field	37.72	-90.72	522	Cremeens et al. (2005)
Block field	37.6	-90.67	366	Cremeens et al. (2005)
Block stream & Summit	37.52	-90.88	518	Cremeens et al. (2005)
Blockfield	37.48	-90.35	396	Cremeens et al. (2005)
Summit feature	37.65	-90.66	375	Cremeens et al. (2005)
Relict, sorted patterned ground	42.25		705	Delcourt & Delcourt (1988)
Relict, sorted patterned ground	42.5		605	Delcourt & Delcourt (1988)
Relict, sorted patterned ground	41		695	Delcourt & Delcourt (1988)
Relict, sorted patterned ground	40.125		700	Delcourt & Delcourt (1988)
Relict, sorted patterned ground	39.8		850	Delcourt & Delcourt (1988)
Relict, sorted patterned ground	39.5		860	Delcourt & Delcourt (1988)
Relict, sorted patterned ground	39		910	Delcourt & Delcourt (1988)
Relict, sorted patterned ground	39		1000	Delcourt & Delcourt (1988)

Table 11 (cont'd).

Relict, sorted patterned ground	37.8	775	Delcourt & Delcourt (1988)
Relict, sorted patterned ground	37.4	1150	Delcourt & Delcourt (1988)
Relict, sorted patterned ground	37.3	1100	Delcourt & Delcourt (1988)
Relict, sorted patterned ground	37	1210	Delcourt & Delcourt (1988)
Relict, sorted patterned ground	35.5	1490	Delcourt & Delcourt (1988)
Relict, sorted patterned ground	35.5	1510	Delcourt & Delcourt (1988)
Relict, sorted patterned ground	35.5	1600	Delcourt & Delcourt (1988)